This file is part of the following work:

Grant, Daniel Shane (2017) *Investigation into the effects of ionising radiation on plasma polymer monoterpene alcohols for applications in organic electronics.* **PhD thesis, James Cook University.**

Access to this file is available from:

https://doi.org/10.4225/28/5acd89dabf350

Investigation into the Effects of Ionising Radiation on Plasma Polymer Monoterpene Alcohols for Applications in Organic Electronics

Thesis submitted by

Daniel Shane GRANT (BEng - Hons)

in October 2017

for the degree of Doctor of Philosophy

in the College of Science and Engineering

James Cook University

Supervisors: A/Prof. Mohan Jacob, Dr. Kateryna Bazaka,

and Prof. James Burnell

DECLARATION

I declare that this thesis is my own work and has not been submitted in any form for another degree or diploma at any other university or institute of tertiary education. Information derived from the published and unpublished work of others has been acknowledged in the text, and a list of references is given.

Daniel S. Grant

October, 2017

STATEMENT OF ACCESS

I, the under-signed, the author of this work, understand that James Cook University may make this thesis available for use within the University Library.

I understand that as an unpublished work, a thesis has significant protection under the Copyright Act and I do not wish to place any further restrictions on access to this thesis. However, any use of its content must be acknowledged and could potentially be restricted by future patents.

Daniel S. Grant

October, 2017

STATEMENT ON THE CONTRIBUTIONS FROM OTHERS

This thesis included contributions from the sources outlined below.

Financial assistance:

- Living assistance whilst studying at James Cook University (JCU), Australia, was provided under the Australian Postgraduate Award over the duration of this thesis. Valued at ~$88,000.
- Living assistance whilst studying at Nangyang Technological University (NTU), Singapore, was provided by the National Institute of Education (NIE), Singapore, for the period of six months. Valued at $4,800.
- Annual funding from the College of Science and Engineering as well as the Graduate Research School facilitated access to characterisation facilities (e.g., the Advanced Analytical Centre), procurement of materials, and attendance at conferences. Valued at ~ $4,500.
- Access to the 10 MV Australian National Tandem Research Accelerator (ANTARES) and X-ray Reflectometer was facilitated by Dr. Rainer Siegele and Dr. Stephen A. Holt under the Australian Institute of Nuclear Science and Engineering (AINSE) Research Award No. ALNGRA14049 valued at $21,735. Further access to ANTARES was facilitated by AINSE Award No. ALNGRA15542 valued at $9,210.
- Access to the Co-60 Gamma Technology Research Irradiator (GATRI) was facilitated by Dr. Justin B. Davies and Connie Banos under the AINSE Research Award No. ALNGRA14554 valued at $6,240.

Editorial assistance was provided by:

- A/Prof. Mohan Jacob (JCU) and Dr. Kateryna Bazaka (JCU) for all content provided within this thesis.
- Co-authors of published papers that constitute Chapters 2 – 6. Included here are Dr. Rainer Siegele (ANSTO), Dr. Stephen A. Holt (ANSTO), Dr. Justin B. Davies (ANSTO), Connie Banos (ANSTO), Dr. Jakaria Ahmad (JCU), Dr. Jason D. Whittle (University of South Australia - UniSA), Dr. Andrew Michelmore (UniSA), Prof. Krasimir Vasilev (UniSA), and A/Prof. Rajdeep S. Rawat (NIE/NTU).

Experimental assistance and data analysis was provided by:

- Dr. Rainer Siegele (ANSTO) for operation of the 10 MV ANTARES instrument, Dr. Stephen A. Holt (ANSTO) for XRR data analysis, Connie Banos (ANSTO) for operation of the GATRI facility, and Dr. Jakaria Ahmad (JCU) for operation of the quadrupole mass spectrometer (UniSA).

Contributions to co-authored publications are detailed as follows:

- The candidate is first author in the following publications:
  - *Comparative Study of Natural Terpenoid Precursors in Reactive Plasmas for Thin Film Deposition Applications* (Chapter 3);
  - *Ion Irradiation as a Tool for Modifying the Surface and Optical Properties of Plasma Polymerised Thin Films* (Chapter 4);
  - *High Fluence Swift Heavy Ion Synthesis of Nanocrystalline and Amorphous Carbon from a Plasma Polymerised Polyterpenol Thin Film Precursor Material* (Chapter 4);
  - *Inelastic Deformation of Plasma Polymerised Thin Films Facilitated by Transient Dense Plasma Focus Irradiation* (Chapter 5); and,
  - *Organic Bioelectronic Plasma Polymerised Polyterpenol Thin Films – Preservation of Properties Relevant to Biomedical and Organic Electronic Applications Following Exposure to Sterilising Doses of Gamma Radiation* (Chapter 6).

  For all of these paper, only partial assistance was provided by co-authors in the form of minor data analysis, editing, and/or access to facilities.

- The candidate is second author in the following publication, with writing and editing responsibilities split equally between Dr. Kateryna Bazaka and the candidate:
  - *Dense Plasma Focus Radiation Processing of Materials for Sustainable Polymer Electronics* (Chapter 2).

ACKNOWLEDGEMENTS

I would like to thank the following people:

ABSTRACT

Plasma polymers are coming to occupy a niche position in the development of functionalised thin films for use in electronic, biomedical, and optical devices. In particular, plasma polymers synthesised from natural organic precursors, such as essential oils, have demonstrated promising properties relating to electronic charge transport/insulation, biocompatibility, and protective device encapsulation. Several of these environmentally friendly precursors, including terpinen-4-ol, are derived from resources native to Australia and their commercial uptake in plasma polymer-enabled technologies holds economic benefits for Australian industry.

This commercial uptake can be advanced through several initiatives. First, the economics of the plasma polymer synthesis process can be improved through better understanding of the relationship between precursor, plasma environment, and polymer properties. Second, efforts can be made to demonstrate the retention of electronically and biomedically relevant properties following exposure to a standardised sterilisation process, such as gamma irradiation. Finally, the range of suitable applications for plasma polymers can be expanded by developing new techniques (such as radiation processing) for tailoring and enhancing their chemical and physical properties.

Resultantly, this thesis focussed on the cold plasma synthesis of polyterpenol thin films from the natural terpinen-4-ol precursor, and the subsequent exposure of these films to a variety of ionising radiation sources and species.

The synthesis process involved the introduction of terpinen-4-ol monomer units (a monocyclic terpene alcohol extracted from the distillation of *Melaleuca alternifolia* oil) into a radio frequency glow discharge. Subsequent fragmentation and recombination/deposition of species within the plasma led to the formation of thin, flexible, and morphologically uniform polyterpenol films. Following synthesis, the polyterpenol films were exposed to ionising radiation in the form of swift heavy ions from an ion beam, gamma rays from a cobalt-60 source, and high-temperature species generated by a dense plasma focus device.

The energy, type, and relative abundance of plasma species was explored using residual gas analysis and positive ion mode quadrupole mass spectrometry. Properties of the irradiated polyterpenol thin films were examined using crystal quartz microbalance analysis, spectroscopic ellipsometry, atomic force microscopy, Fourier transform infrared spectroscopy, X-ray photoelectron spectroscopy, scanning electron spectroscopy, energy dispersive X-ray spectroscopy, Raman spectroscopy, X-ray reflectometry, and two-probe current-voltage and capacitive characterisation.

Specific findings from this thesis include:

- Determination that the plasma environments of terpinen-4-ol and *Melaleuca alternifolia* oil (from which terpinen-4-ol is distilled) show increasing commonalities in plasma species as the applied power is increased. This finding indicates that the less processed *Melaleuca alternifolia* oil may be used as a cost-effective substitute for terpinen-4-ol in applications that are reliant primarily on the mechanical and physical properties of the resultant plasma polymer. Conversely, priority should be given to the use of terpinen-4-ol in a low power plasma environment for the synthesis of films that are required to demonstrate traits that are strongly dependent on chemical functionalities (e.g., antibacterial coatings, or coatings to support endothelialisation).
- Determination that high energy (~50 MeV) iodine ion (I^{10+}) irradiation at low fluence ($\leq 1 \times 10^{12}$ ions/cm^2) can be employed to generate polyterpenol thin films with controlled surface pore density. This opens up the possibility of using porous polyterpenol thin films as nano- or micro-porous filtration membranes, or as loading and controlled dispersal platforms for pharmaceutical products.
- Determination that high energy (~55 MeV) iodine ion (I^{9+}) irradiation at high fluence ($\geq 1 \times 10^{13}$ ions/cm^2) can be employed to convert polyterpenol thin films into graphitic-polymer nanocomposite films, whilst still retaining some degree of polymer chemical functionality. This opens up the possibility of using high fluence ion treatment of polyterpenol to synthesise layers for use in supercapacitors, organic electronics, membranes, and biological assay.

- Determination that the physical and chemical characteristics of polyterpenol exhibit stability following gamma irradiation at doses up to four times in excess of the 25 kGy dose commonly employed to sterilise materials for biomedical applications. The antibacterial properties of polyterpenol (specifically with respect to the *pseudomonas aeruginosa* pathogen) are strongly dependent upon the surface morphology and chemical functionalities of the film. The retention of these characteristics following gamma irradiation at doses well in excess of 25 kGy suggests that polyterpenol antibacterial coatings (for devices such as in-dwelling implants) may be valid targets for gamma sterilisation processes.

- Determination that exposure to extremely high temperature transient irradiation from a dense plasma focus device can induce inelastic deformation of plasma polymer films. Plasma polymers exhibit a high degree of crosslinking, and as such behave in a fashion similar to that of thermosetting polymers when heated (i.e., they char and decompose). The high heating slope and rapid cooldown time associated with dense plasma focus treatment permits chain mobility and plastic behaviour to occur before thermal degradation is expressed. This has implications for reshaping plasma polymers, and enables the formation of novel topographical features (such as hollow bubble-like cavities).

In summary this thesis has enhanced the understanding of plasma chemistry relevant to naturally occurring terpene precursors, and expanded the suite of post-synthesis techniques that can be applied to tailor the properties of plasma polymerised polyterpenol thin films. Applications relating to these developments have been identified, and future avenues for investigation have been proposed.

CONTENTS

LIST OF PUBLICATIONS

The following publications were prepared by the candidate in the course of undertaking this thesis.

Pub. 1.
(Chapter 4)
D. S. Grant, K. Bazaka, R. Siegele, and M. V. Jacob, "Ion irradiation as a tool for modifying the surface and optical properties of plasma polymerised thin films," *Nuclear Instruments & Methods in Physics Research Section B – Beam Interactions with Materials and Atoms*, vol. 360, pp. 54-59, 2015

Pub. 2.
(Chapter 5)
D. S. Grant, R. S. Rawat, K. Bazaka, M. V. Jacob, "Inelastic deformation of plasma polymerised thin films facilitated by transient dense plasma focus irradiation," *Materials Research Express*, vol. 4, pp. 096407(1-5), 2017

Pub. 3.
(Chapter 6)
D. S. Grant, K. Bazaka, J. B. Davies, C. Banos, M. V. Jacob, "Organic bioelectronic plasma polymerised polyterpenol thin films – preservation of properties relevant to biomedical and organic electronic applications following exposure to sterilising doses of gamma radiation," *Journal of Materials Science: Materials in Electronics*, in press

Pub. 4.
(Chapter 3)
D. S. Grant, J. Ahmad, J. D. Whittle, A. Michelmore, K. Vasilev, K. Bazaka, M. V. Jacob, "Comparative study of natural terpenoid precursors in reactive plasmas for thin film deposition applications," submitted to *Polymer Journal*

Pub. 5.
(Chapter 2)
K. Bazaka, D. S. Grant, O. Bazaka, M. V. Jacob, R. S. Rawat, "Dense plasma focus radiation processing of materials for sustainable polymer electronics," submitted to *Renewable & Sustainable Energy Reviews*

Pub. 6.
(Chapter 4)
D. S. Grant, R. Siegele, K. Bazaka, M. V. Jacob, "High fluence swift heavy ion synthesis of nanocrystalline and amorphous carbon from a plasma polymerised polyterpenol thin film precursor material," submitted to the *Journal of Applied Polymer Science*

Additional publications completed, but not directly related to this thesis include:

Pub. 7.   K. Bazaka, D. S. Grant, S. Alancherry, and M. V. Jacob, (2016), "Plasma-Assisted Fabrication and Processing of Biomaterials," in Biomedical Applications of Polymeric Materials and Composites (eds R. Francis and D. Sakthi Kumar), Wiley-VCH Verlag GmbH & Co. KGaA, Weinheim, Germany

Pub. 8.   A. Kumar, D. Grant, S. Alancherry, A. Al-Jumaili, K. Bazaka, M. V. Jacob (2017), "Plasma Polymerization: Electronics and Biomedical Applications," in Plasma Science and Technology for Emerging Economies (eds R. S. Rawat), Springer Nature

Pub. 9.   A. Kumar, D. S. Grant, K. Bazaka, M. V. Jacob, "Tailoring terpenoid plasma polymer properties by controlling the substrate temperature during PECVD," *Journal of Applied Polymer Science*, pp. 45771(1-10), 2017

CHAPTER 1   INTRODUCTION

1.1   RATIONAL

The healthy and equitable continuation of society is challenged by a host of trends spanning aging demographics, resource depletion, climate change, and the rise of antibiotic resistant pathogens. Surmounting these challenges requires the design of new technologies, including bioelectronic and organic electronic devices, built using new materials. These novel materials must satisfy an ever growing suite of performance demands, and should ideally be synthesised from environmentally friendly precursors using green-chemistry techniques.

One such technique, plasma polymerisation, presents as an attractive choice for the solvent-free and dry synthesis of chemically functionalised thin films [1]. Resultantly, from 2009 – 2011, A/Prof. Mohan Jacob and Dr. Kateryna Bazaka successfully synthesised polyterpenol thin films via plasma polymerisation of the terpinen-4-ol monomer, extracted from *Melaleuca alternifolia* essential oil (aka. tea tree oil) [2]. Successive studies into the fundamental and applied properties of this polymer highlighted its suitability for a variety of uses, including as an encapsulating film for electronic devices [3], an antibacterial coating for biomedical devices [4], and an electron-blocking/hole-transport layer in organic electronic devices [5].

The production economics and utility of polyterpenol can be further enhanced by additional exploration into the relationship between precursor selection and plasma environment, and by the post-synthesis tailored modification of its properties via ionising radiation processing.

The desirability of radiation processing (via swift heavy ions, gamma rays, and pinch plasma) is grounded in its ability to induce spatially uniform changes in chemical and physical structure throughout the bulk of the polyterpenol thin film. Alternative processing techniques, including thermal, chemical, and cold plasma treatments are marred by complexities such as thin film degradation, post-treatment presence of chemical residues, and spatial confinement of treatment effects to the surface and near-surface regions of the film.

1

As mentioned, plasma polymerised polyterpenol has prospective applications in biotechnology, electronics, and as a passivation coating for various devices. Whilst being employed in these functions, polyterpenol is liable to be exposed to various forms of radiation (for example, sterilising gamma rays or electron beam processing). Thus, it is essential to understand how such radiation may influence the application-specific properties of the polymer.

The effects of radiation on conventional polymers (i.e., those comprised of regularly repeating monomeric units) are relatively well established, with commercial applications already available for polymer crosslinking, sterilisation, and recycling [6]. Unlike conventional polymers, plasma polymers are synthesised in a radiation-rich environment and as a result demonstrate significant structural disorder and presence of trapped free radicals [1]. Beyond the specific case of cold plasma treatment, very little is known about how the unique structure of plasma polymers responds to ionising radiation. Hence, radiation processing of plasma polymers presents as a virgin field of scientific inquiry with uncultivated potential.

1.2   RESEARCH OBJECTIVES

This thesis aimed to provide new understanding pertinent to both the fundamental elements of polyterpenol thin film synthesis, and the subsequent processing of these films with ionising radiation. In doing so, the following primary research questions were addressed by this thesis:

- Under what conditions does the choice of terpenoid precursor influence the plasma environment used to synthesise polyterpenol and related terpenoid plasma polymer thin films?
- Can the as-deposited physical and chemical properties of polyterpenol thin films be retained following exposure to radiation conditions conducive to biological sterilisation?
- Can the physical and chemical properties of polyterpenol thin films be selectively tailored by exposure to ionising radiation, and if so, what applications are these processed films best suited for?

Specific sub-objectives and their associated rational are detailed as follows:

- *Sub-objective*: to use mass spectrometry to elucidate the relationship between radio frequency power applied during polyterpenol synthesis, and the resulting species formed within the plasma environment.

  Rational: the antibacterial properties of polyterpenol thin films have been established in previous work for films synthesised as low power. This antibacterial behaviour was ascribed to the likely preservation and incorporation of intact terpinen-4-ol monomer units into the polymer deposit. Determination of the species present within the plasma volume as a function of applied power can substantiate the validity of this claim.

- *Sub-objective*: to use mass spectrometry to elucidate the relationship between radio frequency power applied during plasma polymer synthesis, and the resulting species formed within plasma environments supplied with terpinen-4-ol or *Melaleuca alternifolia* oil precursors.

  Rational: the identification of commonalities in the type and relative abundance of species generated within plasma environments supplied with terpinen-4-ol or *Melaleuca alternifolia* oil precursors will enhance the economics of film synthesis. Specifically, it will allow informed selection of the cheapest precursor material capable of forming films with comparable composition and structure to those formed from the more expensive precursor. Conversely, the identification of disparities in the type and abundance of plasma species from precursors excited at a given plasma power permits informed precursor selection with respect to the desired chemical functionality of the final film product.

- *Sub-objective*: to expose polyterpenol thin films to sterilising doses of gamma radiation and assess the effects of this radiation on the chemical and physical characteristics responsible for the material's previously identified bioelectronic and antibacterial properties.

  Rational: if antibacterial polyterpenol coatings are to be applied to biomedical devices, it must first be established that the surface chemical functionality and morphological characteristics responsible for the antibacterial behaviour can be retained following exposure to a commonly employed method of biomedical product sterilisation (viz. gamma

radiation). Post-irradiation retention of electronic properties must also be proven if polyterpenol is to be incorporated into bioelectronic devices for insulating, hole transport, or interlayer adhesion promoting purposes.

- *Sub-objective*: to expose polyterpenol thin films to low fluence swift heavy ions, and determine the effects of this radiation on the material's optical and morphological characteristics.

  Rational: demonstration of the controlled development of latent ion tracks and ion beam etching of polyterpenol thin films can open up new applications for these films as micro- or nano-porous membranes, drug loading architectures, and optical waveguides.

- *Sub-objective*: to expose polyterpenol thin films to high fluence swift heavy ions, and determine the effects of this radiation on the material's chemical composition and structure.

  Rational: demonstration of the ion beam induced conversion of polyterpenol thin films into graphitic-polymer nanocomposites can open up new applications for these films as electrically conductive contacts/layers in supercapacitors, organic electronic devices, and biosensors.

- *Sub-objective*: to expose polyterpenol thin films to dense plasma focus irradiation, and determine the effects of this radiation on the material's morphological structure.

  Rational: the utility of plasma polymers is partially limited by their thermosetting-like behaviour, and limited capacity to withstand thermal annealing. The application of an extremely transient high-temperature DPF treatment environment may present new pathways for circumventing these limitations.

1.3   DOCUMENT ORGANISATION

This thesis is organised into a series of chapters populated by journal papers in various stages of publication. In the interests of modularity each paper has been presented as a self-contained unit with standalone subheadings, experimental methodology, figure/table numbering, and references. The thesis is organised as follows:

Chapter 1 introduces the subject matter of plasma polymers and radiation processing, outlines the objectives to be realised by this thesis, and provides justification for the pursuit of these objectives.

Chapter 2 provides a literature review in the form of a review paper that details the use of plasma technologies, including dense plasma focus, in the environmentally sustainable synthesis and processing of polymers for electronic applications.

Chapter 3 studies the relationship between terpenoid precursors and their associated plasma environment, as a function of applied plasma power. Ion energy probes and quadrupole mass spectrometry provide information about the type, abundance, and energy of neutral and ion species within the plasma environments generated from terpinen-4-ol and *Melaleuca alternifolia* oil precursors respectively. Supplementary information about the polyterpenol deposition rate is also provided by quartz crystal microbalance.

Chapter 4 outlines the response of polyterpenol thin films to swift heavy ion irradiation in two papers. The first of these uses spectroscopic ellipsometry, atomic force microscopy, and X-ray reflectometry to probe changes in material properties following irradiation with 50 MeV I^{10+} ions at low fluences ranging from 1×10^{10} - 1×10^{12} ions/cm^2. Parameters of interest include the optical complex refractive index, air-polymer and polymer-substrate interfacial roughness, and surface morphology.

The second study explores the effects of high fluence ($\geq 1\times10^{13}$ ions/cm^2) 55 MeV I^{9+} ion irradiation on polyterpenol's physical structure and chemical composition. Scanning electron microscopy, spectroscopic ellipsometry, Raman spectroscopy, Fourier transform infrared spectroscopy, and atomic force microscopy are employed to investigate subsequent film restructuring and formation of a chemically functionalised graphitic-polymer nanocomposite.

Chapter 5 outlines the inelastic deformation response of polyterpenol thin films to transient thermal and radiation treatment delivered by a dense plasma focus device. Surface restructuring and the elemental composition of newly formed

microstructures is examined using scanning electron microscopy and energy dispersive X-ray spectroscopy.

Chapter 6 details the preservation of polyterpenol properties relevant to biomedical and organic electronic applications following exposure to gamma radiation (1.17 and 1.33 MeV) at doses ranging from 0.1 – 100 kGy. Post-irradiation stability of optical, electronic, chemical, and surface morphological properties is verified with spectroscopic ellipsometry, capacitive and current-voltage analysis, Fourier transform infrared spectroscopy, and atomic force microscopy.

Chapter 7 summarises the work undertaken throughout the course of this thesis, highlights potential applications stemming from the findings contained herein, and identifies additional avenues for future investigation.

REFERENCES

1.   J. Friedrich, *Mechanisms of Plasma Polymerization - Reviewed from a Chemical Point of View.* Plasma Processes and Polymers, 2011. 8: p. 783.

2.   K. Bazaka and M.V. Jacob, *Synthesis of radio frequency plasma polymerized non-synthetic Terpinen-4-ol thin films.* Materials Letters, 2009. 63(18-19).

3.   M.V. Jacob, et al., *Fabrication and characterization of polyterpenol as an insulating layer and incorporated organic field effect transistor.* Thin Solid Films, 2010. 518(21).

4.   K. Bazaka, et al., *Plasma-Enhanced Synthesis of Bioactive Polymeric Coatings from Monoterpene Alcohols: A Combined Experimental and Theoretical Study.* Biomacromolecules, 2010. 11(8): p. 2016.

5.   M.V. Jacob, et al., *Electron-blocking hole-transport polyterpenol thin films.* Chemical Physics Letters, 2012. 528.

6.   R.L. Clough, *High-energy radiation and polymers: a review of commercial processes and emerging applications.* Nuclear Instruments and Methods in Physics Research Section B, 2001. 185: p. 8.

CHAPTER 2   PLASMA FOR ORGANIC ELECTRONICS

This chapter introduces core concepts integral to understanding the synthesis and radiation processing of polymeric materials employed in the fabrication of organic electronic devices. Factors relating to precursor selection, deposition mechanisms, and the properties of polymeric materials are all considered in the context of organic electronic applications. The chapter also provides a detailed review of dense plasma focus systems and the radiation environment that they generate, with a particular emphasis on the sustainable processing of polymeric materials for electronic applications.

2.1   DENSE PLASMA FOCUS RADIATION PROCESSING OF MATERIALS FOR SUSTAINABLE POLYMER ELECTRONICS

This review paper outlines the need for sustainable polymer-based electronics, and details the role that dense plasma focus processing has played in facilitating this technology. Challenges facing the green and sustainable production of electronic materials are identified, and a case is made for transitioning from traditional silicon-based electronics to carbon-based electronics. Specifically, the advantages associated with polymer electronics are highlighted, along with potential challenges relating to their quality, performance, toxicity, and complex assembly. Non-thermal plasma synthesis routes for polymer electronics are briefly touched on, before progressing to a detailed presentation of fundamental dense plasma focus treatment mechanisms and demonstrated applications in polymer electronics. "Dense plasma focus radiation processing of materials for sustainable polymer electronics," has been submitted to Renewable & Sustainable Energy Reviews. This paper involved collaborations with Olha Bazaka, and A/Prof. Rajdeep S. Rawat.

DENSE PLASMA FOCUS RADIATION PROCESSING OF MATERIALS FOR SUSTAINABLE POLYMER ELECTRONICS

Kateryna Bazaka[a,b,c,#,*], Daniel S. Grant[a,#], Olha Bazaka[a,c], Mohan V. Jacob[a], Rajdeep S. Rawat[c]

[a] College of Science and Engineering, James Cook University, Townsville, Queensland 4811, Australia

[b] CSIRO−QUT Joint Sustainable Materials and Devices Laboratory, Commonwealth Scientific and Industrial Research Organisation, P. O. Box 218, Lindfield, NSW 2070, Australia

[c] School of Chemistry, Physics, and Mechanical Engineering, Queensland University of Technology, Brisbane, Queensland 4000, Australia

[d] Natural Sciences and Science Education, National Institute of Education, Nanyang Technological University, Singapore 637616

[#] These authors contributed equally to this work

[*] Corresponding author: Katia.Bazaka@jcu.edu.au

Abstract

Polymers fill several critical functions in modern photovoltaic and electronic applications, and are commonly found serving as protective coatings, insulators, dielectrics, conductive layers, adhesion promoting layers, and photoresists. Ionising radiation has been used for decades to achieve the synthesis and modification of these polymeric materials, with a varied range of radiation sources, species, and target materials being employed. This paper introduces one such source, the dense plasma focus (DPF), and explores the diverse work that has been undertaken in applying DPF to polymer processing. Revealing the

unique properties of DPF may serve to stimulate specialists presently working in the polymer irradiation domain to consider DPF as an alternative vehicle for accomplishing innovation in polymer processing for sustainable photovoltaic and electronic applications.

1. Introduction

Advances in nanoscale technologies have delivered significant benefits to most industries, from electronics to medical to agricultural fields, leading to substantial advancements in those areas. Indeed, currently available fabrication technologies allow for the deterministic organisation of materials at different length scales, from atomic to macro level, thereby allowing for the nanoscale control of the physicochemical properties and functionality of the materials produced. At the nanoscale, elements behave differently than they do in their bulk form, giving rise to novel effects and unique optical, electronic, chemical or mechanical properties. It is with these unique nanoscale effects and properties that superior performance, energy efficiency, and substantial miniaturisation of a large range of mechanical, optical and electronic devices can be attained, overcoming obstacles that hinder the development of macro and microscale technologies.

Although nanoscale materials and devices continue to become ever more energy efficient and environmentally friendly to operate, the energy and material expenditure associated with their production and post-use management remain disproportionally high. The application of nanomaterials is challenged by the sensitivity of the desirable properties to the presence of undesirable imperfections, such as structural defects, chemical or physical non-uniformity, as well as the quality of the integration of individual components within the device. To operate properly, nanoscale materials and processes demand a high degree of precision in terms of material purity, chemical conformation, dimensions and architecture. This generally translates to high cost, energy-intensive processing of highly purified, often toxic precursors. Indeed, the majority of currently available high-performance precursors are produced using complex synthesis techniques, often in more than one production environment, with significant water, energy and material inputs, and large amounts of waste output. This holds true for inorganic and organic materials, even though the latter are considered having the potential to be a lower-cost, more sustainable alternative to metal salts, metal halides, organic alkoxides, and other materials used in modern electronics. Process energy and material consumption are thus the critical targets for making electronics more sustainable.

This review aims to critically evaluate the use of ionising radiation, specifically that generated by the dense plasma focus family of devices, as an enabling technology for nanoscale processing of polymer materials for application in organic electronics. The review will first briefly discuss the sustainability of current electronics, focusing on the challenges in achieving material and energy efficiency throughout device lifecycle, and outlining the areas where significant improvements are warranted. It will then demonstrate how the highly-reactive physical and chemical effects generated by dense plasma focus radiation can enable innovation in polymer processing for sustainable electronic applications.

2. Challenges in the fabrication of sustainable electronics

Since its emergence in the 1980s, nanotechnology has become a tool to organise and control carbons at atomic- and nanoscales, advancing every aspect of modern electronics, from nanoscale material synthesis, device patterning and assembly, to inspection and metrology capabilities. This enabled unprecedented miniaturisation of device components and large scale integration, leading to the development of highly-efficient, low-cost electronic devices with novel and advanced capabilities while reducing their weight, physical dimensions, and power consumption.

Notwithstanding these benefits, operating at the nanoscale is not trivial. There are general complexities associated with designing devices at these length scales, such as the issues of power dissipation and heat removal in geometrically-scaled conventional silicon devices [1]. Challenges that become prominent during scaling include subthreshold leakage and standby power associated with short channel effects in field effect transistors, increasing operating power due to junction leakage, high standby current associated with gate dielectric thickness scaling, memory scaling being hindered by charge storage and retention, and many others.

The key technical challenge for nanoelectronics, however, is the requirement for nano- or even atomic-scale precision, which increases the complexity, costs and energy requirements for semiconductor material synthesis and processing [2]. According to Gutowski and colleagues, in the past 30 years, an increase by at least six orders of magnitude has been observed in the intensity of materials and

energy used per unit of mass of material processed, with this phenomenon being driven largely by the demands of miniaturisation and nanoscale precision [3]. This means that even though the operational efficiency and environmental credentials of electronics have experience dramatic improvements, the energy and material cost associated with fabrication of these devices remain excessively high.

Although several different types of electronics are being developed, at present, electronics based on silicon and gallium arsenide offers the best combination of performance and stability and as such remains the dominant technology [4]. Most of these photovoltaic and electronic devices use high-purity polycrystalline silicon, scarce elements, such as indium and tantalum, and precious metals, such as gold and platinum, the refinement and processing of which is material- and energy-consuming, costly, and impactful on the environment [5]. The assembly of device components is typically energy-inefficient, requires multi-step processing and the use of potentially environment- and human-health-hazardous auxiliary organic solvents and catalysts. For instance, CVD fabrication of electronic grade silicon is estimated to consume in excess of 20 PJ of electricity per year [3], with the complex multi-step process of silicon wafer fabrication consuming a large fraction of the energy and material expended in the production of an integrated circuit [6].

The cost of post-use management has also remained a considerable impediment on the path to sustainability for modern, highly-integrated electronics. Until recently, excellent long-term stability under as broad of a range of environmental conditions as possible has been highly caveated, as it translated into longevity of device performance over years or even decades. Unsurprisingly, most of the currently used materials are non-biodegradable, that is, they break down at an extremely slow rate and persist in the environment (e.g. remain in the landfill), long after their disposal. Alternatively, these materials need to be post-processed to initiate their decomposition. However, this is logistically challenging: the multi-component, highly integrated nature of modern electronics precludes easy device disassembly; on the other hand, there are few techniques that would be equally suitable for pre-treatment of such a wide variety of materials as those found in modern electronics. Most types of post-use management attract additional material, water and energy costs, including collection of the used articles, their

transportation to landfill or a recycling factory, chemical and/or physical treatment, disposal of end-products, remediation of auxiliary substances and catalysts, and so on. Post-use management (i.e. decomposition and recycling) is complicated by the high degree of integration associated with nanoproducts, as more complex processes are required to decompose or extract specific constituents from the device.

Thus, many nanoproducts that are considered 'green' due to low-cost and energy efficient operation may nonetheless attract significant production and/or end-of-life management costs. Indeed, even though material and energy efficiency and waste management are closely interlinked not only at the production stage, but at the use and post-use stages, the manufacturing, use and disposal are often developed and evaluated separately. From 'green synthesis' that disregard the impact of the work-up chemistry, to 'green waste management' that ignores the transportation costs, the examples are many both in industry protocols and in academic reports. There is a need to converge the advancements in each of these areas to attain the most successful 'green' solution.

3. Carbon vs silicon in electronics

Carbon-based nanomaterials have emerged as a potentially lower-cost, more environmentally sustainable technology that can either replace or supplement silicon-based electronics [7]. Indeed, organic materials are plentiful, versatile and often renewable. It is generally regarded that the production of organic materials, particularly polymers, is more energy-efficient. According to some estimates, up to six orders of magnitude more energy is consumed in the production of high-quality inorganic electronic material than that necessary to produce high-quality plastic [3]. They are also regarded as being more environmentally friendly to source, as carbon and carbon-based materials are omnipresent in nature, and to dispose of, since many are inherently biodegradable or can be manipulated to become more readily degradable. In addition to post-use recycling into lower-value products, used carbon-based materials can also be incinerated to produce energy.

Besides their environmental and economic credentials, the physical and chemical properties of carbon-based materials can enable the development of novel forms

of electronic devices. For instance, in addition to very low-weight and large area coverage, weak Van der Waals bonding between organic molecules enables polymers to endure substantial mechanical deformation [8, 9], which is critical for the development of sensing, energy harvesting and light emitting devices for foldable electronics, smart clothes, electronic skin, and surface conforming foils [10]. Unlike those based on silicon electronics, organic electronic devices can be fabricated using a variety of low-cost, high-throughput, scalable methods, e.g. though inkjet or offset printing of electrically-functional electronic or optical inks, as well as established chemical and physical vapour deposition techniques widely used in modern semiconductor processing [11].

Nonetheless, a large proportion of presently used organics are derived from non-renewable petrochemical resources by means of purification methods that consume and produce hazardous liquid, solid, and gaseous substances. Yet more energy, water and material resources are then required to mitigate these toxic by-products. Toxic substances can also be entrapped within a device itself, potentially leaching out into the environment during operations or post-use.

The use of carbon nanotubes (CNTs) in electronics continues to expand given their unique mechanical, thermal, and electrical properties [12]. At present, controlling the properties and assembly of carbon nanostructures is challenging [13]. CNTs are typically synthesised using arc discharge, laser ablation and chemical vapour deposition [14, 15]. Processing of carbon nanomaterials using traditional methods is also highly energy-demanding, with CNTs and single-walled nanotubes (SWNTs) requiring at least 1 to 2 orders of magnitude higher energy input compared to less-ordered carbon nanofibers.

The temperature at which synthesis is performed is typically significantly higher than a polymer substrate can withstand, and thus CNTs cannot be deposited directly onto the end-substrate. Instead, they are grown on a temporary support, typically patterned with a metal catalyst, and then the synthesised layers of CNTs are either directly transferred onto the end-substrate, or dissolved in a suitable medium for solution processing, e.g. drop-coating, spin-coating, or printing. Nanotubes can be grown in the gas phase using atmospheric-pressure floating-catalyst (aerosol) chemical vapour deposition (FC-CVD), where carbon and catalyst precursors are simultaneously fed into the chamber [16]. A membrane

filter is used to collect the CNTs, and is then dissolved in acetone to transfer the as-grown nanotubes onto the end-substrate. However, these methods are restricted by the size of the initial substrate and may not suit high-throughput, low-cost device assembly. For commercial applications, solution-based processing, particularly spray-coating and printing may be more suitable [17].

Furthermore, the concomitant synthesis and deposition directly onto end-substrate or the direct transfer of the as-deposited layer is also hindered by the difficulties in controlling chirality, diameter, length, and the ratio of semiconducting to metallic NTs [18-20]. Although higher temperature arc discharge and laser ablation produce CNTs with fewer structural defects, the level of contamination with amorphous carbon and metal catalyst is also typically higher than that of CVD process. To address heterogeneity and remove impurities, CNTs are then subjected to a range of post-deposition treatments, such as dispersion, purification and separation. These include density-gradient ultracentrifugation (using structure-discriminating surfactants) [21], gel chromatography [22], substrates with controlled topography [23, 24], alternating current dielectrophoresis [25], and so on. Such post-processing ensures monodispersity of the CNTs [26], yet it limits the yield and increases the cost and the level of waste associated with CNT production.

4. Polymer electronics – opportunities and challenges

As is the case with any other type of nanotechnology, the performance of organic nanoelectronics is reliant on the precision with which materials are fabricated and assembled, as it directly affects circuit density and functionality. A critical determinant of device performance, the efficiency with which charge is transported within the organic layer(s), is dependent on a multitude of factors; among them molecular packing, degree of disorder, presence of impurities, size and molecular weight, and factors associated with the conditions under which the device operates [27].

4.1 Quality vs performance

One of the major parameters governing the transport properties of polymer electronic devices at the microscopic level is the amplitude of the electronic transfer integrals between adjacent oligomer or polymer chains [28]. The transfer

integrals are the function of distance and angles between atoms on adjacent chains, and as such are directly affected by the nature and relative positions of the interacting units [28, 29]. The amplitude of the transfer integrals is extremely sensitive to the molecular packing, e.g. lamella stacking, π−π stacking, chain alignment, etc. For example, by reducing the π–π stacking distance between co-facially stacked, conjugated backbones in a 6,13-bis(triisopropylsilylethynyl) pentacene semiconductor crystal lattice from 3.33 Å to 3.08 Å, it was possible to increase electron orbital overlap between the molecules within the film. This increased the hole mobility in TIPS-pentacene transistors from $0.8\,cm^2\,V^{-1}\,s^{-1}$ to $4.6\,cm^2\,V^{-1}\,s^{-1}$ [30].

Most low-cost printing technologies do not offer the necessary degree of control over the degree of ordering of the chains in the solid state and the density of chemical and/or structural defects [28]. This leads to inferior performance of these devices, particularly when compared to silicon-based devices [4, 7, 31, 32]. Similarly, the use of organic precursors in their 'raw', minimally processed form rarely affords sufficient device performance. A higher order control over the assembly process is typically achieved by using a more stringently controlled environment, pre- and post-processing, which adds to the overall complexity, cost, and energy- and material consumption.

4.2 Material synthesis

The demand for high-quality polymer materials significantly affects the cost and processing complexity of fabrication. For instance, the production energy of $PC_{71}BM$, the acceptor of choice for practically all of the highest-performing research-scale organic photovoltaic (OPV) devices [33, 34], is almost two orders of magnitude greater than that of polysilicon, at approximately $90\,GJ\,kg^{-1}$ [35]. Although the quantities of $PC_{71}BM$ required to produce one OPV is 2–3 orders of magnitude smaller compared to that of polysilicon used in the fabrication of conventional solar cells, the production energy is nonetheless significant.

Conjugated donor polymers, such as P3HT and PCDTBT, are regarded as greener compared to fullerenes, with a production energy of $1.8-1.96\,GJ\,kg^{-1}$ and $5.8\,GJ\,kg^{-1}$ for P3HT and PCDTBT, respectively [36, 37]. However, the polydispersity of the polymers increases fabrication complexity [38]. The

performance of polymer-containing OPVs has been demonstrated to correlate with the molecular weight, e.g. the changes in surface morphology of P3HT and P3HT:PCBM with molecular weight increasing from 34–121 kDa led to a one order of magnitude decrease in hole mobility in the device [39].

Then, there is a matter of declaring a material or process as 'green' while disregarding the environmental and energy credentials of other stages in the product lifecycle, such as the input products, work-up chemistry, auxiliary substances, and potential toxicity of the product during degradation (post-use). For example, the fabrication of many of the organic materials that may themselves be low-cost and benign (e.g., cosmetic and food grade dyes and pigments), also involves and generates harmful by-products and waste [7]. Conversely, the synthesis of the organic semiconductor itself may be sufficiently green, yet the input units can be toxic or be produced via costly, environmentally-harmful pathways. In addition to the toxicity of semiconducting layers, the potential negative effects of additives such as dithio- and diiodooctane [40, 41] and polydimethylsiloxane [42] need to be considered [43].

Certain types of polycondensation, e.g., Knoevenagel condensation, are generally considered 'green' as no or minimal catalyst is used and the reaction by-products are water or CO_2, and are often used for the efficient synthesis of unsaturated semiconducting polymers [44-46]. 'Green' solvent-free reactions facilitated by mechanical grinding have also been reported for Passerini, Grignard and Reformatsky reactions and aldol and Knoevenagel condensations [47-49]. The reactivity here is attributed to the grinding-induced formation of a eutectic melt of uniformly distributed solids; the advantages include high yield, short reaction time, mild reaction conditions (i.e., the use of mild catalyst at room temperature), minimal by-products, and simple purification of the resultant product [50, 51]. However, in order to estimate the net energy and environmental benefits of these technologies, the respective costs of the input materials, assembly methods and disposal have to be incorporated into the analysis.

4.3 Device assembly

Theoretically, printing of solution-processed organic electronics enables fast, large-volume and low-cost production of thin, lightweight and flexible electronic

devices and systems [52]. However, the formation of uniform, flat thin films and alignment and patterning of individual semiconducting nanowires at a desired position in a large area using conventional printing methods is challenging, resulting in relatively poor resolution, electrical performance, and device yield. The non-uniformity is due to the "coffee ring effect", where in the course of solvent evaporation on the surface, the solute is transported from the center of the drop to the contact line [53], forming a ring-like profile. Surface roughness and porosity of solution-processed layers, and difficulties in achieving sample-to-sample consistency of device parameters are also frequently reported [54].

Higher resolution, repeatability, and uniformity can be significantly improved by using more mature techniques, such as vacuum evaporation or lithography techniques [55], or lab-scale techniques, such as doctor blading and spin-coating [56, 57]. However, these techniques are more time-consuming, complex and expensive [58, 59]. The specifics of the processing environment typically restrict the type of organic semiconducting materials that can be deposited/treated using these methods. For instance, few high performance organic semiconductors and insulators can endure conventional photolithographic processes, such as the interactions with developer and acetone in lift-off processes [60].

The use of green solvents in place of toluene, chlorobenzene and o-dichlorobenzene [61, 62], which are environmentally hazardous both when used and when emitted, also typically leads to a decrease in device performance. The issue is particularly evident for conjugated polymer semiconductors, where higher molecular weight is associated with lower solubility for given molecular moieties [63]. Test P3HT:PCBM devices produced with relatively green pristine o-xylene and 1,2,4-trimethylbenzene were characterised by lower power conversion efficiencies of 2.9% and 1.47%, respectively, and the use of mesitylene/acetophenone solvent blend produced only a slightly better result, at 3.38% [64-66].

Devices based on small molecule N(Ph-2T-DCN-Et)$_3$ and PC$_{70}$BM fabricated using 'green' pristine benzaldehyde or a benzaldehyde:mesitylene solvent blend had slightly better efficiencies, at 3.62% and 3.74%, respectively [63], indicating that lower molecular weight small molecule active layers may be better suited to green solvents due to their inherent higher solubility [67]. Solution-processed

multilayers using alcohol- [68, 69] and water-soluble [70, 71] polyelectrolytes would provide a more environmentally-friendly alternative to organic solvents. However, the ionic side groups in polyelectrolytes can induce an undesired electrochemical doping effect [72].

4.4 Potential toxicity

Attractive electrical, thermal, optical and mechanical properties of 2D carbon materials, such as CNTs and nanocrystals, render them well-suited for a range of semiconducting and photoactive thin films in flexible optoelectronics [73, 74]. The nanoscale dimensions of these materials also give rise to chemical and biological activity that can be markedly different from that of the bulk material [75]. For instance, a conductive polymer, poly(3,4-ethylenedioxythiophene), shows cytocompatibility as a coating, but has cytotoxic and apoptotic effects on human and mouse lung cells as a nanoparticle that increases with their decreasing aspect ratio [76]. Indeed, the biochemical activity of nanoparticles is highly dependent on both the geometry and composition of these structures [77]; as such, it is difficult to estimate how these nanostructures will interact with complex systems, such as living organisms or ecosystems [78, 79].

While these biochemical properties can be beneficially exploited to develop novel medical and environmental treatments, they also present challenges for carbon semiconductor manufacturing, especially as the technology transitions from laboratory scale to the scale needed to address global demand [75, 80]. Consider indium tin oxide (ITO), a transparent electrode material frequently used in organic photovoltaics and displays. When immobilised as part of the surface electrode layer, ITO is biocompatible, which supports its use in implantable electronic devices. In particulate form, ITO is toxic, associated with such health issues as pulmonary inflammation in rats [81], mice [82] and hamsters [83], carcinogenicity in rats, and pulmonary fibrosis in workers exposed to ITO aerosols at manufacturing or recycling plants [84-86]. Particles of ITO are significantly more toxic *in vivo* and *in vitro* than In_2O_3, SnO_2, or their unsintered blend [87], with toxicity increasing with decreasing particle size. The smaller size may enable uptake of the poorly soluble ITO particles by cells, where the particles are solubilised via phagolysosomal acidification to release toxic indium ions [88].

Current research indicates that sufficiently long and biopersistent fibrous CNT can deposit in the lungs and exhibit asbestos-like behaviour, causing oxidative stress and provoking inflammation, and potentially fibrosis and cancer in the long term [89]. In addition to pathologic changes, CNTs can elicit direct genotoxic effects on epithelial cells and mesothelium [89, 90]. CNTs introduced into the abdominal cavity of mice show asbestos-like pathogenicity [91].

Although more evidence is required to determine the exact toxicity of various carbon nanomaterials to human health and the environment, it would be prudent to exercise material efficiency to minimise nanomaterial waste, i.e. i) high degree of control over the properties of produced nanomaterials, and ii) efficient incorporation of the synthesised nanomaterials into desired device structures.

4.5 Commercial competitiveness

At present, carbon-based electronic devices are unable to present a competitive level of performance to challenge silicon technology [92-95]. Consider mechanically-flexible solar cells, where thin film inorganic technologies require similar or less energy during production, have shorter energy payback times of 0.75−2 years, longer lifetime, and reach higher conversion efficiency (~ 20.3%) compared to organic photovoltaics, where a lifetime of several years and energy payback of 2−4 years is not uncommon [31, 96]. Thus, in the near future, the large-scale replacement of hard core inorganic components within the presently used devices (e.g., those active in high-speed processors, integrated circuits, and even solar cell modules) remains unlikely.

The critical issue here is the ability to find technologies that would support molecular scale ordering and nanoscale organisation required for fabrication of high-performance electronics without compromising on the economic and environmental advantages of organic semiconductor manufacturing.

5. Ionising radiation

Ionising radiation takes the form of beta particles, protons, alpha particles, heavy ions, photons, and neutrons. To be considered ionising, these particles must possess sufficient energy to liberate bound electrons (typically greater than 10's eV), and can originate from both natural and artificial sources.

The dominant interactions between ionising radiation and matter include the development of atomic displacements, and radiochemistry (manifesting itself in the form of ionisation and free radical production). An assortment of artificial sources of ionising radiation have been developed to take advantage of these interactions, including electron beams, synchrotrons, radioisotopes, and non-thermal plasmas. This assortment of sources has, in turn, been applied to an equally diverse spread of polymer-related fields [97], including for the synthesis of electrically insulating polymers [98-105], heat-shrink polymers, the curing of coatings and inks, synthesis and functionalisation of antibacterial surfaces [106-108], and the sterilisation of disposable plastic medical devices [109].

Among these artificial sources, plasmas are unique in that they can provide environments in which virtually all species of ionising radiation can be found. The majority of plasma-based techniques for synthesising or modifying materials, especially polymers, in electronics have employed non-thermal plasmas. Included here are radio frequency, microwave, direct current, and dielectric barrier discharges. Dense plasma focus (DPF) stands out in contrast to these sources as one of the few high temperature plasmas employed in polymer processing.

The DPF device was developed separately in both the United States by Mather [110] and the Soviet Union by Fillipov, Fillipova, and Vinogradov [111]. Initially DPF attracted considerable attention for its ability to generate neutrons, with hopeful applications in controlled thermonuclear fusion research [112, 113]. More promising avenues for achieving fusion resulted in the attention of DPF research groups being directed towards more fruitful pursuits, with practical applications being developed in X-ray lithography [114], radiography [115], and in studying the effects of neutron radiation on materials to assess their suitability for use in fusion reactors [116].

With respect to materials research, the vast majority of DPF effort has been devoted to studying the synthesis of graphene or diamond like coatings [117, 118], and the synthesis or nano-structuring of metallic films [119]. This review paper aims to introduce non-thermal plasma processing, before extending the general discussion and course of research for DPF applications to enclose the domain of polymer synthesis and modification via DPF processing.

5.1 Non-thermal plasmas in silicon electronics

In semiconductor manufacturing, plasma-assisted synthesis and surface modification is widely used for highly controlled removal and deposition of material, including etching, ashing, sputtering, and chemical vapour deposition. Mild plasma treatments, such as those using oxygen gas, are used to activate the surface to facilitate or promote subsequent interactions with other materials in a predefined fashion. For example, exposure to mild oxygen plasma improves bonding adhesion for lattice-mismatched semiconducting material systems (e.g., Si and GaAs, or Si and InP), without the need for high-temperature annealing. The treatment results in a high density of chemically active species on the surface that can undergo spontaneous bonding at near-room temperature.

Low-pressure, low-voltage plasmas are particularly useful for anisotropic, highly selective etching, where the goal is to limit excessive heating and ion bombardment that may damage the fine structures on the surface of the wafer. Enabled by mostly vertical delivery of reactive ions, high fidelity transfer of patterns and highly anisotropic etch profiles on a variety of substrates can be attained, not only at the microscale, but also in the nano- and sub-nm range, yielding highly-resolved, well-defined and ordered morphologies with high aspect ratio. The mechanism involves electric-field-driven, fast delivery of reactive ion species to the unmasked areas of the substrate, where they bond with the substrate atom, resulting in the formation of volatile species that can be effectively removed from the reactor by the action of the vacuum pump.

For example, Si nanowires with radii < 100 nm, aspect ratios above 100:1, and perpendicular orientation to underlying substrate are fabricated using time-multiplexed deep reactive ion etching at room temperature (*Figure 1*) [120]. Because of their highly mobile, energetic nature and the effect of the electric field which pulls them towards the substrate, plasma-generated ions can penetrate deep inside the fine features, e.g. trenches or pits, without inflicting substantial damage on their walls, thus enabling fabrication of very deep, closely-spaced features. Densely-packed sub-10 nm fine features with aspect ratios greater than 10:1 and vertical Si wire features with 15 nm diameter, 26 nm feature-to-feature spacing, and aspect ratios of up to 17:1 were produced using block copolymer lithography and low-temperature etching [121].
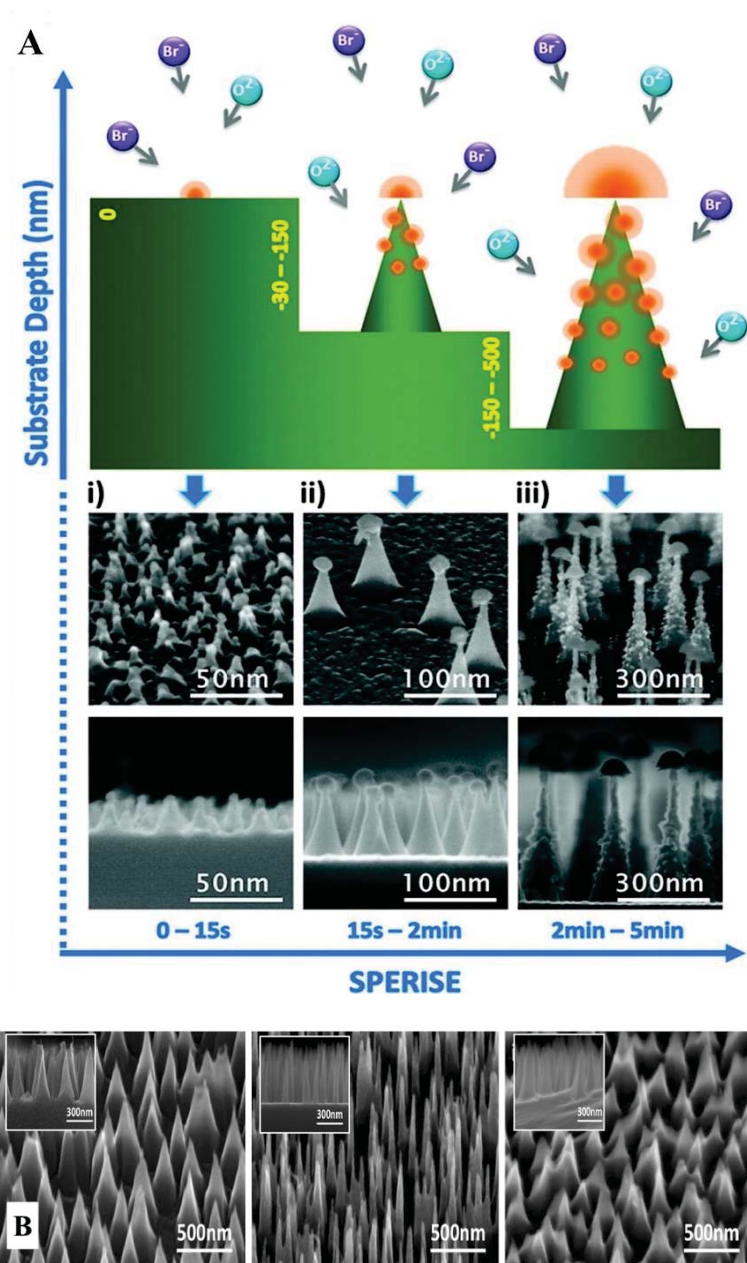
Figure 1. (A) An example of the mechanism of formation for Si nanocones via simultaneous plasma enhanced reactive ion synthesis and etching (SPERISE) process using oxygen and bromine plasma. Exposure to plasma results in the formation of pseudorandomly distributed silicon oxybromide nanodots (orange), which then grow into hemispheres via a phase-transition nucleation process. These hemispheres act as a protective nanomask for the simultaneous reactive ion etching of the underlying silicon cone structures (green). Wet oxide etchant removes the hemispheres to reveal nanocones. **(B)** The growth rate of the hemispheres and the crystalline structures of the silicon determine the aspect ratio of nanocones. SEM images of nanostructure profiles on single crystalline,

polycrystalline, and amorphous silicon substrates after oxide removal show cones with extremely smooth sidewall and sharp tips. Reproduced from [122]

Self-organised arrays of inorganic nanotips can be effectively produced at low temperature over large areas using self-masked plasma etching [123]. The mask is deposited using nanostructure-forming plasmas, e.g. methane and silane; the deposition is followed by Ar+H_2 plasma etching [124]. Since this method uses self-organised nanoclusters to define the radius of the tip, very sharp tips (~1 nm) can be fabricated [125]. In a similar way, tall polymer nanowires (d < 50 nm, aspect ratio > 20:1) for sensor, optoelectronic and energy storage devices can be produced using a layer of polymer photoresist as a base for mask-less fabrication [126].

Plasma deposition, such as plasma-enhanced chemical vapour deposition (PECVD) and sputter deposition, is widely used for fast-rate fabrication of inorganic, organic and composite films on a variety of substrates, including temperature-sensitive polymer substrates and thin film structures [127]. The properties of these films can vary from smooth, highly-uniform with respect to surface nanoscale features and chemistry, to rough, porous, chemically graded structures by controlling processing conditions, namely applied power, input gas, pressure, temperature, reactor geometry, etc. For instance, mixed plasmas containing dichlorosilane, silane, or tetraethoxysilane (as Si precursor) and O_2 is used to deposit high quality silicon dioxide layers, where silane+O_2+Ar plasmas produce films containing minimal hydrogen impurities. Plasma-specific effects can be effectively used for the quasi-deterministic assembly of 0D, 1D, 2D and 3D nanostructures. For example, using SiH_4+N_2 or SiH_4+H_2 plasmas, amorphous and crystalline Si quantum dots (QDs) can be grown in an inorganic matrix at low-temperatures, with low power densities and a relatively high growth rate.

Plasma can be used to produce photoluminescent Si and Ge nanocrystals with clear facets and high degree of surface hydrogenation, where the non-equilibrium nature of plasmas promotes shape retention and fast recrystallisation of the grown nanostructures [128]. As nanocrystals are produced in the plasma bulk, they can be easily deposited onto a wide range of substrates, for example, pre-patterned glass substrates for light-emitting diodes. Distinct thermal and chemical

effects of low-temperature, non-equilibrium plasmas also enable fabrication and *in situ* functionalisation of nanoparticles in gas and liquid phases, where plasma serves as a catalyst driving the electrochemical reaction [129, 130]. For the growth of Si nanowires, plasma-enhanced environment, e.g. chemical vapour deposition (PECVD), is used to improve selectivity and reduce the temperature of fabrication. This enables deposition of thinner preferentially-ordered nanostructures that are more sparsely distributed across the surface of the substrate. Similarly, plasmas are well-suited for highly-controlled lower-temperature deposition of ultra-thin semiconducting layers, e.g. InGaCaGdN/GaN, InGaZnO, and diamond superlattice structures.

In non-thermal plasmas, the difference in the velocities between electrons and ions lead to the formation of a plasma sheath, a thin region near the surface of the substrate that separates this surface from the plasma bulk. The thickness of the sheath is dependent on plasma density, electron temperature and other factors, and can be used to control the deposition process. The sheath is the result of a large flux of highly mobile electrons arriving to the surface of the substrate well ahead of slower-travelling ions. To balance the negative charge on the substrate surface, a layer with a much higher density of ions (i.e., the sheath) is formed. As the electric field is at its highest value at the surface of the substrate, ionised atoms and molecules are electrostatically accelerated towards the surface as they traverse the sheath [131]. For material fabrication, it is important to balance the speed with which ions arrive at the surface, so as to maximise the speed of material formation yet minimise excessive ion bombardment which may cause formation of defects or etch the newly formed deposit. As such, electrons play a key role in the generation of radical species in the plasma bulk, within the sheath and on the substrate surface, whereas plasma-produced ions, atoms and radicals interact with the surface to induce heating, deposition, etching, recombination, and other processes.

5.2 Non-thermal plasma processing of polymers

Ionising radiation processing enables tailorable variations in the physical and chemical characteristics of polymeric materials. These variations can be induced in both the bulk volume of the materials or, as is most commonly encountered in plasma irradiation, at their surfaces.

Regardless of the species in question (ion, electron, high energy photon, etc.), ionising radiation predominantly induces two elementary processes within polymers, namely: bond scissioning, and bond formation. With respect to the first of these, the ionising particle supplies sufficient energy to induce a scission either along the main chain (e.g., C−C scission), or with side groups (e.g., C−H scission). Natural consequences of these scission events include a reduction in the molecular weight of the polymer, the production of free radicals within the polymer, and possibly the evolution of gases such as H_2, HCl, N_2 etc (depending upon side group species) [132].

Scissioning events are followed by recombination, leading to either unsaturated bond formation within a chain, or crosslinking between carbon atoms in adjacent chains. This crosslinking results in the formation of a three-dimensional network with an increase in the average molecular weight of the polymer. Polymers crosslinked in this manner also exhibit increased insolubility and reinforced dimensional stability in hostile environments [133]. In addition to these elementary processes, ionising radiation with ions is also prone to inducing lattice defects within crystalline materials, ion implantation, and etching of surface matter [134].

It bears mentioning that these elementary processes hold true at low temperatures and in the absence of oxygen. Outside of these conditions, additional avenues for energy conversion or dissipation (including molecular movement, the formation of oxidised species, or interactions with additives) serve to complicate the diversity of material responses to the applied radiation [132]. Such complications may be prevalent in DPF devices, where the plasma serves to expose the irradiated material to electrons with temperatures into the keV range and ions with energies into the MeV range [119].

6. Dense plasma focus as a radiation source

To better understand the potential for DPF in the processing of polymeric materials, the typical operation of the device is first be presented, along with a discussion of the components and properties of the plasma and ionising species formed by the device.
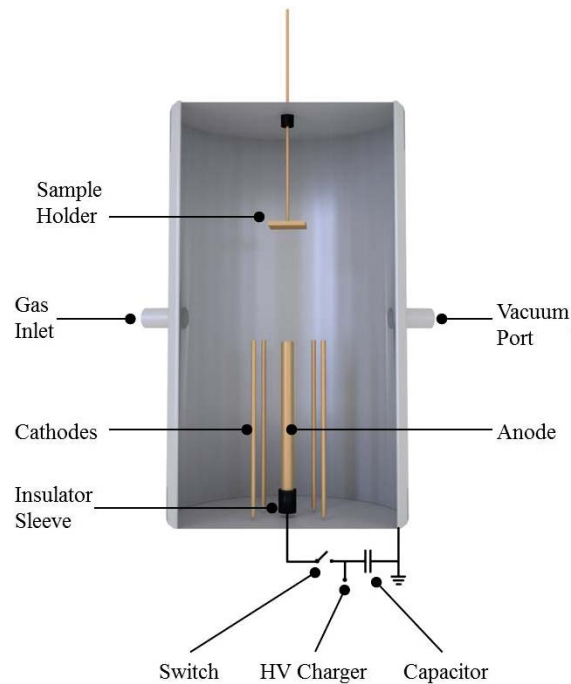
Figure 2. Typical dense plasma focus device configuration

The DPF device is typically arranged as shown in *Figure 2*. In brief, its general mode of operation involves the sample being mounted on the sample holder platform. The height of the sample holder platform is then adjusted to enable control over the total fluence received across the surface of the sample. The chamber is evacuated down to working pressure. If desired, a process gas is introduced to the chamber, and the chamber pressure is adjusted to facilitate optimum focussing action (typically between 0.5−10 mbar, depending on the gas used). The capacitor bank is charged to the desired voltage (typically between 10−30 kV). High-current short reaction time switches are triggered, allowing the energy stored within the capacitor bank to be transferred to the chamber electrodes, initiating the formation of a plasma sheath across the insulator sleeve, as illustrated in *Figure 3A*. The plasma sheath accelerates along the electrode assembly under the presence of a *J x B* force, as shown in *Figure 3B*. Once the plasma sheath reaches the end of the anode, it undergoes radial compression and collapses in on itself, thus forming the dense pinch plasma, as shown in *Figure 3C*. This pinch plasma persists for up to several tens of nanoseconds, until it is broken up by m = 0 and m = 1 instabilities. Following degradation of the pinch plasma the electrons contained within the pinch are accelerated towards the positively charged anode at relativistic energies (>100 keV). Concurrently, the

pinch plasma ions develop an ionisation wavefront, travelling at up to 120 cm/µs, which is subsequently projected towards the sample holder platform, as shown in *Figure 3D*.

In instances where it is advantageous to ensure that the sample is only treated with energetic electrons, it is alternatively possible to mount the sample beneath the hollowed-out anode. Additional modifications to the DPF's typical mode of operation include the use of masks, guards, and various filters to selectively control the spatial distribution, type, and energy of species arriving at the sample surface.
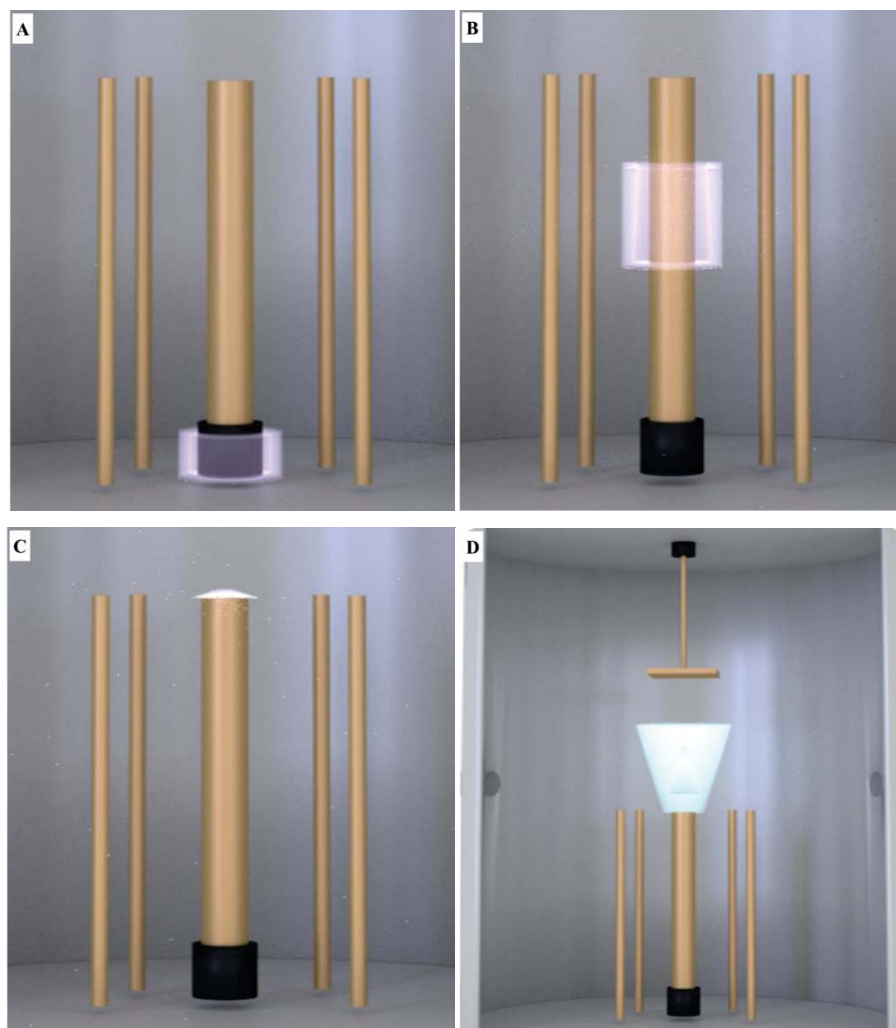

Figure 3. Evolution of the DPF operating phases: **(A)** initiation, **(B)** axial acceleration, **(C)** radial collapse, **(D)** pinch plasma destabilisation and subsequent irradiation

The DPF device generates a material processing environment that cannot be readily emulated by common forms of non-thermal plasma-enabled processing techniques. For instance, the instability-accelerated electrons operate at an energy regime on the order of tens to hundreds of keV [135, 136], whilst the accelerated ions have energies ranging from tens of keV to a few MeV [137, 138]. These energies, coupled with the transient nature of the plasma discharge (tens to a few hundreds of nanoseconds [139-141]), allow for rapid treatment and thermal annealing of target samples, and increased ion penetration and implantation depths within polymer films. In addition to ionising species common to non-thermal plasma such as electrons, ions, and energetic UV photons, DPF can also supply additional ionising species such as X-ray photons and neutrons [142]. Furthermore, despite the myriad of differing DPF device designs and dimensions, these devices all produce plasmas with comparable temperatures and densities within the focus volume (when properly configured) [143]. This uniformity across platforms enables a degree of reproducibility throughout research groups and DPF facilities that is difficult to recreate with non-thermal plasma processing techniques [144].

7. Dense plasma focus processing of polymeric materials

A concentrated collection of DPF papers relating to matters of import in the processing of polymeric materials for electronic applications are presented hereafter.

7.1 Polymeric photoresist lithography

Lithography is a key technique employed in the electronics industry to fabricate semiconductor devices. The technique utilises a mask with localised absorption regions to permit the patterned irradiation of the underlying material (typically a viscous polymer deposited over a silicon substrate). Depending upon the chemical composition of the resist, it may exhibit preferential crosslinking (for negative resists) or chain-scissioning (for positive resists) in response to this irradiation. Subsequent chemical solvent treatments can then be applied to remove the soluble (i.e., non-crosslinked) regions [145].

Optical processes presently dominate the lithography industry, though limitations relating to the techniques' resolution have led to sustained interest in developing

a number of supplementary or alternative processes, including ion beam [146], electron beam [147], extreme ultraviolet (EUV) [148] and X-ray lithography [145]. The viability of applying DPF as a source for the generation of several of these radiations in lithography has been successfully demonstrated in a number of studies that predominantly focus on the exposure of SU-8 polymeric photoresist [149].

Given the preference for extending pre-existing optical processes to operate at shorter wavelengths, a variety of admixtures of nitrogen, neon, argon, xenon, krypton, and lithium vapour have been employed in DPF to generate photon radiation with energies ranging from 10's eV to 10's keV (i.e., UV to hard X-rays) [150]. The characteristic line energies of these species (associated with de-excitation radiation) is also accompanied by Bremsstrahlung and recombination radiation, leading to a broadening of the radiation energies [151]. To compensate for this, DPF devices are commonly fitted with filters (e.g., beryllium, molybdenum, silver, etc.) to facilitate greater selectivity over the applied lithography wavelength [152-154].
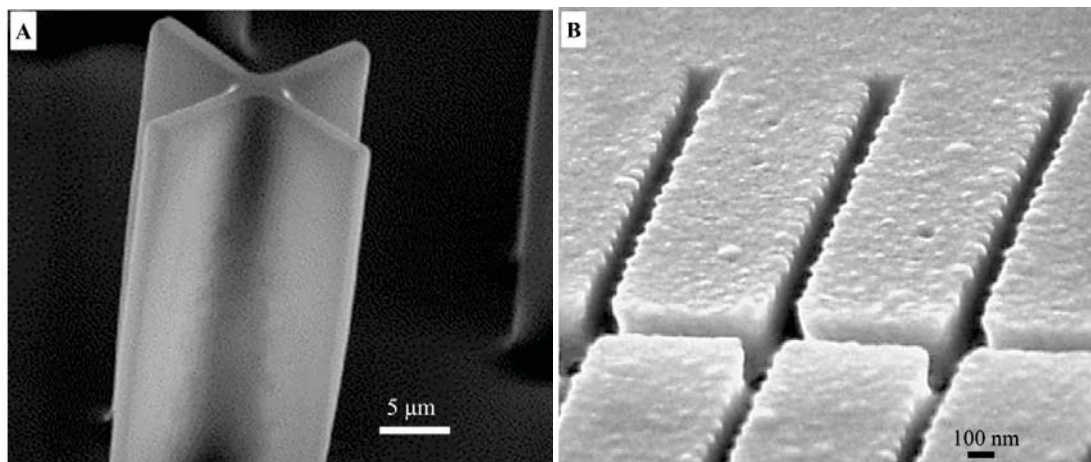
Figure 4. Early studies demonstrating DPF X-ray lithography of SU-8 photoresist, highlighting **(A)** the high aspect ratio of 20:1 on 25 μm thick resist [153], and **(B)** fine resolution that can be achieved following SU-8 exposure to 500 X-ray shots [155]

Relative to synchrotron and laser produced plasma, DPF shares a number of advantageous characteristics with other discharge produced plasmas (DPPs), including low cost, compact form factor, and ease of use [156, 157]. Efforts to enhance the durability and emission yield of DPF devices are ongoing [158, 159],

with the intent of realising the large-scale utility of DPF driven lithography (along with its accompanying excellent aspect ratios and fine feature resolutions, as evidenced in *Figure 4*).

7.2 Polymer synthesis

In addition to organic conducting and semiconducting materials, polymers are used extensively within the electronics industry for insulating layers, dielectrics, and device encapsulation. Traditionally radiation such as UV rays and non-thermal plasmas have been extensively employed in the synthesis of these polymeric materials to accomplish crosslinking and curing [160, 161].

One exemplar polymer, polyacrylic acid, finds utility in industrial applications [162], and has also been investigated for applications in gas detection [163], nanowire passivation [164], binding or adhesion promotion [165], and as a dopant in electrically conductive polymers [166]. Furthermore, when fabricated as a plasma polymer, polyacrylic acid has attracted attention for covalent immobilisation of biomolecules by virtue of its carboxyl functional groups [167, 168].

Whilst plasma synthesis techniques for polyacrylic acid have predominantly focussed on the application of cold plasma, in 2011 Alavi et al. [169] demonstrated for the first time the synthesis of polyacrylic acid with a DPF device. Using a 4.5 kJ Mather type DPF device powered by a 36 µF, 16 kV capacitor, the researchers in this study were able to fabricate plasma polymerised acrylic acid after 15 shots. The polymer was formed on a styrene-butadiene-rubber (SBR) substrate coated in a layer of acrylic acid in the presence of a nitrogen process gas. Following irradiation, the samples were rinsed with water to remove soluble residue, and the subsequent presence of the polymer was confirmed using ATR FTIR, with the spectra and associated peak assignment presented in *Figure 5* and Table 1, respectively.
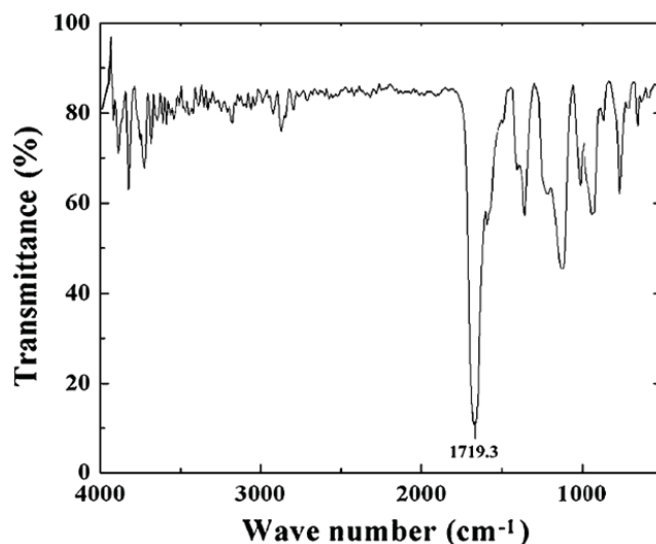
Figure 5. FTIR-ATR spectra of plasma-polymerised acrylic acid over SBR substrate

Table 1. Assignment of FTIR-ATR absorption bands (excluding SBR)

Type of vibration	Wave number (cm^{-1})
OH broad band	2,800–3,500
CH stretch band	2,800–3,000
C=O	1,695–1,725
OH deformation	910–950
C=C	1,617–1,634
CH_2 bending	1,430
C–O vibration	1,167–1,250
C–N stretch band	1,055–1,175

Beyond validating the viability of using high-temperature DPF to synthesise a polymer, the researchers were also able to demonstrate increased substrate adhesion following plasma treatment using 30 DPF shots, though increased copper sputtering (from the anode material) may partially mitigate the utility of this development. The findings presented here indicate that DPF is a viable technique for the synthesis of polyacrylic acid with carboxyl surface functionalities. This, in turn, suggests that DPF may be able to play a role in the development of common plasma polymerised acrylic acid applications, such as biofunctional surfaces, or

32

as adhesion-promoting layers in polymer-polymer and polymer-metal interfaces [170-172]. This research may also open up interesting avenues of future enquiry by prospectively coupling single-step polymer synthesis with DPF's other salient nanofabrication and modification applications (such as nano-structuring the bulk substrate, implanting nitrogen or carbon to form nitrides or carbides in metallic substrates, or depositing metallic thin films) [119].

7.3 Organic p-n junctions

A p–n junction is an interface between two types of semiconductor material, p-type and n-type, and is a critical element in the fabrication of diodes and transistor devices, enabling the subsequent development of LEDs, amplifiers, digital logic circuits, photovoltaics, processors, and a whole host of other microelectronic devices [173, 174]. In contrast to silicon based p−n junctions, in which impurity doping is used to produce n- and p-type regions within a single crystal [174], the vast majority of processes used to fabricate organic p-n junctions employ solution and thermal deposition techniques to produce defined interfaces consisting of one of a great many distinct n-type (electron transporting) and p-type (hole transporting) materials [175]. Such methods suffer from a number of limitations, including limited ambient environmental stability and the common inclusion of polar groups in organic n-type materials (leading to reduced solution processability) [176, 177].

Srivastava et al, has demonstrated diode like behaviour in polyaniline films subjected to DPF irradiation [178]. Polyaniline is a low cost intrinsically conducting polymer with attractive prospective applications in a number of fields, including tissue engineering [179], display devices [180, 181], and energy storage devices [182, 183].

The polyaniline employed in Srivastava's study was synthesised by chemical oxidation of aniline in aqueous acidic media using ammonium perdisulphate as the oxidant, resulting in p-type semiconducting films. These films were then subjected to argon ion irradiation in a 3.3 kJ Mather type DPF device powered by a 30 μF, 15 kV Maxwell capacitor. XPS analysis of these films indicated a reduction in the presence of nitrogen following argon irradiation treatment and this, coupled with an increase in crosslinking, is believed to be the primary factors

in developing the n-type nature of those portions of the polyaniline film exposed to the DPF radiation. In this manner, films were developed with p-n junctions that demonstrated diode like properties, as evidenced by the I-V measurement results presented in *Figure 6*. Furthermore, this doping was accomplished with no visible damage to the thin film when the sample was mounted at distances of 4 cm or greater from the DPF anode.
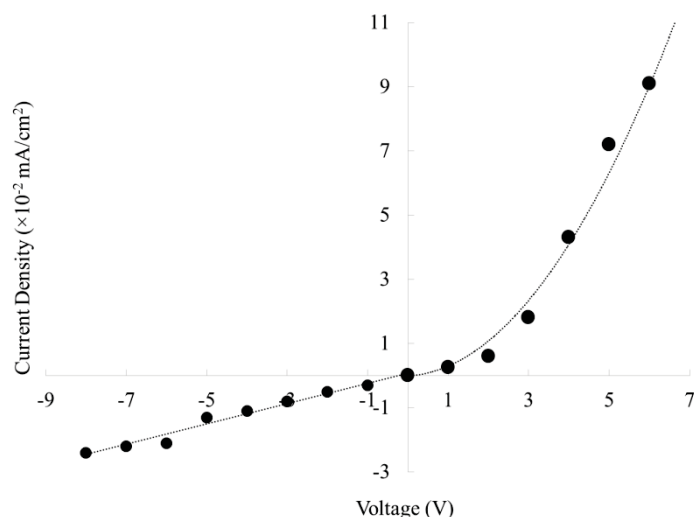
Figure 6. I−V characteristics of a junction formed on a single p-type doped polyaniline due to DPF argon ion irradiation [178]

The capacity to produce p-n junctions in polymeric films that have been cation doped chemically on one side and anion doped via DPF ion irradiation may suggest interesting applications in the development of organic electronic devices, specifically with respect to employing more traditional doping processes, as opposed to being constrained to synthesising devices using dissimilar n- and p-type polymers.

7.4 Conductive polymer nanowires

Conductive nanowires represent a field of one-dimensional (1D) materials that exhibit a number of novel properties by virtue of their high surface-to-volume ratio [184], and the increasing influence exerted by quantum effects at the scale in question [185]. These properties include significantly higher electron mobility and a capacity to suppress the absorption or emission of photons [184], and mark nanowires as attractive components for incorporation into a variety of nanoscale

electronic devices relating to biosensors [186, 187], photonics [188], and energy scavenging [189, 190].

Among candidate polymers, the environmental stability, conductivity, and high specific pseudocapacitance of polyaniline nanowires in particular make them especially promising for applications relating to supercapacitors and actuators (among others) [191, 192]. The vast majority of literature relating to the synthesis of polyaniline nanowires (and organic nanowires in general) has focussed on vapour deposition and solution-based methods [193]. Large scale fabrication of nanostructured polyaniline surfaces continues, however, to be hampered by the complexity of these methods, coupled with their long process times and small treatment areas. By using irradiation to circumvent these dominant synthesis techniques, Mohanty et al [194] was able to demonstrate a method for synthesising polyaniline nanowires via single-shot exposure to a pulsed electron beam generated by DPF.

In the study a 2.2 kJ Mather type DPF device powered by a 7.1 µF, 25 kV capacitor was used as the source for a pulsed electron beam. Irradiation was performed in a nitrogen atmosphere at 40 Pa, providing electrons with energies ranging from approximately 10 keV up to greater than 200 keV [195]. Following irradiation with a single shot, FESEM micrographs demonstrated the synthesis of polyaniline nanowires in less than 2 µs, with dimensions ranging from 50-80 nm in diameter and up to a few micrometers in length, as evidenced in *Figure 7*.
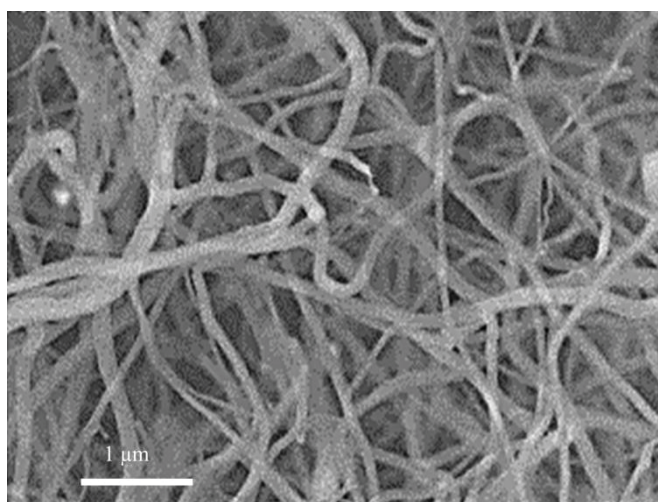

Figure 7. FESEM micrograph of self-organised nanowires grown on polyaniline films using DPF [194].

This physical approach to nanowire synthesis obviates the need for complex chemical processing techniques, and for certain template-based synthesis methods it mitigates complications associated with retaining nanowire integrity following removal of the template. The rapid in-situ formation of nanowires on whatever topography the polyaniline happens to possess may be coupled with masking techniques to spatially localise the synthesis, and subsequently eliminates the need to employ transfer processes to relocate the nanowires from their site of synthesis to their final locus. Taken in concert, these prominent features of DPF nanowire synthesis may serve to hasten the commercial production and uptake of electronic devices deploying nanowire components.

7.5 Modification of polymer surface chemistry and morphology

The physical and chemical characteristics of polymers are often modified to enhance their suitability for a wide variety of roles. With respect to polymers employed in the electronics domain, radiation-induced surface chemistry modification is often applied to increase the concentration of polar groups at surfaces, with the intention of enhancing the polymer's printability, wettability, adhesion, and compatibility [109]. Additional morphological variations following irradiation often include increased surface roughening coupled with a subsequent increase in surface area, resulting in further variations in the polymer's surface wettability and adhesion properties [196-198].
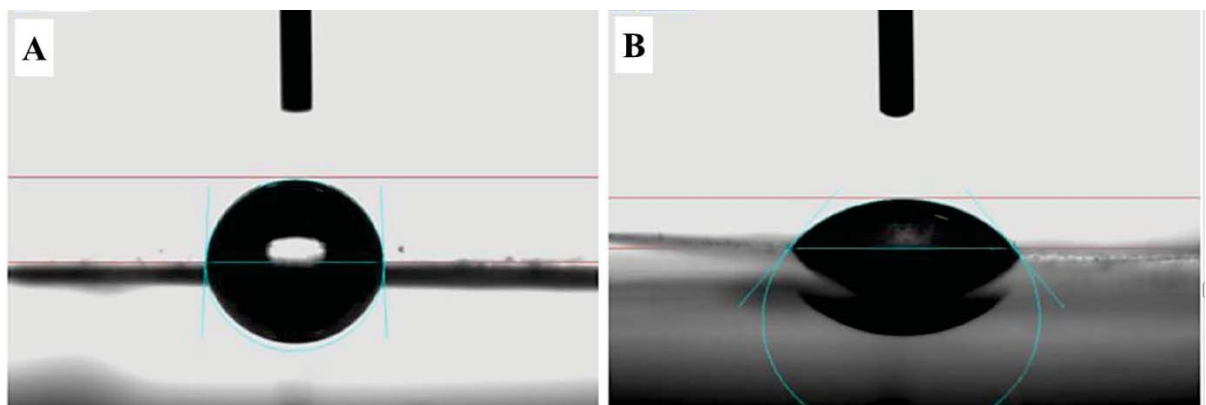

Figure 8. Water contact angle measurements for **(A)** pristine PET at 88º, **(B)** and PET following 10 shots of argon DPF at 51.2º [199]

In 2014 Habibi and Alavi employed a DPF device to modify the surface properties of polyethylene terephthalate (PET) [199]. PET is a commercially important

polymer employed in the fabrication of plastic bottles, packaging materials, textiles [200], and is attracting growing interest in the biomedical field [201, 202]. Furthermore, PET has been extensively used as a flexible substrate in electronics research [203-205]. Whilst its bulk properties make it an ideal candidate for utilisation in these fields, its surface properties (such as adhesion, wettability, and biocompatibility) may serve to limit its utility [206].

In the study a 4.5 kJ Mather-type DPF device operated at 12.5 kV and powered by a 40 µF capacitor was used to expose PET sheets to argon pulsed plasma at a working pressure of 3 mbar. Following irradiation via 10 shots at a distance of 10 cm from the central anode, water contact angle measurements (CAM) were carried out using the sessile drop method (Dataphysics OCA-20 device). CAM results revealed a reduction in contact angle from 88° ± 5° for pristine PET sheets to 51° ± 5° for PDF irradiated PET sheets, as evidenced in *Figure 8*.

As with other plasma processing techniques, the authors attributed the increase in hydrophilicty to an increase in the presence of oxygen functional groups via post-irradiation interactions between the carbon radicals at the PET surface and oxygen present within the atmosphere. It is also interesting to note that this increase in hydrophilicity was accomplished with a very short process time. Other forms of plasma discharges used to enhance PET hydrophilicity can require plasma exposure times ranging from 10s to 100s of seconds [206, 207]. In contrast, DPF was able to produce comparable variations in wettability after 10 shots, with an associated total plasma exposure time of ~ 10^{-6} s. In addition to the reduced exposure time, the energetic species generated by the DPF source are also liable to approach greater penetration depths than their non-thermal plasma counterparts, facilitating the modification of a greater volume of the polymer's properties.

8. Concluding comments

In this review we have demonstrated that irrespective of whether the electronics is based on inorganic materials or carbon-based precursors, its performance is directly linked to dimensions and properties of the nanostructures and the precision with which these nanostructures are organised and assembled [2]. Indeed, advancement and uptake of sustainable electronics, such as that based

on polymer materials, is inherently linked with the development of technologies that can enable fast, efficient, and highly controlled synthesis and organisation of polymers on a variety of surfaces.

The applications reviewed in this paper demonstrate that DPF is a viable tool for the synthesis, doping, surface modification, nanostructuring, and lithography of polymeric materials for electronics. Furthermore, these outputs can be achieved using a process which, in addition to sharing several traits with other (typically) non-thermal plasma techniques (e.g., dry, single-step processing requiring minimal substrate/material preparation), also exhibits a number of unique salient features. Included here are DPF's capacity to produce a wide variety of energetic species (e.g., hard X-rays, EUV, ions, electrons, and neutrons), selectivity over the irradiating species and energy (by modifying sample locus, process gas, filter material, etc.), and transient thermal effects coupled with an extremely short processing time.

DPF is a novel source of energetic radiation species, and fundamental investigations into the synthesis and modification of polymeric materials using varied DPF treatment regimens have the potential to play a leading role in the development of new electronic applications for polymers, and in the enhancement of the utility of polymers in existing applications. Furthermore, the aforementioned characteristics of DPF suggest that the technique is well positioned to deliver advances in organic electronics, bioelectronics, and micro/nano-scale technologies.

Acknowledgements

References

1. D. Vasileska, *Modeling thermal effects in nano-devices.* Microelectronic Engineering, 2013. 109(0).
2. T. Gao, et al., *Monodisperse Hollow Silica Nanospheres for Nano Insulation Materials: Synthesis, Characterization, and Life Cycle Assessment.* ACS Applied Materials & Interfaces, 2013. 5(3).

3.   T.G. Gutowski, et al., *Thermodynamic Analysis of Resources Used in Manufacturing Processes.* Environmental Science & Technology, 2009. 43(5).

4.   N. Krishnan, et al., *A Hybrid Life Cycle Inventory of Nano-Scale Semiconductor Manufacturing.* Environmental Science & Technology, 2008. 42(8).

5.   M. Woodhouse, et al., *Perspectives on the pathways for cadmium telluride photovoltaic module manufacturers to address expected increases in the price for tellurium.* Solar Energy Materials and Solar Cells, 2013. 115(0).

6.   C.F. Murphy, et al., *Development of Parametric Material, Energy, and Emission Inventories for Wafer Fabrication in the Semiconductor Industry.* Environmental Science & Technology, 2003. 37(23).

7.   M. Irimia-Vladu, *"Green" electronics: biodegradable and biocompatible materials and devices for sustainable future.* Chemical Society Reviews, 2014. 43(2).

8.   T. Sekitani, et al., *Flexible organic transistors and circuits with extreme bending stability.* Nat Mater, 2010. 9(12).

9.   H.T. Yi, et al., *Ultra-flexible solution-processed organic field-effect transistors.* Nat Commun, 2012. 3.

10.   M. Kaltenbrunner, et al., *Ultrathin and lightweight organic solar cells with high flexibility.* Nat Commun, 2012. 3.

11.   T.R. Andersen, et al., *Scalable, ambient atmosphere roll-to-roll manufacture of encapsulated large area, flexible organic tandem solar cell modules.* Energy & Environmental Science, 2014. 7(9).

12.   L.J. Dahlben, et al., *Environmental Life Cycle Assessment of a Carbon Nanotube-Enabled Semiconductor Device.* Environmental Science & Technology, 2013. 47(15).

13.   C. Wang, et al., *Carbon nanotube electronics - moving forward.* Chemical Society Reviews, 2013. 42(7).

14.   M.M. Shulaker, et al., *Carbon nanotube computer.* Nature, 2013. 501(7468).

15.   A. Thess, et al., *Crystalline Ropes of Metallic Carbon Nanotubes.* Science, 1996. 273(5274).

16. D.-m. Sun, et al., *Flexible high-performance carbon nanotube integrated circuits.* Nat Nano, 2011. 6(3).

17. S. Kim, et al., *Spin- and Spray-Deposited Single-Walled Carbon-Nanotube Electrodes for Organic Solar Cells.* Advanced Functional Materials, 2010. 20(14).

18. L. Ding, et al., *Selective Growth of Well-Aligned Semiconducting Single-Walled Carbon Nanotubes.* Nano Letters, 2009. 9(2).

19. N. Rouhi, D. Jain, and P.J. Burke, *High-Performance Semiconducting Nanotube Inks: Progress and Prospects.* ACS Nano, 2011. 5(11).

20. J.M. Lobez, et al., *Surface Selective One-Step Fabrication of Carbon Nanotube Thin Films with High Density.* ACS Nano, 2014. 8(5).

21. M.S. Arnold, et al., *Sorting carbon nanotubes by electronic structure using density differentiation.* Nat Nano, 2006. 1(1).

22. H. Liu, et al., *Large-scale single-chirality separation of single-wall carbon nanotubes by simple gel chromatography.* Nat Commun, 2011. 2.

23. M.C. LeMieux, et al., *Self-Sorted, Aligned Nanotube Networks for Thin-Film Transistors.* Science, 2008. 321(5885).

24. L.S. Liyanage, et al., *Wafer-Scale Fabrication and Characterization of Thin-Film Transistors with Polythiophene-Sorted Semiconducting Carbon Nanotube Networks.* ACS Nano, 2011. 6(1).

25. R. Krupke, et al., *Separation of Metallic from Semiconducting Single-Walled Carbon Nanotubes.* Science, 2003. 301(5631).

26. D.-M. Sun, et al., *A Review of Carbon Nanotube- and Graphene-Based Flexible Thin-Film Transistors.* Small, 2013. 9(8).

27. V. Coropceanu, et al., *Charge Transport in Organic Semiconductors.* Chemical Reviews, 2007. 107(4).

28. J.L. Brédas, et al., *Organic semiconductors: A theoretical characterization of the basic parameters governing charge transport.* Proceedings of the National Academy of Sciences, 2002. 99(9).

29. K. Kolata, et al., *Molecular Packing Determines Singlet Exciton Fission in Organic Semiconductors.* ACS Nano, 2014. 8(7).

30. G. Giri, et al., *Tuning charge transport in solution-sheared organic semiconductors using lattice strain.* Nature, 2011. 480(7378).

31.   E.A. Chandross, *Not-So-Sunny Outlook for Organic Photovoltaics.* Science, 2011. 333(6038).

32.   K. Nakayama, et al., *Patternable Solution-Crystallized Organic Transistors with High Charge Carrier Mobility.* Advanced Materials, 2011. 23(14).

33.   J. You, et al., *A polymer tandem solar cell with 10.6% power conversion efficiency.* Nat Commun, 2013. 4.

34.   G. Dennler, M.C. Scharber, and C.J. Brabec, *Polymer-Fullerene Bulk-Heterojunction Solar Cells.* Advanced Materials, 2009. 21(13).

35.   A. Anctil, et al., *Material and Energy Intensity of Fullerene Production.* Environmental Science & Technology, 2011. 45(6).

36.   S. Lizin, et al., *Life cycle analyses of organic photovoltaics: a review.* Energy & Environmental Science, 2013. 6(11).

37.   A. Anctil, et al., *Cumulative energy demand for small molecule and polymer photovoltaics.* Progress in Photovoltaics: Research and Applications, 2013. 21(7).

38.   G.D. Sharma, et al., *Efficient bulk heterojunction devices based on phenylenevinylene small molecule and perylene-pyrene bisimide.* Journal of Materials Chemistry, 2010. 20(3).

39.   A.M. Ballantyne, et al., *The Effect of Poly(3-hexylthiophene) Molecular Weight on Charge Transport and the Performance of Polymer:Fullerene Solar Cells.* Advanced Functional Materials, 2008. 18(16).

40.   J. Peet, A.J. Heeger, and G.C. Bazan, *"Plastic" Solar Cells: Self-Assembly of Bulk Heterojunction Nanomaterials by Spontaneous Phase Separation.* Accounts of Chemical Research, 2009. 42(11).

41.   J. Peet, et al., *Efficiency enhancement in low-bandgap polymer solar cells by processing with alkane dithiols.* Nat Mater, 2007. 6(7).

42.   K.R. Graham, et al., *Polydimethylsiloxane as a Macromolecular Additive for Enhanced Performance of Molecular Bulk Heterojunction Organic Solar Cells.* ACS Applied Materials & Interfaces, 2011. 3(4).

43.   D.J. Burke and D.J. Lipomi, *Green chemistry for organic solar cells.* Energy & Environmental Science, 2013. 6(7).

44.   J. Kim, et al., *Efficient small molecule organic semiconductor containing bis-dimethylfluorenyl amino benzo[b]thiophene for high open circuit*

voltage in high efficiency solution processed organic solar cell. RSC Advances, 2012. 2(7).

45. X. Shi, J. Chang, and C. Chi, *Solution-processable n-type and ambipolar semiconductors based on a fused cyclopentadithiophenebis(dicyanovinylene) core.* Chemical Communications, 2013. 49(64).

46. S. Nagamatsu, et al., *Long-Term Air-Stable n-Channel Organic Thin-Film Transistors Using 2,5-Difluoro-1,4-phenylene-bis{2-[4-(trifluoromethyl)phenyl]acrylonitrile}.* ACS Applied Materials & Interfaces, 2014. 6(6).

47. K. Sato, T. Ozu, and N. Takenaga, *Solvent-free synthesis of azulene derivatives via Passerini reaction by grinding.* Tetrahedron Letters, 2013. 54(7).

48. M.A. Pasha and B. Datta, *Mechanochemistry: An efficient method of solvent-free synthesis of 3-amino-2,4-dicarbonitrile-5-methylbiphenyls.* Journal of Saudi Chemical Society, 2014. 18(1).

49. A.F.M.M. Rahman, et al., *A Facile Solvent Free Claisen-Schmidt Reaction: Synthesis of α,α'-bis-(Substituted-benzylidene)cycloalkanones and α,α'-bis-(Substituted-alkylidene)cycloalkanones.* Molecules, 2012. 17(1): p. 571.

50. A.K. Singh and L.D.S. Yadav, *Rapid Synthesis of Benzodiazepines by Ring Expansion of Aziridines with Anthranilic Acids by Using a Grinding Technique.* Synthesis, 2012. 2012(04): p. 591.

51. S. Kumar, et al., *An efficient, catalyst- and solvent-free, four-component, and one-pot synthesis of polyhydroquinolines on grinding.* Tetrahedron, 2008. 64(3).

52. Y. Gao, et al., *Fabrication of both the photoactive layer and the electrode by electrochemical assembly: towards a fully solution-processable device.* Chemical Communications, 2014. 50(72).

53. R.D. Deegan, et al., *Capillary flow as the cause of ring stains from dried liquid drops.* Nature, 1997. 389(6653).

54. K. Fukuda, et al., *Fully Solution-Processed Flexible Organic Thin Film Transistor Arrays with High Mobility and Exceptional Uniformity.* Sci. Rep., 2014. 4.

55. J. Ahmad, et al., *Materials and methods for encapsulation of OPV: A review.* Renewable and Sustainable Energy Reviews, 2013. 27.

56. S.-Y. Min, et al., *Large-scale organic nanowire lithography and electronics.* Nat Commun, 2013. 4.

57. J.-H. Choi, et al., *Enhancement of organic solar cell efficiency by patterning the PEDOT:PSS hole transport layer using nanoimprint lithography.* Organic Electronics, 2013. 14(12).

58. A. Teichler, J. Perelaer, and U.S. Schubert, *Inkjet printing of organic electronics - comparison of deposition techniques and state-of-the-art developments.* Journal of Materials Chemistry C, 2013. 1(10).

59. S.J. Kang, et al., *High-performance electronics using dense, perfectly aligned arrays of single-walled carbon nanotubes.* Nat Nano, 2007. 2(4).

60. D. Ji, et al., *Large scale, flexible organic transistor arrays and circuits based on polyimide materials.* Organic Electronics, 2013. 14(10).

61. C.J. Brabec, et al., *Polymer–Fullerene Bulk-Heterojunction Solar Cells.* Advanced Materials, 2010. 22(34).

62. B. Walker, C. Kim, and T.-Q. Nguyen, *Small Molecule Solution-Processed Bulk Heterojunction Solar Cells†.* Chemistry of Materials, 2010. 23(3).

63. I. Burgués-Ceballos, et al., *Solubility Based Identification of Green Solvents for Small Molecule Organic Solar Cells.* Advanced Functional Materials, 2014. 24(10).

64. F. Machui, et al., *Determination of the P3HT:PCBM solubility parameters via a binary solvent gradient method: Impact of solubility on the photovoltaic performance.* Solar Energy Materials and Solar Cells, 2012. 100(0).

65. K. Tada, *Yet another poor man's green bulk heterojunction photocells: Annealing effect and film composition dependence of photovoltaic devices using poly(3-hexylthiophene):C70 composites prepared with chlorine-free solvent.* Solar Energy Materials and Solar Cells, 2013. 108(0).

66. C.-D. Park, et al., *High performance bulk-heterojunction organic solar cells fabricated with non-halogenated solvent processing.* Organic Electronics, 2011. 12(9).

67. T. Earmme and S.A. Jenekhe, *High-performance multilayered phosphorescent OLEDs by solution-processed commercial electron-transport materials.* Journal of Materials Chemistry, 2012. 22(11).

68. F. Huang, et al., *High-Efficiency, Environment-Friendly Electroluminescent Polymers with Stable High Work Function Metal as a Cathode: Green- and Yellow-Emitting Conjugated Polyfluorene Polyelectrolytes and Their Neutral Precursors.* Journal of the American Chemical Society, 2004. 126(31).

69. S. Sax, et al., *Efficient Blue-Light-Emitting Polymer Heterostructure Devices: The Fabrication of Multilayer Structures from Orthogonal Solvents.* Advanced Materials, 2010. 22(18).

70. H. Wu, et al., *Efficient Electron Injection from a Bilayer Cathode Consisting of Aluminum and Alcohol-/Water-Soluble Conjugated Polymers.* Advanced Materials, 2004. 16(20).

71. S. Sax, et al., *Intrinsic electrochemical doping in blue light emitting polymer devices utilizing a water soluble anionic conjugated polymer.* Organic Electronics, 2007. 8(6).

72. W. Jiang, et al., *Alcohol-Soluble Electron-Transport Small Molecule for Fully Solution-Processed Multilayer White Electrophosphorescent Devices.* Organic Letters, 2014. 16(4).

73. S.H. Jin, et al., *Solution-processed single-walled carbon nanotube field effect transistors and bootstrapped inverters for disintegratable, transient electronics.* Applied Physics Letters, 2014. 105(1).

74. X. Wang, et al., *Transparent Carbon Films as Electrodes in Organic Solar Cells.* Angewandte Chemie International Edition, 2008. 47(16).

75. G.J. Horbach, et al., *The Safety of Nanomaterials: Translation from Academic Research to Industrial and Regulatory Applications.* Journal of Translational Toxicology, 2014. 1(1).

76. W.-K. Oh, et al., *Shape-Dependent Cytotoxicity and Proinflammatory Response of Poly(3,4-ethylenedioxythiophene) Nanomaterials.* Small, 2010. 6(7).

77. M.P. Monopoli, et al., *Biomolecular coronas provide the biological identity of nanosized materials.* Nature Nanotechnology, 2012. 7(12).

78. S. Lanone, et al., *Determinants of carbon nanotube toxicity.* Advanced Drug Delivery Reviews, 2013. 65(15).

79. K. Bhattacharya, et al., *Mechanisms of carbon nanotube-induced toxicity: Focus on pulmonary inflammation.* Advanced Drug Delivery Reviews, 2013. 65(15).

80. Y.-S. Zimmermann, et al., *Organic photovoltaics: Potential fate and effects in the environment.* Environment International, 2012. 49(0).

81. K. Nagano, et al., *Two- and 13-week Inhalation Toxicities of Indium-tin Oxide and Indium Oxide in Rats.* Journal of Occupational Health, 2011. 53(2).

82. K. Nagano, et al., *Inhalation Carcinogenicity and Chronic Toxicity of Indium-tin Oxide in Rats and Mice.* Journal of Occupational Health, 2011. 53(3).

83. A. Tanaka, et al., *Pulmonary Toxicity of Indium-Tin Oxide and Indium Phosphide after Intratracheal Instillations into the Lung of Hamsters.* Journal of Occupational Health, 2002. 44(2).

84. S. Homma, et al., *Pulmonary fibrosis in an individual occupationally exposed to inhaled indium-tin oxide.* European Respiratory Journal, 2005. 25(1).

85. T. Hamaguchi, et al., *Exposure to hardly soluble indium compounds in ITO production and recycling plants is a new risk for interstitial lung damage.* Occupational and Environmental Medicine, 2008. 65(1).

86. T. Chonan, O. Taguchi, and K. Omae, *Interstitial pulmonary disorders in indium-processing workers.* European Respiratory Journal, 2007. 29(2).

87. D. Lison, et al., *Sintered Indium-Tin-Oxide (ITO) Particles: A New Pneumotoxic Entity.* Toxicological Sciences, 2009. 108(2).

88. W.M. Gwinn, et al., *Macrophage Solubilization and Cytotoxicity of Indium-Containing Particles In Vitro.* Toxicological Sciences, 2013. 135(2).

89. K. Donaldson, et al., *Pulmonary toxicity of carbon nanotubes and asbestos — Similarities and differences.* Advanced Drug Delivery Reviews, 2013. 65(15).

90. K. Donaldson, et al., *Carbon nanotubes: A review of their properties in relation to pulmonary toxicology and workplace safety.* Toxicological Sciences, 2006. 92(1).

91. C.A. Poland, et al., *Carbon nanotubes introduced into the abdominal cavity of mice show asbestos-like pathogenicity in a pilot study.* Nature Nanotechnology, 2008. 3(7).

92. R.A.J. Janssen and J. Nelson, *Factors Limiting Device Efficiency in Organic Photovoltaics.* Advanced Materials, 2013. 25(13).

93. M. Jørgensen, et al., *Stability of Polymer Solar Cells.* Advanced Materials, 2012. 24(5).

94. F. Ante, et al., *Contact Resistance and Megahertz Operation of Aggressively Scaled Organic Transistors.* Small, 2012. 8(1).

95. F.C. Krebs, *Air stable polymer photovoltaics based on a process free from vacuum steps and fullerenes.* Solar Energy Materials and Solar Cells, 2008. 92(7).

96. R.B. Ross, et al., *Endohedral fullerenes for organic photovoltaic devices.* Nat Mater, 2009. 8(3).

97. K. Bazaka and M.V. Jacob, *Implantable devices: issues and challenges.* Electronics, 2012. 2(1).

98. K. Bazaka, M.V. Jacob, and B.F. Bowden, *Optical and chemical properties of polyterpenol thin films deposited via plasma-enhanced chemical vapor deposition.* Journal of Materials Research, 2011. 26(08).

99. M.V. Jacob, et al., *Electron-blocking hole-transport polyterpenol thin films.* Chemical Physics Letters, 2012. 528.

100. M.V. Jacob, et al., *Plasma polymerised thin films for flexible electronic applications.* Thin Solid Films, 2013. 546.

101. D. Taguchi, et al., *Analyzing hysteresis behavior of capacitance–voltage characteristics of IZO/C 60/pentacene/Au diodes with a hole-transport electron-blocking polyterpenol layer by electric-field-induced optical second-harmonic generation measurement.* Chemical Physics Letters, 2013. 572.

102. J. Ahmad, K. Bazaka, and M.V. Jacob, *Optical and surface characterization of radio frequency plasma polymerized 1-isopropyl-4-methyl-1, 4-cyclohexadiene thin films.* Electronics, 2014. 3(2).

103. K. Bazaka, et al., *Investigation of interfacial charging and discharging in double-layer pentacene-based metal-insulator-metal device with*

polyterpenol blocking layer using electric field induced second harmonic generation. Chemical Physics Letters, 2011. 503(1).

104. K. Bazaka and M. Jacob, *Synthesis of radio frequency plasma polymerized non-synthetic Terpinen-4-ol thin films.* Materials Letters, 2009. 63(18).

105. M.V. Jacob, et al., *Fabrication and characterization of polyterpenol as an insulating layer and incorporated organic field effect transistor.* Thin Solid Films, 2010. 518(21).

106. K. Bazaka, et al., *Plasma-assisted surface modification of organic biopolymers to prevent bacterial attachment.* Acta biomaterialia, 2011. 7(5).

107. K. Bazaka, et al., *Plasma-enhanced synthesis of bioactive polymeric coatings from monoterpene alcohols: a combined experimental and theoretical study.* Biomacromolecules, 2010. 11(8).

108. K. Bazaka, et al., *Efficient surface modification of biomaterial to prevent biofilm formation and the attachment of microorganisms.* Applied microbiology and biotechnology, 2012. 95(2).

109. R.L. Clough, *High-energy radiation and polymers: a review of commercial processes and emerging applications.* Nuclear Instruments and Methods in Physics Research Section B, 2001. 185: p. 8.

110. J.W. Mather, *Investigation of the high-energy acceleration mode in the coaxial gun.* Physics of Fluids Supplement, 1964. 7(11): p. 28.

111. T.I.F. N.V. Fillipov, V.P. Vinogradov, *Dense high-temperature plasma in a non-cylindrical Z-pinch compression.* Nuclear Fusion Supplement, 1962. 2: p. 577.

112. H.C. P. Cloth, *Neutronics of a Dense Plasma Focus - An Investigation of a Fusion Plasma.* Nuclear Science and Engineering, 1977. 62(4): p. 591.

113. G.G.L. B. Brunelli, ed. *Unconventional Approaches to Fusion.* Ettore Majorana International Science Series, ed. A. Zichichi. 1982, Plenum Press: New York and London.

114. A.P. D. Wong, T.L. Tan, R.S. Rawat, P. Lee, *Soft X-ray Optimization Studies on a Dense Plasma Focus Device Operated in Neon and Argon in Repetitive Mode.* IEEE Transactions on Plasma Science, 2004. 32(6): p. 2227.

115. R.S.R. R. Verma, P. Lee, M. Krishnan, S.V. Springham, T.L. Tan, *Miniature plasma focus device as a compact hard x-ray source for fast radiography applications.* IEEE Transactions on Plasma Science, 2010. 38(4): p. 652.

116. E.V.D. V.N. Pimenov, L.I. Ivanov, S.A. Maslyaev, V.A. Gribkov, R. Miklaszewski, M. Scholz, A.V. Dubrovsky, I.V. Volobuev, Yu.E. Ugaste, F. Mezzetti, P. De Chiara, L. Pizzo, B. Kolman, A. Szydlowski, *Damage of structure materials for fusion devices under pulsed ion and high temperature plasma beams.* Journal of Nuclear Materials, 2002. 307-311: p. 95.

117. R.S.R. E. Ghareshabani, R. Verma, S. Karamat, S. Sobhanian, *Low energy repetitive miniature plasma focus device as high deposition rate facility for synthesis of DLC thin films.* Applied Surface Science, 2010. 256: p. 4977.

118. M.S. S. Zeb, A. Qayyum, G. Murtaza, M. Zakaullah, *Deposition of diamond-like carbon film using dense plasma focus.* Materials Chemistry and Physics, 2007. 103: p. 235.

119. R.S. Rawat, *High-Energy-Density Pinch Plasma: A Unique Nonconventional Tool for Plasma Nanotechnology.* IEEE Transactions on Plasma Science, 2013. 41: p. 701.

120. A. Zeniou, et al., *Ultra-high aspect ratio Si nanowires fabricated with plasma etching: plasma processing, mechanical stability analysis against adhesion and capillary forces and oleophobicity.* Nanotechnology, 2014. 25(3).

121. L. Zuwei, et al., *Low-temperature plasma etching of high aspect-ratio densely packed 15 to sub-10 nm silicon features derived from PS-PDMS block copolymer patterns.* Nanotechnology, 2014. 25(28).

122. Y. Chen, et al., *Ultrahigh Throughput Silicon Nanomanufacturing by Simultaneous Reactive Ion Synthesis and Etching.* ACS Nano, 2011. 5(10).

123. R. Di Mundo, et al., *On the "Growth" of Nano-Structures on c-Silicon via Self-Masked Plasma Etching Processes.* Plasma Processes and Polymers, 2013. 10(10).

124. Y. Song, et al., *Antireflective grassy surface on glass substrates with self-masked dry etching.* Nanoscale Research Letters, 2013. 8(1).

125. C.-H. Hsu, et al., *Generally Applicable Self-Masked Dry Etching Technique for Nanotip Array Fabrication.* Nano Letters, 2004. 4(3).

126. D. Ke, et al., *Fabrication of polymer nanowires via maskless O 2 plasma etching.* Nanotechnology, 2014. 25(16).

127. M.V. Jacob, et al., *Catalyst-free plasma enhanced growth of graphene from sustainable sources.* Nano letters, 2015. 15(9).

128. R.J. Anthony, et al., *An All-Gas-Phase Approach for the Fabrication of Silicon Nanocrystal Light-Emitting Devices.* Nano Letters, 2012. 12(6).

129. X.Z. Huang, et al., *Plasmonic Ag nanoparticles via environment-benign atmospheric microplasma electrochemistry.* Nanotechnology, 2013. 24(9).

130. D. Mariotti, et al., *Silicon Nanocrystals in Liquid Media: Optical Properties and Surface Stabilization by Microplasma-Induced Non-Equilibrium Liquid Chemistry.* Advanced Functional Materials, 2012. 22(5).

131. Q. Wang, et al., *Low-temperature plasma synthesis of carbon nanotubes and graphene based materials and their fuel cell applications.* Chemical Society Reviews, 2013. 42(23).

132. J. Davenas, et al., *Stability of polymers under ionising radiation: The many faces of radiation interactions with polymers.* Nuclear Instruments and Methods in Physics Research Section B, 2002. 191(1): p. 653.

133. S. Rouif, *Radiation cross-linked polymers: Recent developments and new applications.* Nuclear Instruments and Methods in Physics Research Section B, 2005. 236: p. 68.

134. S.A. Mehboob Sadiq, Muhammad Shafiq, Muhammad Zakaullah, *Enhanced Crystallinity of PTFE by Ion Irradiation in a Dense Plasma Focus.* Plasma Processes and Polymers, 2007. 4: p. 186.

135. J.L. T. Zhang, A. Patran, D. Wong, S.M. Hassan, S. Mahmood, T. White, T.L. Tan, S.V. Springham, S. Lee, P. Lee, R.S. Rawat, *Optimization of a plasma focus device as an electron beam source for thin film deposition.* Plasma Sources Science and Technology, 2007. 16(2): p. 250.

136. C.D. P. Choi, H. Herold, C.S. Wong, *Characterization of self-generated intense electron beams in a plasma focus.* Laser Particle Beams, 1990. 8(3): p. 469.

137. S.R.M. H. Bhuyan, T.K. Borathakur, R.S. Rawat, *Analysis of nitrogen ion beam produced in dense plasma focus device using faraday cup.* Indian Journal of Pure and Applied Physics, 2001. 39: p. 698.

138. S.V.S. M.V. Roshan, A. Talebitaher, R.S. Rawat, P. Lee, *Magnetic spectrometry of high energy deuteron beams from pulsed plasma system.* Plasma physics and controlled fusion, 2010. 52(8): p. 085007.

139. N.K.N. S.R. Mohanty, H. Bhuyan, R.K. Rout, R. S. Rawat, P. Lee, *Effect of anode designs on ion emission characteristics of a plasma focus device.* Japanese Journal of Applied Physics, 2007. 46(5A): p. 3039.

140. L.C.T. A. Patran, D. Stoenescu, M.S. Rafique, R.S. Rawat, S.V. Springham, T.L. Tan, P.Lee, M. Zakaullah, S. Lee, *Spectral study of the electron beam emitted from a 3 kJ plasma focus.* Plasma Sources Science and Technology, 2005. 14(3): p. 549.

141. A.L. H. Kelly, A. Marquez, M.J. Sadowski, J. Baranowski, E. Skladnik-Sadowska, *Analysis of the nitrogen ion beam generated in a low-energy plasma focus device by a Faraday cup operating in the secondary electron emission mode.* IEEE Transactions on Plasma Science, 1998. 26(1): p. 113.

142. A.V.N. V.P. Vinogradov, V.I. Krauz, G.E. Remnev, Yu. V. Vinogradova, G.G. Kanaev, K.N. Mitrofanov, V.V. Myalton, *Development and study of a portable plasma focus neutron source.* Plasma Physics Reports, 2014. 40(2): p. 146.

143. M. Krishnan, *The Dense Plasma Focus: A Versatile Dense Pinch for Diverse Applications.* IEEE Transactions on Plasma Science, 2012. 40(12): p. 3189.

144. J.D. Whittle, et al., *Variability in Plasma Polymerization Processes - An International Round-Robin Study.* Plasma Processes and Polymers, 2013. 10: p. 767.

145. J.R. Maldonado and M. Peckerar, *X-ray lithography: Some history, current status and future prospects.* Microelectronic Engineering, 2016. 161: p. 87.

146. J.E.E. Baglin, *Ion beam nanoscale fabrication and lithography - A review.* Applied Surface Science, 2011. 258: p. 4103.

147. Y. Chen, *Nanofabrication by electron beam lithography and its applications: A review.* Microelectronic Engineering, 2015. 135: p. 57.

148. T. Itani, *Recent status and future direction of EUV resist technology.* Microelectronic Engineering, 2009. 86: p. 207.

149. P. Lee, et al., *Electron lithography using a compact plasma focus.* Plasma Sources Science and Technology, 1997. 6(3): p. 343.

150. W.N. Partlo, et al. *Development of an EUV (13.5 nm) light source employing a dense plasma focus in lithium vapor.* in *Proceedings of SPIE - The International Society for Optical Engineering.* 2000.

151. M. Akel, *Soft X-ray Emission Optimization Studies with Krypton and Xenon Gases in Plasma Focus Using Lee Model.* Journal of Fusion Energy, 2013. 32: p. 523.

152. R. Petr, et al., *Performance summary on a high power dense plasma focus x-ray lithography point source producing 70 nm line features in AlGaAs microcircuits.* Review of Scientific Instruments, 2004. 75(8): p. 2551.

153. T.L. Tan, et al., *Characterization of chemically amplified resist for X-ray lithography by Fourier transform infrared spectroscopy.* Thin Solid Films, 2005. 504: p. 113.

154. F.N. Beg, et al., *Study of x-ray emission from a table top plasma focus and its application as an x-ray backlighter.* Journal of Applied Physics, 2000. 88(6): p. 3225.

155. M.A.O. Vladimir A. Gribkov, *On various possibilities in pulsed radiation biochemistry and chemistry.* Radiation and Environmental Physics, 2004. 43: p. 303.

156. S.R. Mohanty, et al., *Miniature hybrid plasma focus extreme ultraviolet source driven by 10 kA fast current pulse.* Review of Scientific Instruments, 2006. 77: p. 043506.

157. S.M.P. Kalaiselvi, et al., *Optimization of neon soft X-rays emission from 200 J fast miniature dense plasma focus device: A potential source for soft X-ray lithography.* Physics Letters A, 2013. 377: p. 1290.

158. T. Sodekoda, et al. *Repetitive operation of counter-facing plasma focus device: Toward a practical light source for EUV lithography.* in *Extreme Ultraviolet (EUV) Lithography V.* 2014. San Jose, California, United States.

159. M. Zakaullah, et al., *Characteristics of x-rays from a plasma focus operated with neon gas.* Plasma Sources Science and Technology, 2002. 11(4): p. 377.

160. V. Shukla, et al., *Review of basic chemistry of UV-curing technology.* Pigment and Resin Technology, 2004. 33(5): p. 272.

161. K. Bazaka, M.V. Jacob, and K. Ostrikov, *Sustainable Life Cycles of Natural-Precursor-Derived Nanocarbons.* Chemical reviews, 2015. 116(1).

162. F.L. Buchholz, *Polyacrylamides and Poly(Acrylic Acid).* Wiley-VCH Verlag GmbH & Co. KGaA: Weinheim, Germany, 2012. 28.

163. U.W. A. Oprea, *High sensitivity polyacrylic acid films for ammonia detection with field effect devices.* Sensors and Actuators B: Chemical, 2005. 111-112: p. 572.

164. K. Rasool, M.A. Rafiq, and Z.A.K. Durrani, *Tailoring transport and dielectric properties by surface passivation of silicon nanowires with Polyacrylic acid/TiO2 nanoparticles composite.* Microelectronic Engineering, 2014. 119: p. 141.

165. Y.L. Z.P. Cai, W.S. Li, L.D. Xing, Y.H. Liao, *Preparation and performances of LiFePO4 cathode in acqueous solvent with polyacrylic acid as binder.* Journal of Power Sources, 2009. 189(1): p. 547.

166. C.Y.T. X. Lu, J. Xu, C. He, *Thermal degradation of electrical conductivity of polyacrylic acid doped polyaniline: effect of molecular weight of the dopants.* Synthetic Metals, 2003. 138(3): p. 429.

167. N.A.B. J.D. Whittle, R.D. Short, C.W.I. Douglas, A.P. Hollander, J. Davies, *Adsorption of vitronectic, collagen and immunoglobulin-G to plasma polymer surfaces by enzyme linked immunosorbent assay (ELISA).* Journal of Materials Chemistry, 2002. 12: p. 2726.

168. C.P. B. Gupta, I. Bisson, P. Frey, J. Hilborn, *Plasma-induced graft polymerization of acryclic acid onto poly(ethylene terephthalate) films: characterization and human smooth muscle cell growth on grafted films.* Biomaterials, 2002. 23(3): p. 863.

169. M.H. M.H.S. Alavi, R. Amrollahi, F. Afshar Taromi, *A Study on Plasma Polymerization of Acrylic Acid Using APF Plasma Focus Device.* Journal of Fusion Energy, 2011. 30: p. 184.

170. U.V. V. Sciarratta, D. Hegemann, M. Muller, C. Oehr, *Plasma functionalization of polypropylene with acrylic acid.* Surface and Coatings Technology, 2003. 174-175: p. 805.

171. N.M. I.L.J. Dogue, *Improvement of polypropylene film adhesion in multilayers by various chemical surface modifications.* International Journal of Adhesion and Adhesives, 1995. 15(4): p. 205.

172. E.K. Dirk Hegemann, Sebastien Guimond, *Plasma Polymerization of Acrylic Acid Revisited.* Plasma Processes and Polymers, 2009. 6: p. 246.

173. C. Reese, et al., *Organic thin film transistors.* Materials Today, 2004(September): p. 20.

174. M. Grundmann, *The Physics of Semiconductors.* 2nd ed. 2010, Berlin: Springer.

175. C. Wang, et al., *Semiconducting Pi-Conjugated Systems in Field-Effect Transistors: A Material Odyssey of Organic Electronics.* Chemical Reviews, 2011. 112: p. 2208.

176. X. Zhao and X. Zhan, *Electron transporting semiconducting polymers in organic electronics.* Chemical Society Reviews, 2011. 40(7): p. 3728.

177. X. Gao and Y. Hu, *Development of n-type organic semiconductors for thin film transistors: a viewpoint of molecular design.* Journal of Materials Chemistry C, 2014. 2: p. 3099.

178. S.R.M. M.P. Srivastava, S. Annapoorni, R.S. Rawat, *Diode like behaviour of an ion irradiated polyaniline film.* Physics letters A, 1996. 215: p. 63.

179. R.R. Taimoor H. Qazi, Aldo R. Boccaccini, *Tissue engineering of electrically responsive tissues using polyaniline based polymers: A review.* Biomaterials, 2014. 35: p. 9068.

180. L.Z. Lu Zhao, Yuxi Xu, Tengfei Qiu, Linjie Zhi, Gaoquan Shi, *Polyaniline electrochromic devices with transparent graphene electrodes.* Electrochimica Acta, 2009. 55: p. 491.

181. G.N. Anna De Girolamo Del Mauro, Valentina Bizzarro, Immacolata Angelica Grimaldi, Fulvia Villani, Carla Minarini, *Analysis of the Performances of Organic Light-Emitting Devices with a Doped or an Undoped Polyaniline-Poly(4-styrenesulfonate) Hole-Injection Layer.* Journal of Applied Polymer Science, 2011. 122: p. 3618.

182. Y.Z. Yao Liu, Shiming Zhang, Junxi Zhang, Ping Ren, Chao Qian, *Amorphous iron phosphate/carbonized polyaniline nanorods composite as cathode material in sodium-ion batteries.* Journal of Solid State Electrochemistry, 2016. 20(2): p. 479.

183. M.R. Xiaogang Li, Weishan Li, *Sulfur encapsulated in porous carbon nanospheres and coated with conductive polyaniline as cathode of lithium-sulfur battery.* Journal of Solid State Electrochemistry, 2016. 20(1): p. 153.

184. L. Garwin and P. Ball, *Science at the Atomic Scale.* Nature 1992. 355(6363): p. 761.

185. A.P. Alivisatos, *Semiconductor Clusters, Nanocrystals, and Quantum Dots.* Science, 1996. 271: p. 933.

186. F. Patolsky, G. Zheng, and C.M. Lieber, *Nanowire-Based Biosensors.* Analytical Chemistry, 2006. 78: p. 4260.

187. F. Patolsky and C.M. Lieber, *Nanowire nanosensors.* Materials Today, 2005. 8(4): p. 20.

188. P.J. Pauzauskie and P. Yang, *Nanowire photonics.* Materials Today, 2006. 9(10): p. 36.

189. J. Chang, et al., *Piezoelectric nanofibers for energy scavenging applications.* Nano Energy, 2012. 1(3): p. 356.

190. S. Xu, et al., *Self-powered nanowire devices.* Nature Nanotechnology, 2010. 5: p. 366.

191. K. Wang, J. Huang, and Z. Wei, *Conducting Polyaniline Nanowire Arrays for High Performance Supercapacitors.* Journal of Physical Chemistry C, 2010. 114: p. 8062.

192. C. Zhang, et al., *Synthesis and applications of organic nanorods, nanowires and nanotubes.* Annual Reports on the Progress of Chemistry. Section C. Physical Chemistry, 2013. 109: p. 211.

193. S.-Y. Min, et al., *Organic Nanowire Fabrication and Device Applications.* Small, 2015. 11(1): p. 45.

194. N.K.N. S.R. Mohanty, R.S. Rawat, P. Lee, B.B. Nayak, B.S. Acharya, *Self-organized transformation to polyaniline nanowires by pulsed energetic electron irradiation in a plasma focus device.* Physics Letters A, 2009. 373: p. 1962.

195. S.R.M. N.K. Neog, *Study on electron beam emission from a low energy plasma focus device.* Physics letters A, 2007. 361(4-5): p. 377.

196. D.Y. Kwok and A.W. Neumann, *Contact angle measurement and contact angle interpretation.* Advances in Colloid and Interface Science, 1999. 81: p. 167.

197. A.N. Netravali, et al., *Surface modification of ultra-high strength polyethylene fibers for enhanced adhesion to epoxy resins using intense pulsed high-power ion beam.* Journal of Adhesion Science and Technology, 1999. 13(11): p. 1331.

198. A.A. Olgun Güven, Erdal Tan, *An atomic force microscopic study of the surfaces of polyethylene and polycarbonate films irradiated with gamma rays.* Radiation Physics and Chemistry, 1997. 50(2): p. 165.

199. M.H.S.A. Morteza Habibi, *Argon ion beam interaction on polyethylene terephthalate surface by a 4 kJ plasma focus device.* Pramana - Journal of Physics, 2014. 86(3): p. 599.

200. R.G. Brandon Kuczenski, *Material flow analysis of polyethylene terephthalate in the US, 1996-2007.* Resources, Convservation and Recycling, 2010. 54: p. 1161.

201. A.A. Afra Hadjizadeh, Martin N. Bureau, *Preparation and characterization of NaOH treated micro-fibrous polyethylene terephthalate nonwovens for biomedical application.* Journal of the Mechanical Behaviour of Biomedical Materials, 2010. 3(8): p. 574.

202. J.I. Lim, J.H. Kim, and H.-K. Park, *Artificial nerve scaffold of fascicles of poly (L-lactide) microfiber and knitted polyethylene terephthalate protector.* Microelectronic Engineering, 2012. 96: p. 6.

203. J.-H. Lee, et al., *Fabrication of 70 nm narrow metal nanowire structure on flexible PET film by nanoimprint lithography.* Microelectronic Engineering, 2008. 85: p. 710.

204. J. Taniguchi, et al., *Nanoprint lithography of gold nanopatterns on polyethylene terephthalate.* Microelectronic Engineering, 2009. 86.

205. F.F. Vidor, et al., *ZnO nanoparticle thin-film transistors on flexible substrate using spray-coating technique.* Microelectronic Engineering, 2016. 159: p. 155.

206. K.N. Norihiro Inagaki, Norio Tuchida, Kohji Miyazaki, *Surface Characterization of Plasma-Modified Poly(ethylene terephthalate) Film Surfaces.* Journal of Polymer Science: Part B, 2004. 42: p. 3727.

207. N.D. Geyter, et al., *Treatment of polymer films with a dielectric barrier discharge in air, helium and argon at medium pressure.* Surface and Coatings Technology, 2007. 201: p. 7066.

CHAPTER 3   TERPENOID PLASMA ENVIRONMENT

Identifying the type and relative abundance of species present within a terpenoid plasma environment is a vital step towards improving the quality and production economics of terpenoid-based plasma polymers. This information facilitates informed selection of the lowest-cost terpenoid precursor and applied plasma power combination that can be employed to produce a plasma polymer demonstrating the requisite physical and chemical properties for a particular application. When applied to a single precursor, such as terpinen-4-ol, it also allows for the identification of applied power thresholds that must not be exceeded if certain molecular structures or functionalities are to be preserved within the plasma environment and subsequently be made available for retention within the deposit. Furthermore, greater insight into the structure of the resulting plasma polymer may be provided by identifying species within the plasma environment that are available for incorporation into the deposit. This stands in contrast to common chemical characterisation techniques (such as FTIR, EDX, XPS, etc.) which, while useful for understanding chemical composition, are typically incapable of providing insight into the chemical structure of plasma polymers given their high degree of disorder.

3.1   COMPARATIVE STUDY OF NATURAL TERPENOID PRECURSORS IN REACTIVE PLASMAS FOR THIN FILM DEPOSITION APPLICATIONS

This paper compares terpinen-4-ol and *Melaleuca alternifolia* oil plasma environments as a function of applied power. A quadrupole mass spectrometer was operated in residual gas analysis and positive ion mode to provide information about the type and relative abundance of neutral and ionic species present within glow discharges supplied with terpinen-4-ol or *Melaleuca alternifolia* oil precursors. Ion energy distributions were compiled using data provided by an energy analyser integrated into the quadrupole mass spectrometer, and deposition rates within the glow discharge were captured by a crystal quartz microbalance. Thin films prepared from both precursors, and at various power settings, were subjected to supplementary biological assay to

assess antibacterial action (against *S. aureus* proliferation and biofilm formation) and cytocompatibility (with respect to human fibroblasts and Balb/c mice macrophages). "Comparative study of natural terpenoid precursors in reactive plasmas for thin film deposition applications," has been submitted to Polymer Journal. This paper involved collaborations with Dr. Jakaria Ahmad, A/Prof. Jason D. Whittle, Dr. Andrew Michelmore, and Prof. Krasimir Vasilev.

COMPARATIVE STUDY OF NATURAL TERPENOID PRECURSORS IN REACTIVE PLASMAS FOR THIN FILM DEPOSITION APPLICATIONS

Daniel S. Grant[1], Jakaria Ahmad[1], Jason D. Whittle[2,3], Andrew Michelmore[2,3], Krasimir Vasilev[2,3], Kateryna Bazaka[1,4], Mohan V. Jacob[1,*]

[1] College of Science and Engineering, James Cook University, Townsville, Queensland 4811, Australia

[2] Future Industries Institute, University of South Australia, Mawson Lakes Campus, South Australia 5095, Australia

[3] School of Engineering, University of South Australia, Mawson Lakes Campus, South Australia 5095, Australia

[4] School of Chemistry, Physics, and Mechanical Engineering, Queensland University of Technology, Brisbane, Queensland 4000, Australia

* Corresponding author. Tel: +61-7-47814379 E-mail: mohan.jacob@jcu.edu.au

Abstract

If plasma polymer thin films are to be synthesised from sustainable and natural precursors of chemically heterogeneous composition, it is important to understand the extent to which this composition influences the mechanism of polymerisation. To this end a well-studied monoterpene alcohol, terpinen-4-ol, has been targeted for a comparative study with the naturally-occurring mix of terpenes (viz. *Melaleuca alternifolia* oil) from which it is commonly distilled. Positive ion mode mass spectra of both terpinen-4-ol and *M. alternifolia* oil showed a decrease in disparities between the type and abundance of cationic species formed in their respective plasma environments as applied plasma power was increased. Supplementary biological assay revealed the antibacterial action of both terpinen-4-ol and *M. alternifolia* derived coatings with respect to *S. aureus*

bacteria, whilst cytocompatibility was demonstrated by comparable eukaryotic cell adhesion to both coatings. Elucidating the processes occurring within the reactive plasmas can enhance the economics of plasma polymer deposition by permitting use of the minimum power, time and precursor pre-processing required to control the extent of monomer fragmentation and fabricate a film with the desired physical and chemical properties.

1. Introduction

Plasma polymerisation is a well-established technique for the fabrication of thin films from volatile precursor species, and represents a complex interplay between species within the plasma volume itself and those at the plasma-substrate interface [1]. The chemical and physical properties of these films are heavily dependent upon a number of process parameters, including precursor species, flow rate, applied power, pressure, and substrate temperature [2]. By quantifying the role that each of these parameters play in influencing the nature and energies of plasma species, it is possible to precisely manipulate the deposition process in order to fabricate films exhibiting specific properties.

The drive for sustainability has spurred growing interest in replacing synthetic or highly purified organic precursors with natural, minimally-processed, and abundant low-cost alternatives [3]. One exemplar of this drive is polyterpenol, a plasma polymer synthesised from the terpinen-4-ol precursor monomer, a non-synthetic monocyclic terpene derived from the distillation of *M. alternifolia* oil (aka. tea tree oil). By virtue of the plasma polymerisation process, polyterpenol thin films share a number of attributes common to other plasma polymers including smooth, pin-hole free surfaces, and optical transparency [4]. Beyond this, post-deposition retention of terpinen-4-ol functionality within polyterpenol thin films fabricated at low power demonstrates a promising capacity to support antibacterial action [5-8], piquing interest in their potential use for biomedical applications.

For most high-tech thin film applications there is a direct relationship between the consistency of nanoscale properties and subsequent material or device performance. In this respect the chemical heterogeneity and batch variability of natural precursors poses a challenge to their commercial uptake. Resultantly, to realise reproducible fabrication of quality high-value films from essential oils it is imperative to understand the input chemistry and how it relates to the subsequent chemistry of the film. Whilst the complexity of the plasma polymerisation process makes it difficult to arrive at this understanding, mass spectrometry (MS) presents itself as a capable tool for tackling the challenge.

MS utilises an ion source, analyser, and detector to generate a two dimensional plot of signal intensity versus *m/z* (mass-to-charge ratio), with the product given as the mass spectrum. These spectra yield a wealth of information relating to chemical processes occurring within the plasma, including fragmentation, recombination, and the abundance of species involved in these reactions. By virtue of the fact that MS processes occur under high vacuum (resulting in long mean free paths), it permits one to examine the gas phase chemistry of isolated ions that arrive at the grounded surface beneath the plasma sheath at the sampling entrance. This, in turn, has resulted in MS being identified as a useful tool for understanding the processes occurring within the plasma volume following the introduction of a volatile plasma polymer precursor candidate. To this end, MS has been employed to generate a mechanistic understanding of the plasma chemistry of a number of precursors with biomaterial applications, including acrylic acid, allylamine, and ethanol [9-11].

Plasma polymerisation is an exceptionally complex process, owing to the diverse range of species present within the plasma and the extent to which interplay between these species is reliant upon deposition parameters. This poorly defined and complex chemistry can lead to the formation of films with variable structure and surface functionalities, the desired tuning of which may require considerable empirical investigations. Comparisons between terpinen-4-ol and *M. alternifolia* oil plasma environments at various powers allows for informed and cost-optimised decision making with respect to the choice of precursor and plasma power, depending on the desired properties of the thin film to be deposited.

2. Materials and methods

The high-purity non-synthetic precursor monomer, terpinen-4-ol (*Figure 1 a)*), was sourced from Australian Botanical Products and the parent *M. alternifolia* essential oil (with major components given in *Figure 1 a) – d)*) was procured from G.R. Davis Pty Ltd. Both were subjected to freeze-thaw degassing to remove dissolved oxygen prior to being introduced into the glow discharge. Deposition was performed on 1 cm^2 silicon wafers that were subjected to pre-deposition ultrasonic treatment in acetone and ethanol before being blown dry with nitrogen gas.
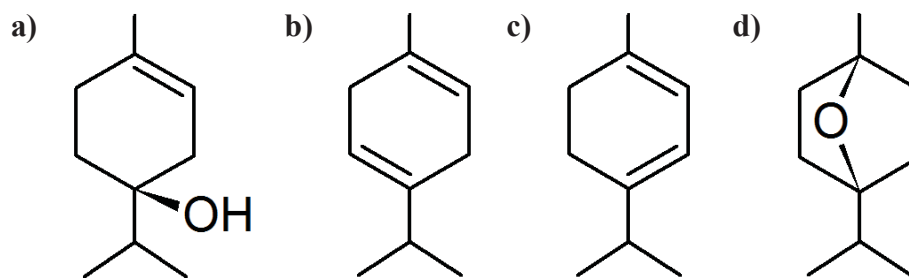
Figure 1. Major components and typical composition of M. alternifolia: a) terpinen-4-ol (40.1%), b) γ-terpinene (23.0%), c) α-terpinene (10.4%), d) 1,8-cineole (5.1%)

Continuous wave plasma polymerisation was undertaken within a stainless steel vacuum reactor vessel (length: 0.25 m, internal diameter: 0.3 m) evacuated to a working pressure $< 3 \times 10^{-3}$ mbar with a two-stage rotary vane pump. The reactor setup has been described in detail elsewhere [12]. Power was delivered to the reactor vessel via a 13.56 MHz R.F. generator at 5, 25, and 50 W. Actual power coupled into the plasma (distinct from the output power of the R.F. generator) was obtained from the electrode voltage, current, and phase measurements of an OctIV Probe (Impedans, Dublin). The deposition rate was measured using a Sycon Instruments (USA) crystal quartz microbalance (QCM) with a 6 MHz gold crystal (diameter: 7 mm), mounted at the centre of the grounded bottom electrode within the reactor.

A combined quadrupole mass spectrometer and energy analyser (Hiden EQP1000) was situated along the reactor midline. Sampling was accomplished using a grounded 100 μm orifice through which the reactor vessel was differentially pumped using a turbomolecular pump so as to ensure that system pressure was kept below 8×10^{-6} mbar during the sampling process. This low pressure provided an ion mean free path that is much longer than the ion trajectory in the MS [13]. It must be noted that species extraction was confined to occur at a single grounded orifice, and as such there is an implied assumption in this work that the measurements thus obtained are generally representative of the plasma environment experienced by likewise grounded samples.

Ion optics were tuned to provide maximum signal strength at the monomer unit mass (i.e., m/z = 154). For positive ion spectra the ion optics were re-tuned for each run by sampling at the peak ion energy, and an electron impact source (2

µA, 70 eV) was used for electron impact ionisation of neutral species. The mass spectrometer was operated in RGA and PIM to acquire the mass spectra for neutral and cation plasma species respectively.

3. Results and discussion

3.1 Plasma characteristics – commonly reported parameters

Table 1 outlines a number of key plasma and polymer parameters characterised throughout the course of this experiment. Specifically, it details nominal generator power (i.e., the output power from the R.F. generator), actual power coupled into the plasma (as measured with the OctIV Probe), terpinen-4-ol monomer flow rate into the reactor vessel, reactor vessel pressure, and the mass rate at which the polymer was deposited (obtained via crystal quartz microbalance (QCM)).

It is common to report various plasma and thin film properties as a function of the nominal generator output power, which may be readily obtained from the display on the generator unit. Unfortunately, this figure ignores parasitic energy losses within the system, and thus inevitably over-represents the actual power delivered to the plasma. For this study, however, access to an OctIV Probe permitted quantification of the actual transmitted power. The disparity between the nominal generator power and the actual transmitted power can be attributed to various energy losses and inefficiencies inherent to the deposition assembly employed for this study. These inefficiencies include transmission line losses, matching network losses, and coupling losses between the electrodes and plasma volume [14].

Table 1. Plasma parameters

Nominal Generator Power [W]	Actual Transmitted Power [W]	Flow Rate, ϕ [sccm]	Pressure*, P [mbar]	P/ϕ	Mass Deposition Rate [µg·m^{-2}·s^{-1}]
5	4.8	1.0	2.53×10^{-2}	4.8	5.6
25	19.2	0.7	3.10×10^{-2}	27.4	55.2
50	35.1	0.9	3.97×10^{-2}	39.0	42.3

  * Working pressure with the plasma turned on

The rate (ϕ) at which the terpinen-4-ol monomer flowed into the reactor vessel was controlled by a needle valve, and is expressed in standard cubic centimeters

per minute (sccm). By observing that the maximum deposition rate occurs for the minimum flow rate (i.e., at 0.7 sccm), we can speculate that the flow rate (and thus the number of monomeric units delivered to the plasma volume and available for fragmentation/deposition) is not a limiting factor in film formation. It must be noted, however, that this observation is only relevant if one discounts the influence of applied power on the deposition rate (which is also varied). Pressure exhibited an increasing trend in response to increases in the actual transmitted power, as one would expect following the associated increase in the density of energetic species within the plasma [2].

The Yasuda Factor given in *Equation (1)* (where W = wattage in J/s, M = monomer molecular weight in kg/mol, and F = monomer flow rate in mol/s) provides a measure of a system's plasma energy density [15], and allows for a general comparison of plasmas operating at different conditions within the same reactor vessel [16].

$$YF = W/MF \qquad (1)$$

In this instance M is held constant and as such the YF can be reduced to an applied power-to-flow rate ratio (P/ϕ) to facilitate comparison between the plasmas generated in this study. It must be noted when interrogating information presented in *Table 1* (and subsequent figures) that it was not possible to undertake mass deposition rate and MS measurements at precisely the same P/ϕ.

Deposition rates for plasma polymers derived from non-synthetic sources have been shown to demonstrate both a positive correlation with power (e.g., γ-terpinene [17]) and a negative correlation with power (e.g., linalool [18]). This deposition rate is highly dependent upon the energy invested per particle of gas mixture flowing through the glow discharge zone. For a given plasma reactor setup this is a function of several process parameters, including pressure, applied power, flow rate, and monomer species [1, 2]. Beyond these parameters, it is known that substrate thermal and energetic conditions also influence plasma polymerisation processes, including adsorption, desorption, diffusion, and chemical reactions [19-21]. These substrate conditions are themselves a function of the energy per bombarding particle, and the flux density of these particles [22].

Hence, the reduction in mass deposition rate from 25 W to 50 W may indicate that an adsorption-desorption equilibrium is beginning to become a rate limiting process in polyterpenol deposition at higher powers.

The decreasing deposition rate at 50 W may also be interpreted with respect to the ion energy distributions presented in *Figure 2*. Here we can assume that there is a shift in the balance from molecular physisorption, soft landing and chemisorption process (occurring between ~ 0.1-15 eV), to abstraction and sputtering processes at collision energies above ~ 15 eV [23, 24]. It is also known that below a certain YF threshold the rate of plasma polymerisation is strongly dependent upon the structure of the feed gas or monomer. At higher YFs the structure of the feed gas exerts less influence on the rate of deposition owing to increased monomer fragmentation [25, 26].

Developing a macroscopic understanding of the role that the R.F. power plays in the deposition rate may permit further control over the plasma polymerisation process. Knowing the mass deposition rate under a particular deposition scheme (i.e., pressure, flow rate, etc.) also provides the means to selectively control polyterpenol film thickness by selecting an appropriate deposition time. Furthermore, the deposition rate may now prospectively be used as a metric for providing generalisations about the process conditions that exist within the plasma system.

3.2 Ion energy distribution functions

The ion energy distribution function (IEDF) for positive ions arriving at the substrate is influenced by a number of parameters, including system pressure and instantaneous local electric field at the substrate [27]. Given that ion energy is not mass dependent, the IEDFs presented below are representative of all positive ions present within the plasma (not just those appearing at *m/z* 154).

The lack of a narrow ion energy band within *Figure 2 a) - c)* can be attributed to pressure (or more precisely, the ratio of the mean free path of the ions to the sheath thickness). In this instance, increases in pressure lead to an increase in the prevalence of collisional processes in the sheath, which in turn serve to bring about a broadening of the IEDFs and a decrease in the mean energy [28, 29]. Conversely, we can attribute the narrowing of the IEDFs as the transmitted power

is reduced to ion transit time effects related to the extent of precursor monomer fragmentation. Specifically, at lower powers the monomer units exhibit minimal fragmentation (relative to higher powers), and these heavier ion fragments are not accelerated as rapidly as light ions. This, in turn, contributes to longer transit times and an associated reduction in the width of the IEDF [30].
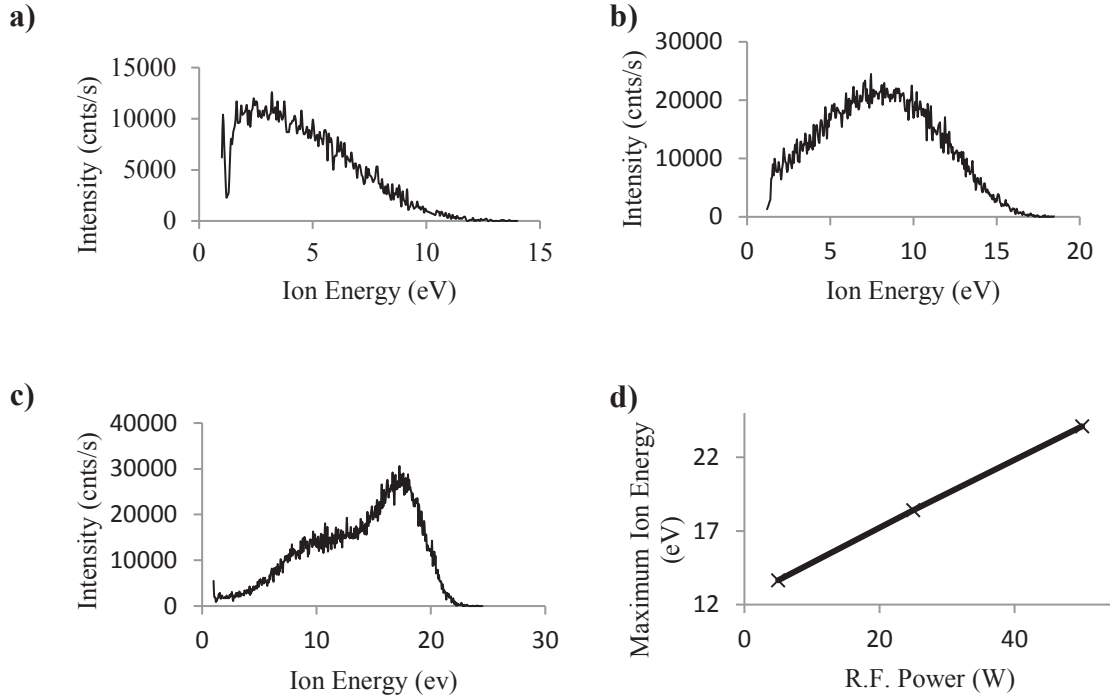

Figure 2. Positive ion energy distribution functions for *m/z* 154 and fragment ions arriving at the self-biased surface for powers and pressures of a) 5 W 2.17 Pa, b) 25 W 1.95 Pa, and c) 50 W 1.69 Pa; d) Ion energy as a function of applied R.F. power

Within non-thermal low pressure R.F. plasmas the maximum ion energy is given by $e_0 V_{sh}$, where e_0 is the electron charge and V_{sh} is the electric potential drop across the sheath in front of the substrate [22]. Thus, allowing for the electron charge to remain constant, the maximum ion energy is determined by the voltage drop across the substrate's plasma sheath, V_{sh}, [31], given as the difference between plasma potential V_{pl} and substrate potential V_s :

$$V_{sh} = V_{pl} - V_s \qquad (2)$$

The maximum ion energies given in *Figure 2 a) - c)* and summarised in *d)* indicate an increase in the maximum ion energy of the IEDFs as the generator and

transmitted R.F. power is increased; a finding that is in keeping with those reported by other studies [32]. This relationship can be interpreted with respect to e_0V_{sh} and *Equation (2)* by asserting that the increases in R.F. power serve to produce an increase in the sheath potential. Furthermore, given that the substrate is grounded (ensuring that $V_s = 0$) these increases in sheath potential can be solely attributed to an increase in the plasma potential, V_{pl}.

It is well known that the kinetic energy of bombarding ions plays a significant role in modifying the properties of thin films [33, 34]. Specifically, processes such as ion implantation, etching, and chain-scissioning/cross-linking can result in variations in the density, adhesion, hardness, and conductivity of plasma polymer thin films [35-37]. For this reason it is common for many plasma systems to employ a capacitively coupled R.F. biased substrate electrode to control the kinetic energy of the ions bombarding the substrate [30, 38]. In this instance, however, our findings indicate that we can control this kinetic energy simply by careful selection of the generator power. This, in turn, may play an important role in controlling processes that are sensitive to energetic ion bombardment including etching rates, selectivity of the etched material, and material degradation [27, 39].

3.3 Plasma characteristics – residual gas analysis of terpinen-4-ol

Figure 3 depicts the electron impact ionisation residual gas analysis (RGA) mass spectra of the neutral terpinen-4-ol species, and *m/z* ratios present at R.F. powers of 5, 25, and 50 W. The spectra have been corrected to account for the instrument's transmission function by assuming that peak intensity was proportional to m^{-1}, as advised by the manufacturer. All spectra were also normalised with respect to the total area under the spectra peaks.

The *no plasma* spectrum was analysed by direct interpretation of signal peaks for ions produced by impact ionisation of the neutral species. Here each peak represents a linear summation of all fragment ions with the corresponding *m/z* ratio, and it is probable that each such *m/z* relates to only a single fragment species (given that analysis is only being carried out on a single monomer and not a mixture of differing monomer species).
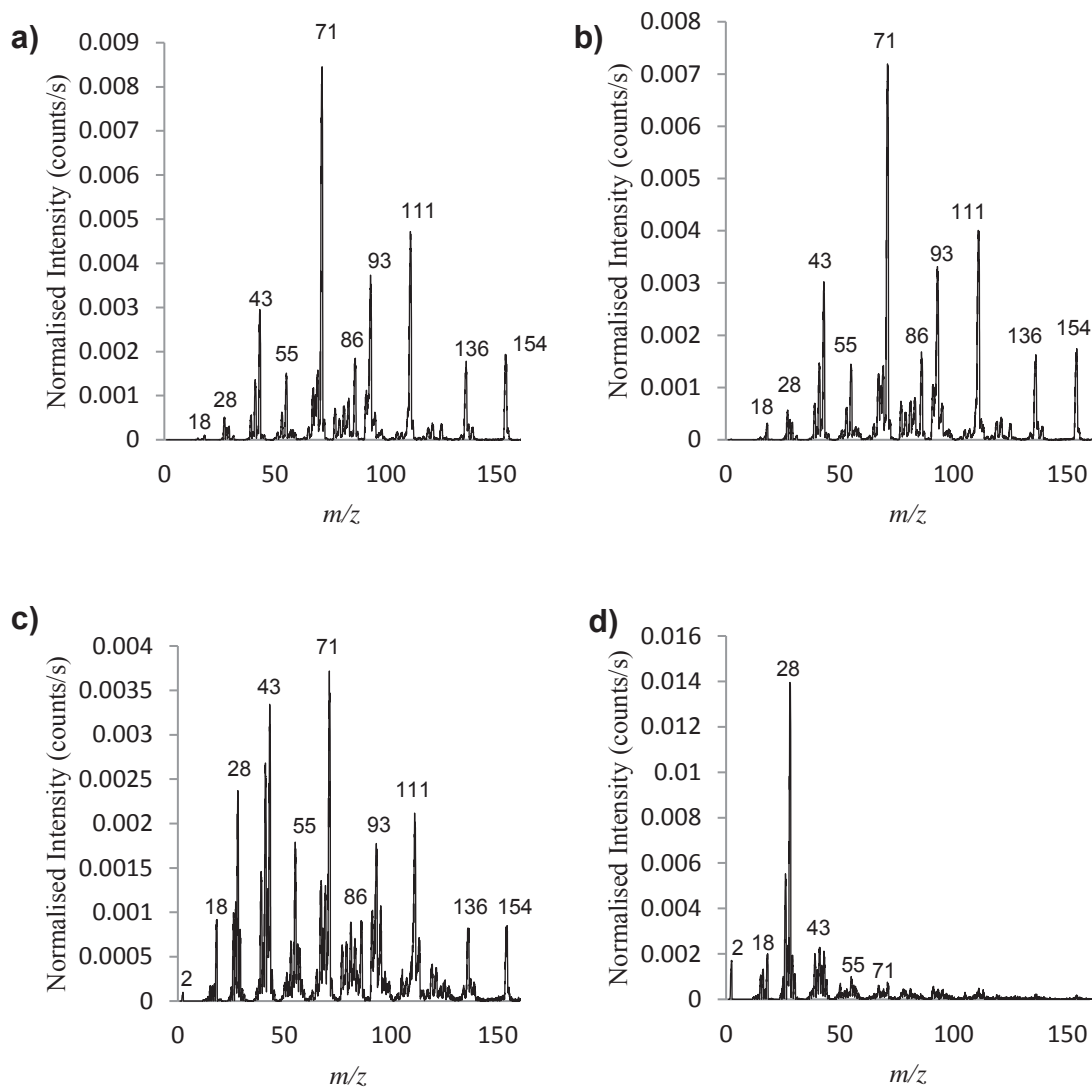
67

Figure 3. RGA mass spectra for a) monomer with no plasma; and plasma-phase neutrals at b) 5 W, c) 25 W, and d) 50 W

Table 2. Peak assignment in terpinen-4-ol RGA mass spectra

Peak (m/z)	Assignment
2	$H_2^{\cdot+}$
17	OH^+
18	$H_2O^{\cdot+}$
28	$CO^{\cdot+}$ or $C_2H_4^{\cdot+}$
43	$C_3H_7^+$
55	$C_4H_7^+$ or $C_3H_3O^+$

71	$C_5H_{11}^+$ or $C_4H_7O^+$
93	$C_7H_9^+$
111	$C_8H_{15}^+$
136	$C_{10}H_{16}^{\cdot+}$
154	$C_{10}H_{18}O^{\cdot+}$

+ positive even-electron ions

+· positive radical ions

For *no plasma* the base peak is located at *m/z* 71, and additional molecular weight species are present at *m/z* 154 (representing the terpinen-4-ol monomer, either with or without scissioning), 136, 111, 93, 71, and 43. In this instance $C_{10}H_{16}$ is liable to degrade into *m/z* 93 with a loss of forty-three mass units (corresponding to C_3H_7), as evidenced by the comparable abundance of the complementary *m/z* 93 and 43 units. Increases in power resulted in a noticeable shift in intensities towards lower *m/z* species, including the detectable formation of H_2 as evidenced by *m/z* 2.

RGA of the plasma-phase neutrals suggests extensive fragmentation of terpinen-4-ol. However, the mode of fragmentation at low power (i.e., at 5 W) is similar to that provided by electron impact in the *no plasma* sample, indicating that this power stimulates minimal plasma-induced fragmentation of the monomer. It is interesting to note that even at an applied power of 25 W (and to a lesser extent, 50 W), there remains a non-trivial source of precursor monomer within the plasma volume. This also indicates that some of the spectral intensity of *m/z* ratios less than that of the monomer may be wholly or partially attributed to the RGA electron impact fragmentation of these precursor monomers, as opposed to plasma-induced fragmentation. This stands in contrast to similar studies conducted on lower molecular weight monomers such as acrylic acid where virtually total monomer fragmentation was achieved at 15 W. This disparity between spectral intensity of the monomer ions from an acyclic structure (such as acrylic acid) and the cyclic terpenin-4-ol may be partially accounted for by scissioning of the cyclic structure, which would result in a change in the ion's molecular structure, but not its molecular weight. However, the relatively low intensity of *m/z* 154 peaks in *b)* - *d)* suggests that such contributions are likely to be of a modest nature. The

remaining peaks can be attributed to plasma-induced fragmentation of the terpinen-4-ol monomer, with the resulting neutral fragments being ionised by the mass spectrometer.

At low YF we observe minimal fragmentation, and considerable preservation of monomeric units. By assuming that these relatively intact monomeric units are incorporated into the plasma polymer, we can further substantiate findings presented in [40] which attribute the enhanced antibacterial properties of polyterpenol thin films fabricated at low YF to the preservation of monomer functionalities (i.e., -OH and double bonds) within the polymer film. Incorporation of monomeric units into the final deposit may be further advanced by increased adsorption of non-fragmented units at low substrate temperatures [41] eventuating as a natural by-product of the low applied power.

This finding permits us to tune the plasma parameters, and in particular the plasma power, in order to achieve the desired fragmentation scheme and subsequent incorporation of specific fragment and monomer species within the plasma volume and resulting plasma polymer deposit.

3.4 Plasma characteristics – positive ion mode analysis of terpinen-4-ol and M. alternifolia Oil

As detailed in *Table 3*, the monomer of interest in this study, terpinen-4-ol, is the primary subcomponent of *M. alternifolia* oil. Subsequently, a comparative analysis of the positive ion mode (PIM) mass spectra for the cationic species generated by the plasma environment alone (without any further electron impact ionisation-induced fragmentation) was performed for both the monomer and the parent oil, as shown in *Figure 4*. Associated peak assignments for terpinen-4-ol fragments are provided in *Table 4*.

Table 3. Major components of *M. alternifolia* oil [5, 42]

Component	Chemical formula	Molecular weight	Typical composition (%)
Terpinen-4-ol	$C_{10}H_{18}O$	154.25	40.1
γ-Terpinene	$C_{10}H_{16}$	136.24	23.0
α-Terpinene	$C_{10}H_{16}$	136.24	10.4

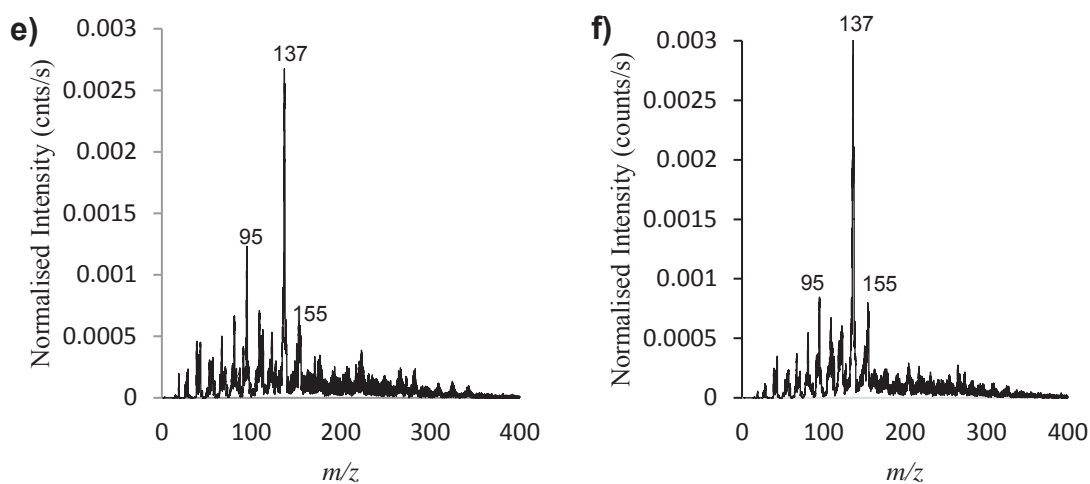| 1,8-Cineole | $C_{10}H_{18}O$ | 154.25 | 5.1 |
Terpinolene	$C_{10}H_{16}$	136.24	3.1
ρ-Cymene	$C_{10}H_{14}$	134.21	2.9
α-Pinene	$C_{10}H_{16}$	136.24	2.6
α-Terpineol	$C_{10}H_{18}O$	154.25	2.4
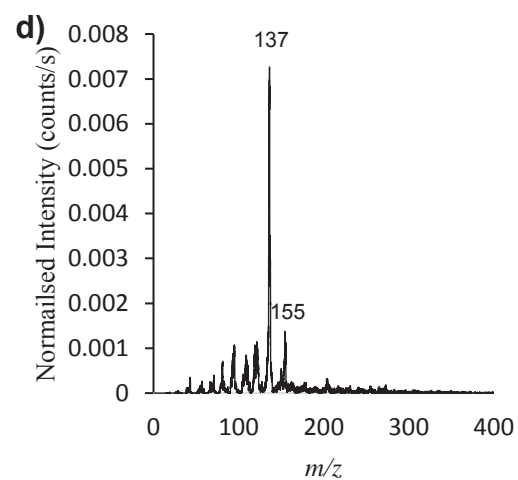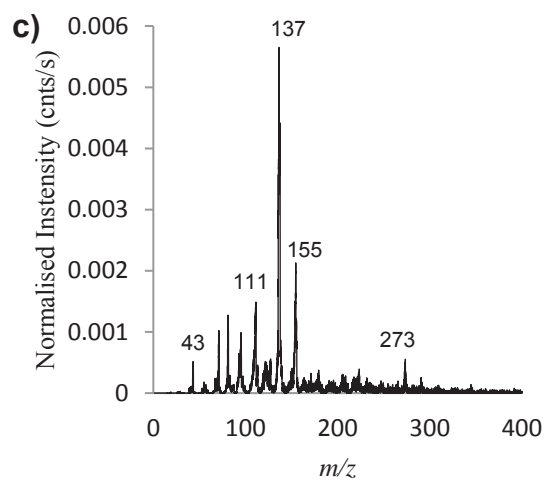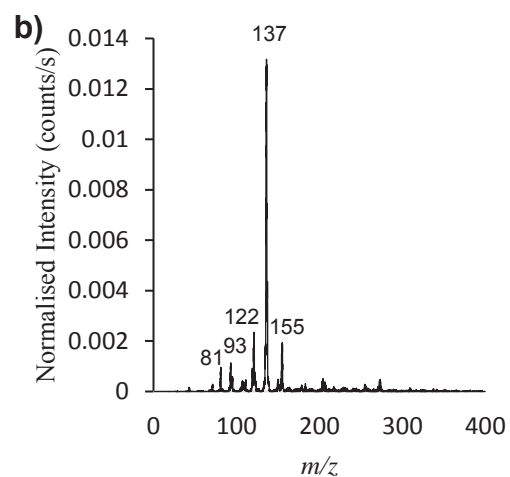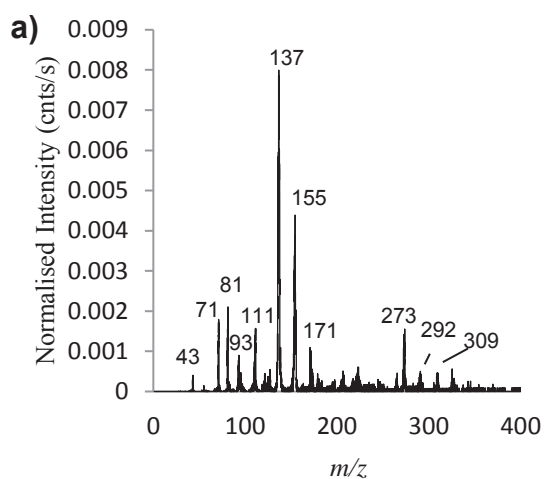
Figure 4. PIM mass spectra for terpinen-4-ol at R.F. plasma powers of a) 5 W, c) 25 W, and e) 50 W, and the parent *M. alternifolia* oil at R.F. plasma powers of b) 5 W, d) 25 W, and f) 50 W

Elimination of water (18 amu) from the monomer gives rise to the base peak at *m/z* 137 for all terpinen-4-ol spectra. Other features of note in the monomer spectra include the low intensity presence of a dimer at *m/z* 309, with a concomitant peak at *m/z* 292 following elimination of OH. With respect to the *M. alternifolia* PIM spectra, we again observe the presence of the base peak at *m/z* 137, associated with the presence of any number of the oil's myriad of protonated $C_{10}H_{16}$ species and fragmentation of $C_{10}H_{18}O$ species following water elimination. As with the terpinen-4-ol PIM spectra, successive increases in the applied R.F. power correlate with a decrease in the intensity of all prominent peaks identified at the lower power setting, and an accompanying increase in the variety of both low and high *m/z* fragmentation/recombination products.

Despite the preponderance of terpinen-4-ol monomeric units in *M. alternifolia* oil, a disparity exists between the abundance and variety of cationic species present in the low power plasma environments for these two respective precursors, as evidenced by *Figure 4 a)* and *b)*. In explanation, consideration must be given to the possibility that the difference in vapour pressure for the multitude of species present in *M. alternifolia* oil favours the introduction and prevalence of lower molecular weight species (i.e., $C_{10}H_{16}$) into the plasma environment. This possibility is given further credence by the close resemblance of the spectrum in *Figure 4 b)* to that of the low power PIM spectrum of a single $C_{10}H_{16}$ species

72

(namely γ-terpinene) presented in a previous study [17]. As the applied power is increased, however, disparities begin to disappear as increased molecular fragmentation of both terpinen-4-ol (*Figure 4 c)* and *e)*) and *M. alternifolia* oil (*Figure 4 d)* and *f)*) ensures convergence towards comparable cationic plasma environments.

Based on these findings we can assert that if retention of the terpinen-4-ol peak and associated functionality is of relevance to the final application of the thin film (e.g., in eukaryotic cell compatible coatings), utilisation of the pure monomer in a low R.F. power plasma environment is essential. Conversely, if the thin film is to be synthesised at an elevated R.F. power (say, to produce a protective coating with enhanced crosslinking), the choice of precursor becomes trivial from a properties point of view. Here the less processed (and hence less costly) parent *M. alternifolia* oil may serve to produce films with comparable composition to those formed from the terpinen-4-ol monomer alone.

Table 4. Peak assignment in terpinen-4-ol PIM mass spectra

Dominant Peaks	Possible Species
309	$[2M + H]^+$
292	$[2M + H]^+ - OH$
282	
273	
267	
223	
171	
155	$[M + H]^+$
137	$[M + H]^+ - H_2O$
122	
111	$C_8H_{15}^+$
109	
93	

81	
71	$C_5H_{11}^+$ or $C_4H_7O^+$
68	
55	$C4H7+$ or $C_3H_3O^+$
43	$C_3H_7^+$
30	
18	$H_2O^{\cdot+}$

3.5 Biological assay

Plasma polymerised films from terpinen-4-ol and *M. alternifolia* (i.e., tea tree oil) precursors were subjected to supplementary antibacterial assay, as depicted in *Figure 5*. Uncoated glass control displayed the highest *S. aureus* biofilm thickness and biovolume, at 15.3 ± 1.92 µm and 8.5 ± 1.58 µm^3/µm^2 respectively. Relative to the control, terpinen-4-ol and *M. alternifolia* coatings demonstrated significantly reduced biofilm thickness (2.5 ± 0.75 µm and 2.3 ± 0.72 µm respectively) and biovolume (1.4 ± 0.95 µm^3/µm^2 and 1.5 ± 0.87 µm^3/µm^2 respectively). Given the similarity in biofilm reduction for the two coatings, it is possible that their antibacterial action is supported by fragments species common to their respective mass spectra, such as *m/z* 81, 93, 137, and 155 (as revealed in *Figure 5 a) and b)*). This finding also indicates that if antibacterial action is the prime characteristic required of the coating, then preference may be given to the less processed and cheaper tea tree oil as the precursor material.
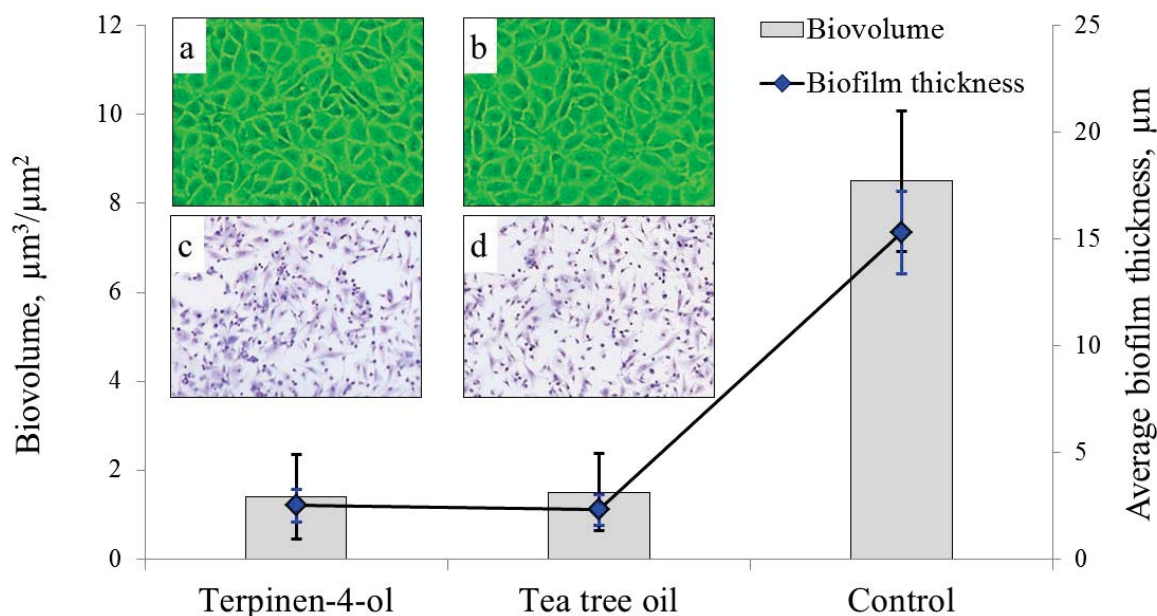
Figure 5. Biofilm thickness and biovolume of *S. aureus* biofilm grown for 18 hr at 37°C on the surface of thin films deposited from terpinen-4-ol and tea tree oil precursors, with unmodified glass used as a control. Inset: a-b) phase contrast images of wells containing human fibroblasts grown in the presence of the coatings. c-d) attachment of Balb/c mouse macrophages incubated in the presence of coatings (attachment to control not shown)

Phase contrast images of human fibroblasts incubated in the presence of the coatings (*Figure 5 a* and *b*) revealed healthy cell size and morphology similar to that of cells incubated in the presence of the inert glass control, suggesting cytocompatibility of the coatings and limited leaching of the biologically-active agents into the liquid media. To investigate cytocompatibility of these coatings on contact, mice macrophage cells were seeded at a density of 5×10^5 cells per mL into 24–well plates by adding 1 mL of cell suspension to each well containing substrates coated by terpinene-4-ol or *M. alternifolia* films, with glass cover slips used as a control. After incubation at 37°C and 5% CO_2 for 48 hr, macrophage attachment was quantified at $2.1 \pm 0.2 \times 10^2$ cells/mm² for control, $2.3 \pm 0.2 \times 10^2$ cells/mm² for terpinene-4-ol, and $2.0 \pm 0.3 \times 10^2$ cells/mm² for *M. alternifolia* samples (*Figure 5 c* and *d*). Whilst being within the margin of error for control and terpinene-4-ol treated samples, slightly reduced attachment of eukaryotic cells to coatings derived from the *M. alternifolia* precursor is to be expected, given that

M. alternifolia is comprised of a multitude of molecules (such as 1,8-cineole, α-terpinene, aromadendrene, etc) that can be toxic to these cells [43, 44]. These findings indicate that whilst plasma polymers synthesised from either terpinen-4-ol or tea tree oil precursors are suitable for antibacterial coatings, slight priority may be given to terpinen-4-ol coatings for indwelling implant surfaces requiring interaction with, and attachment of, eukaryotic cells.

4. Conclusion

This work elucidated the relationship between applied R.F. power, and the subsequent fragmentation of terpinen-4-ol monomeric units. The use of MS coupled with ion energy spectroscopy analysis facilitated identification of neutral and cationic fragmentation species, and the aggregate kinetic energy of cationic species. Monomer fragmentation was found to increase with applied power, and this is accompanied by an increase in the spread of *m/z* values. On a comparative basis, this increased fragmentation served to diminish disparities between the plasma environment of the monomer, and that of its parent *M. alternifolia* oil. Conversely, operating at reduced power levels is liable to produce films exhibiting an increase in the selective retention of terpinen-4-ol monomeric units and their associated biologically relevant functionalities.

These findings can be employed to correlate the various properties of terpenoid-based plasma polymer thin films to the power and plasma environmental conditions under which they were fabricated. For example, the specific choice of precursor (i.e., terpinen-4-ol monomer, or the less-costly *M. alternifolia* oil from which it is distilled) may now be justified with respect to the plasma environment generated for each precursor as a function of the plasma power. Such correlations underlay the financially- and physically-driven fine-tuning of the deposition process to achieve the development of films derived from natural precursors that exhibit appropriate qualities for particular applications.

Acknowledgements

References

1.   J. Friedrich, *Mechanisms of Plasma Polymerization - Reviewed from a Chemical Point of View.* Plasma Processes and Polymers, 2011. 8: p. 783.

2.   F.F. Shi, *Recent advances in polymer thin films prepared by plasma polymerization: Synthesis, structural characterization, properties and applications.* Surface and Coatings Technology, 1996. 82: p. 1.

3.   K. Bazaka, M.V. Jacob, and K. Ostrikov, *Sustainable Life Cycles of Natural-Precursor-Derived Nanocarbons.* Chemical Reviews, 2016. 116(1): p. 163.

4.   K. Bazaka and M.V. Jacob, *Synthesis of radio frequency plasma polymerized non-synthetic Terpinen-4-ol thin films.* Materials Letters, 2009. 63: p. 1594.

5.   C.F. Carson;, K.A. Hammer;, and T.V. Riley, *Melaleuca alternifolia (Tea Tree) Oil: a Review of Antimicrobial and Other Medicinal Properties.* Clinical Microbiology Reviews, 2006. 19(1): p. 50.

6.   S.D. Cox, et al., *The mode of antimicrobial action of the essential oil of Melaleuca alternifolia (tea tree oil).* Journal of Applied Microbiology, 2000. 88: p. 170.

7.   K. Bazaka, et al., *Plasma-Enhanced Synthesis of Bioactive Polymeric Coatings from Monoterpene Alcohols: A Combined Experimental and Theoretical Study.* Biomacromolecules, 2010. 11(8): p. 2016.

8.   K. Bazaka, et al., *Anti-bacterial surfaces: natural agents, mechanisms of action, and plasma surface modification.* RSC Advances, 2015. 5: p. 48739.

9.   H.D. Hazrati, J.D. Whittle, and K. Vasilev, *A Mechanistic Study of the Plasma Polymerization of Ethanol.* Plasma Processes and Polymers, 2014. 11: p. 149.

10.   D.B. Haddow, et al., *A Mass Spectrometric and Ion Energy Study of the Continuous Wave Plasma Polymerization of Acrylic Acid.* Langmuir, 2000. 16: p. 5654.

11.   Z. Zhang, W. Knoll, and R. Forch, *Amino-functionalized plasma polymer films for DNA immobilization and hybridization.* Surface and Coatings Technology, 2005. 200: p. 993.

12.   A. Michelmore, et al., *An Experimental and Analytical Study of an Asymmetric Capacitively Coupled Plasma Used for Plasma Polymerization.* Plasma Processes and Polymers, 2014. 11(9): p. 833.

13.   J. Benedikt, et al., *Quadrupole mass spectrometry of reactive plasmas.* Journal of Physics D: Applied Physics, 2012. 45: p. 403001.

14.   S. Pizzini, *Advanced Silicon Materials for Photovoltaic Applications*. 2012: John Wiley and Sons.

15.   H.K. Yasuda, *Plasma Polymerization*. 1985, London: Academic Press.

16.   J.D. Whittle, et al., *Variability in Plasma Polymerization Processes - An International Round-Robin Study.* Plasma Processes and Polymers, 2013. 10: p. 767.

17.   J. Ahmad, et al., *Structural Characterization of γ-Terpinene Thin Films Using Mass Spectroscopy and X-Ray Photoelectron Spectroscopy.* Plasma Processes and Polymers, 2015. 12(10): p. 1085.

18.   M.V. Jacob, et al., *Plasma polymerised thin films for flexible electronic applications.* Thin Solid Films, 2013. 546.

19.   J.A. Thornton, *Influence of apparatus geometry and deposition conditions on the structure and topography of thick sputtered coatings.* Journal of Vacuum Science and Technology, 1974. 11(4): p. 666.

20.   B. Hussla, et al., *In Situ Silicon-wafer Temperature Measurements During RF Argon-ion Plasma Etching via Fluoroptic Thermometry.* Journal of Physics D: Applied Physics, 1987. 20(7): p. 889.

21.   H. Deutsch, H. Kersten, and A. Rutscher, *Basic Mechanisms in Plasma Etching.* Contributions to Plasma Physics, 1989. 29(3): p. 263.

22.   H. Kersten, et al., *The energy balance at substrate surfaces during plasma processing.* Vacuum, 2001. 63: p. 385.

23. D.C. Jacobs, *Reactive Collisions of Hyperthermal Energy Molecular Ions with Solid Surfaces.* Annual Review of Physical Chemistry, 2002. 53: p. 379.

24. L. Stafford, et al., *Energy dependence of ion-assisted chemical etch rates in reactive plasmas.* Applied Physics Letters, 2005. 87(7): p. 071502.

25. H. Yasuda, *Glow discharge polymerization.* Journal of Polymer Science: Macromolecular Reviews, 1981. 16(1): p. 199.

26. G. Czeremuszkin, A.M. Wrobel, and M. Kryszewski, *Plasma polymerization of organoisothiocyanates. I. Characterization of deposition process and deposited materials.* Journal of Applied Polymer Science, 1992. 44(5): p. 883.

27. J. Meichsner, et al., *Plasma diagnostics for surface modification of polymers.* Surface and Coatings Technology, 1998. 98: p. 1565.

28. W. Schwarzenbach, et al., *Sheath impedance effects in very high frequency plasma experiments.* Journal of Vacuum Science and Technology, 1996. 14(1): p. 132.

29. M. Zeuner, H. Neumann, and J. Meichsner, *Ion energy distributions in a dc biased rf discharge.* Journal of Applied Physics, 1997. 81(7): p. 2985.

30. M.A. Sobolewski, J.K. Olthoff, and Y. Wang, *Ion energy distributions and sheath voltages in a radio-frequency-bioased, inductively coupled, high-density plasma reactor.* Journal of Applied Physics, 1999. 85: p. 3966.

31. F.L. Buzzi, Y.-H. Ting, and A.E. Wendt, *Energy distribution of bombarding ions in plasma etching of dielectrics.* Plasma Sources Science and Technology, 2009. 18: p. 1.

32. S. Kadlec, et al., *Energy distribution of ions in an unbalanced magnetron plasma measured with energy-resolved mass spectrometry.* Surface and Coatings Technology, 1997. 89: p. 177.

33. Y. Takagi, et al., *Generation processes of super-high-energy atoms and ions in magnetron sputtering plasma.* Vacuum, 2006. 80(6): p. 581.

34.   M. Mišinaa, et al., *Investigation of the pulsed magnetron discharge by time- and energy-resolved mass spectrometry.* Vacuum, 2002. 68(2): p. 171.

35.   J.P.A. Anders, *Plasma-Based Ion Implantation and Deposition: A Review of Physics, Technology, and Applications.* IEEE Transactions on Plasma Science, 2005. 33(6): p. 1944.

36.   A. Anders, *A structure zone diagram including plasma-based deposition and ion etching.* Thin Solid Films, 2010. 518: p. 4087.

37.   E. Krikorian and R.J. Sneed, *Nucleation, growth and transformation of amorphous and crystalline solids condensing from the gas phase.* Astrophysics and Space Science, 1979. 65(1): p. 129.

38.   X. Li, et al., *Fluorocarbon-based plasma etching of SiO2: Comparison of C4F6/A and C4F8/A discharges.* Journal of Vacuum Science and Technology, 2002. 20(6): p. 2052.

39.   X.V. Qin, Y.-H. Ting, and A.E. Wendt, *Tailored ion energy distributions at an rf-biased plasma electrode.* Plasma Sources Science and Technology, 2010. 19: p. 1.

40.   K. Bazaka, et al., *Plasma-assisted surface modification of organic biopolymers to prevent bacterial attachment.* Acta Biomaterialia, 2011. 7(5): p. 2015.

41.   G.P. Lopez and B.D. Ratner, *Substrate Temperature Effects on Film Chemistry in Plasma Deposition of Organics. 1. Nonpolymerizable Precursors.* Langmuir, 1991. 7: p. 766.

42.   J.J. Brophy, et al., *Gas chromatographic quality control for oil of Melaleuca terpinen-4-ol type (Australian tea tree).* Journal of Agricultural and Food Chemistry, 1989. 37(5): p. 1330.

43.   K.A. Hammer, et al., *A review of the toxicity of Melaleuca alternifolia (tea tree) oil.* Food and Chemical Toxicology, 2006. 44: p. 616.

44.   C.F. Carson, T.V. Riley, and B.D. Cookson, *Efficacy and safety of tea tree oil as a topical antimicrobial agent.* Journal of Hospital Infection, 1998. 40(3): p. 175.

CHAPTER 4   SWIFT HEAVY ION IRRADIATION

This chapter examines the restructuring and development of new properties for polyterpenol thin films following irradiation with high energy swift heavy ions (SHIs). SHIs (i.e., ions with an energy greater than ~1 MeV) deposit energy within target polymer materials via electronic and nuclear stopping mechanisms. Energy deposition is spatially localised within a cylindrical region along each ion track, with track lengths that can extend into the tens of µm. The resulting excitation, ionisation, and displacement interactions that occur within this region precipitate a multitude of physiochemical processes, including chain-scissioning, crosslinking, outgassing, and etching.

Section 4.1 focusses on the exposure of polyterpenol to 50 MeV I^{10+} SHIs at fluence values $\leq 10^{12}$ ions/cm^2. This low fluence ensures isolated energy deposition and material modification within a single track regime. In Section 4.2 the fluence is increased above 10^{13} ions/cm^2, allowing for uniform film restructuring within an overlapping multiple track regime provided by 55 MeV I^{9+} SHIs.

4.1   ION IRRADIATION AS A TOOL FOR MODIFYING THE SURFACE AND OPTICAL PROPERTIES OF PLASMA POLYMERISED THIN FILMS

This paper examined the processing of polyterpenol thin films with 50 MeV I^{10+} SHIs at fluence values $\leq 10^{12}$ ions/cm^2. Air-polyterpenol and polyterpenol-substrate interfacial roughness was probed with X-ray reflectometry (Cu-K$_\alpha$), and verified with supplementary data provided by atomic force microscopy and spectroscopic ellipsometry characterisation. Radiation-induced variations in film refractive index and extinction coefficient were also extracted from modelling of spectroscopic ellipsometry experimental data over the 250 – 1000 nm region. "Ion irradiation as a tool for modifying the surface and optical properties of plasma polymerised thin films." is published in Nuclear Instruments and Methods in Physics Research B: Beam Interactions with Materials and Atoms (Elsevier). This paper involved collaboration with Dr. Stephen Holt, and Dr. Rainer Siegele.

ION IRRADIATION AS A TOOL FOR MODIFYING THE SURFACE AND OPTICAL PROPERTIES OF PLASMA POLYMERISED THIN FILMS

Daniel S. Grant[a], Kateryna Bazaka[a,b], Rainer Siegele[c], Stephen A. Holt[d], and Mohan V. Jacob*[a]

[a] College of Science, Technology and Engineering, James Cook University, Townsville, Queensland 4811, Australia

[b] School of Chemistry, Physics, and Mechanical Engineering, Queensland University of Technology, Brisbane, QLD 4000, Australia

[c] Institute for Environmental Research, Australian Nuclear Science and Technology Organisation, Lucas Heights, New South Wales 2234, Australia

[d] Bragg Institute, Australian Nuclear Science and Technology Organisation, Lucas Heights, New South Wales 2234, Australia

* Corresponding Author: Mohan.Jacob@jcu.edu.au

Abstract

Radio Frequency (R.F.) glow discharge polyterpenol thin films were prepared on silicon wafers and irradiated with I^{10+} ions to fluences of 1×10^{10} and 1×10^{12} ions/cm^2. Post-irradiation characterisation of these films indicated the development of well-defined nano-scale ion entry tracks, highlighting prospective applications for ion irradiated polyterpenol thin films in a variety of membrane and nanotube-fabrication functions. Optical characterisation showed the films to be optically transparent within the visible spectrum and revealed an ability to selectively control the thin film refractive index as a function of fluence. This indicates that ion irradiation processing may be employed to produce plasma-polymer waveguides to accommodate a variety of wavelengths. XRR probing of the substrate-thin film interface revealed interfacial roughness values comparable to those obtained for the uncoated substrate's surface

(i.e., both on the order of 5Å), indicating minimal substrate etching during the plasma deposition process.

1. Introduction

Swift heavy ion (SHI) irradiation (energies above 1 MeV) is known to induce a number of characteristic radiation-chemical processes in polymeric materials. In common with other types of ionising radiation (e.g., gamma rays, electrons, etc.), SHIs can produce cross-linking, chain scissions, free radicals, and unsaturated bonds in hydrogenated polymers [1]. Unique to SHI irradiation however, is that as the ion traverses the polymeric medium (with penetration depths that can be tailored in the order of tens of micrometres) its large deposited energy density produces a latent track of well-defined dimensions [2, 3]. Furthermore, the energy and species of the ion employed in the irradiation process exert considerable influence on the extent of crosslinking or chain-scissions within the structure of the polymer in question [4]. Many of the aforementioned radiation-chemical processes are confined to occur within the penumbra of this track [5]. The capacity for SHIs to modify physical and chemical properties of polymers has fostered a number of studies aimed at developing and enhancing commercial applications. These include lithography processes, the fabrication of nanotube templates, and nanoporous membranes [6-8].

Radio frequency (R.F.) glow discharge is a well-established dry process for the fabrication of organic thin films [9]. Typically, energy is supplied to a process gas (such as helium, argon, or atmospheric gas) leading to the formation of a non-equilibrium cold plasma within either an internal, external, or electrodeless reactor vessel [10]. Monomer units are then introduced to the plasma glow, where they are subjected to fragmentation, excitation, and ionisation by the energetic plasma. The resulting species subsequently adhere to the substrate material via either physical absorption or chemical bonding processes. The result is the formation of highly crosslinked and structurally disordered films possessing a number of advantageous physical and chemical properties, including strong substrate adhesion, pin-hole free surface topologies, and chemically functionalised surfaces. Furthermore, a large variety of deposition parameters (including vacuum pressure, precursor selection, R.F. power, reactor geometry, monomer flow rate, plasma gas, deposition time, etc.) can be varied to achieve polymer films with specific properties or combinations thereof [11]. For these reasons, R.F. glow discharge polymers have found numerous current and

prospective applications as conformal coatings for inorganic electronic assemblies [12], encapsulation films for organic electronic devices [13], and coatings for various other substrate materials (exhibiting an assortment of tailored anti-fogging, corrosion resistant, and abrasion resistant properties) [14].

In this research, we focus on the application of 50 MeV I[10+] SHIs to polyterpenol thin films fabricated using an R.F. glow discharge polymerisation technique. The precursor monomer for these films, terpinen-4-ol, is a non-synthetic monocyclic terpene derived from the distillation of tea tree oil. Studies undertaken by our group have demonstrated that in addition to possessing the aforementioned generic plasma polymer properties [15, 16], polyterpenol thin films demonstrate rectifying electron-blocking hole-transport behaviour [17], and the retention of terpinen-4-ol functional groups within the polymerised film imbues this polymer with antibacterial properties [18]. The primary objective of this research is to characterise the effects of iodine SHI irradiation on the surface and optical properties of polyterpenol, and, to the extent that it is possible to do so, to interpret these property changes in the context of the elementary ion energy loss mechanisms. These findings will tailor the direction of future investigations into coupling polyterpenol's attractive material traits with SHI irradiation's capacity to modify polymeric material properties.

2. Material preparation methods

2.1 Substrates

Plasma polymerised polyterpenol thin films were deposited on highly polished 500 μm thick 1×1 cm <100> photoresist coated single crystal silicon wafers (n-type Sb doped), sourced from Fondazione Bruno Kessler.

Prior to plasma deposition the wafers were rinsed in acetone to remove the photoresist coating. The wafers were then washed in a solution of Extran and distilled water, ultrasonically cleaned in a sonicator (distilled water, 50 °C, 30 min), and rinsed in isopropanol to remove inorganic contaminants. Residual organic contaminants were then removed using piranha solution (3:1 mixture of 25% H_2SO_4 in concentrated H_2O_2). The wafers were then subjected to a final rinse in distilled water and blown dry. The cleaning procedure produced a hydrophilic surface and led to no variation in surface roughness.

2.2 Plasma polymer deposition

Plasma polymerisation of terpinen-4-ol (99%, Australian Botanical Products) was carried out using a custom-made cylindrical glass reactor chamber, with an approximate volume of 0.0029 m^3, a length of 0.75 m, and internal diameter of 0.07 m. Radio frequency power was supplied to the chamber at 13.56 MHz via two externally coupled copper electrodes spaced 0.07 m from one another and 0.11 m from the monomer inlet. Prior to plasma formation, the chamber was flushed with argon gas for 60 s to dislodge loose contaminant particles and displace atmospheric gas. Films were fabricated at 25 W over a deposition time of 15 s, yielding film thicknesses of less than 500 Å.

2.3 Iodine ion irradiation

The polyterpenol thin films were irradiated under vacuum with 50 MeV I^{10+} ions, generated using the 10 MV ANTARES tandem accelerator (ANSTO). Specimens were irradiated at < 20 nA over a 2 cm^2 area to minimise macroscopic heating, and irradiation time was varied to achieve total fluences of 1×10^{10} and 1×10^{12} ions/cm^2. Beam current was ascertained before and after each irradiation run using a Faraday cup, and irradiation was undertaken at a temperature of 293 K and a pressure of 10^{-5} mbar.

The choice of ion energy and species employed in this study is liable to influence a number of interaction processes between the radiation and the polymeric material. These include the large number of nucleons (relative to say, H or He) leading to an increased prevalence and importance of nuclear stopping (i.e., atomic displacements and phonons) in the ion-specimen interaction as a result of the larger Rutherford cross-section and momentum transfer. The high ion energy also results in an ion velocity well in excess of the Bohr velocity, leading to a shorter interaction time between the ion and its surrounding medium, and a reduction in electronic stoppage (i.e., reduced electron excitation and ionisation) [1].

3. Characterisation

3.1 Surface properties

XRR (Cu-K_α) measurements were performed at the air-solid interface using a PANanalytical X-Pert PRO reflectometer (high tension = 45 kV, current = 40 mA).

These measurements were performed as a function of incident angle (θ), observing the specularly reflected beam as a function of the momentum change perpendicular to the surface ($Q_z = 4\pi\sin\theta/\lambda$).

The XRR data was modelled using the Motofit [19] reflectivity analysis software package running in the IGOR Pro environment. These data were fitted as log(R) vs. Q using a Differential Evolution [20] algorithm, with corrections for a linear background, resolution smearing, and Gaussian roughness at each interface. As a reflectivity instrument, XRR measures the square of the amplitude. Consequently, phase information is lost, and this presents the possibility of being able to develop multiple different models that produce similar reflectivity curves. Given that the wrong physical model is unlikely to provide agreeable fits to different specimens, this issue was mitigated to some extent by measuring and co-refining multiple specimens, and through cross comparison with values provided by ellipsometry. The lack of well-defined stoichiometry in plasma polymers (and the difficulties associated with determining chemical structure of plasma polymers) precluded the use of XRR for determining film density.

Optical methods for surface feature interrogation of pristine and irradiated polyterpenol coated silicon substrates were supported by AFM (NT-MDT NTEGRA Prime), with subsequent data analysis undertaken using the Nova software package. The instrument was fitted with an NSG10 probe (255 kHz cantilever resonant frequency, 11.5 Nm^{-1} force constant, 3:1 tip aspect ratio and 10 nm curvature radius). Scans were undertaken in tapping mode to eliminate lateral tip-sample forces and limit the formation of inelastic specimen deformations. No AFM-specific specimen preparation was performed prior to undertaking the measurements, and scans were obtained at 3×3 µm resolution to reveal nano-scale features.

3.2 Optical properties

A J.A. Woollam variable angle spectroscopic ellipsometer (VASE) was used to probe specimen optical properties, including the complex refractive index $N(\lambda)$ = $n - ik$. Data was collected across the 250 – 1000 nm wavelength region and at five angles of incidence (50 - 70°, in increments of 5°). Data analysis and modelling was carried out using the WVASE32 software package, following

supplier recommended procedures outlined within the software package manual. Specifically, specimens were modelled using a stratified model consisting of si_jaw, sio2_jaw, and Cauchy components to model the silicon substrate, oxide, and polyterpenol thin film layers respectively. The optical constants of the silicon substrate and oxide layer were approximated using literature values contained within the software package (i.e., si_jaw and sio2_jaw respectively), and the good fit between the substrate experimental data and model fit obviated the need to adjust the literature values.

The optical constants of the polyterpenol thin films were obtained by fitting a Cauchy function to the polymeric layer experimental data across the measured spectral range. Strong parameter correlation precluded simultaneous fitting of both the film's thickness and complex refractive index. Thus, the spectral range was reduced to 400 – 1000 nm (over which the extinction coefficient k is assumed to equal zero), and normal fitting was performed solely for the layer's thickness, long-wavelength asymptotic index (A_n), and the (B_n) dispersion term. Thereafter, point-by-point fitting was undertaken for n and k across the entire measured spectral range. The Cauchy function was then converted to a GenOsc by fitting with two Gaussian oscillators, with specific fit parameters including the amplitude (A), centre energy (E_c), and broadening (B).

4. Results and discussion

4.1 Surface topography - AFM

AFM imaging in *Figure 1* details the progression in surface pore density (i.e., number of pores/unit of surface area) as a function of fluence. *Figure 1A* shows the surface profile of pristine polyterpenol films, and *Figure 1B* shows the formation of discreet pores following irradiation to a fluence of 1×10^{10} ions/cm^2. Irradiation to the fluence of 1×10^{12} ions/cm^2 resulted in significant etching of and damage to the polymer film, coupled with the elimination of discernible discreet ion tracks.

The well-defined geometry of entry tracks, coupled with the ability to control surface pore density by varying the ion fluence, highlights the prospective application of ion beam irradiation to polyterpenol thin films for the production of nanoporous surfaces and membranes. Other researchers have demonstrated

that these entry tracks and latent ion tracks beneath the polymer surface can be converted into uniform cylindrical channels using chemical etching processes such as immersion in NaOH solution [21, 22]. Such ion track technology has found industrial application in filters (Whatman, Trackpore, Oxyphen) and printed circuit boards (IST) [23], with active ongoing research in the fields of controlled drug release and nanotube technology [24-26].
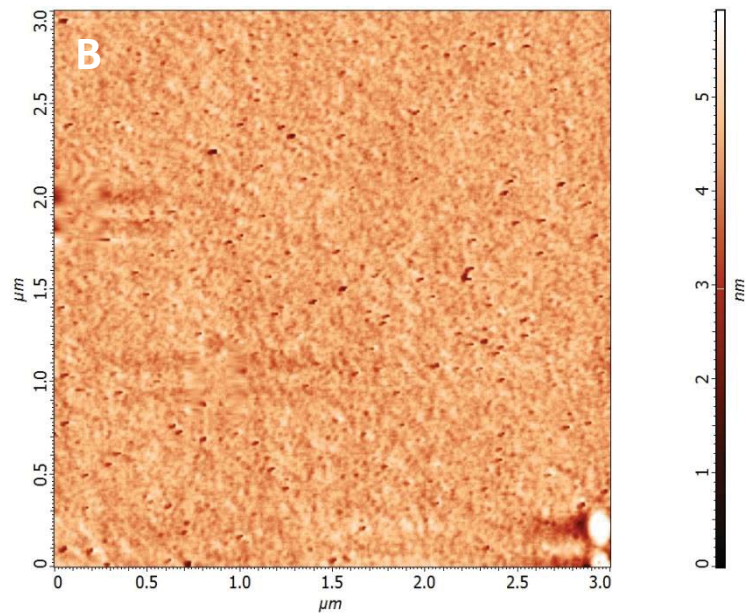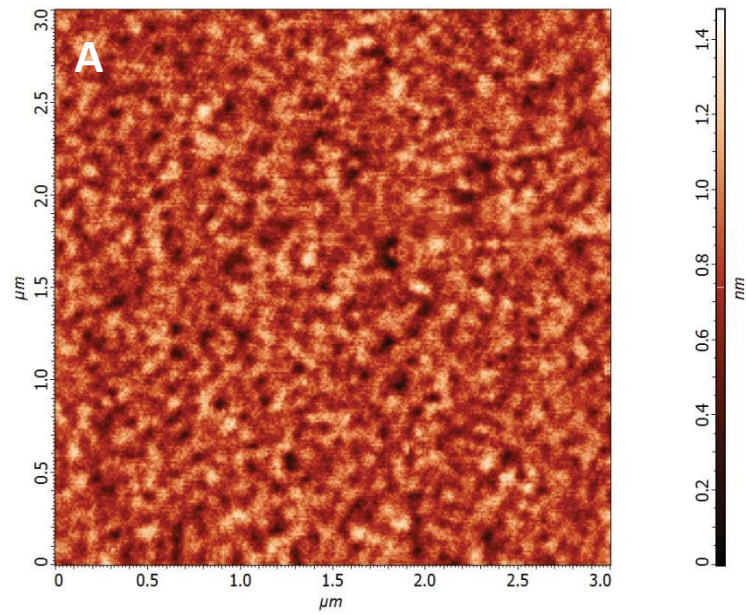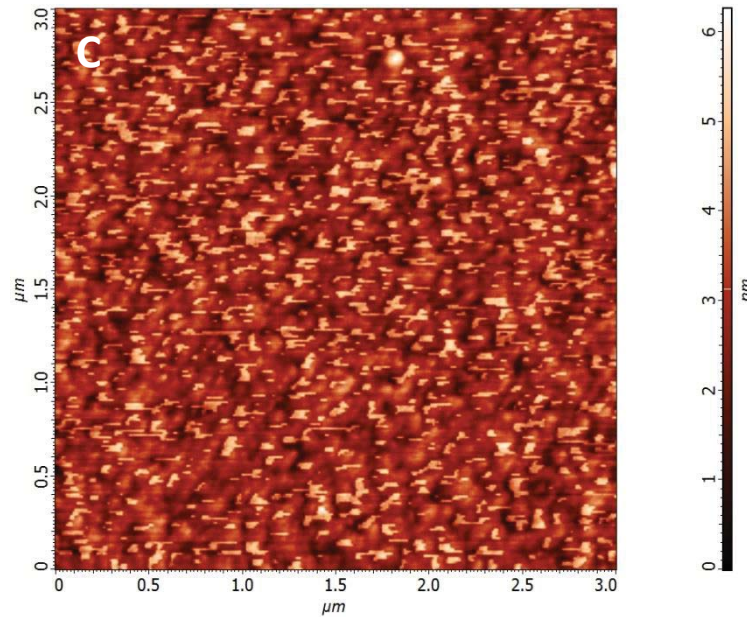
Figure 1. Surface profile of pristine polyterpenol **(A)**, and thin films irradiated at fluences of 1×10^{10} **(B)**, 1×10^{12} **(C)**

Specimen irradiated at a fluence of 1×10^{10} ions/cm^2 exhibited a surface skewness value less than 0, indicating that the height profile is dominated by troughs (representing the pores exhibited in *Figure 1B*). Kurtosis (R_{kur}) values, found to be greater than 3, indicate that deviations in the surface profile are primarily the result of a sparse number of high-magnitude deviations. Taken together, these measures indicate that these specimen exhibit a dominance of troughs (relative to peaks), which may be readily explained by the relatively scarce presence of ion tracks, resulting in subsequently small deviations from the planar nature of the specimen. Irradiation at maximum fluence, 1×10^{12} ions/cm^2, produced specimens exhibiting positive skewness, and a small degree of positive kurtosis. These findings indicate that height deviations from the mean are dominated by peaks, and that these deviations are of a modest though numerable nature.

Visual inspection of the pristine specimen demonstrates the pin-hole free nature and nano-scale smoothness of the plasma polymerised thin film, whilst the latter two images highlight the high degree of uniformity in pore dispersion or coverage. Average roughness values were found to be 0.19, 0.29, and 0.75 nm for pristine samples, and samples irradiated at 1×10^{10}, and 1×10^{12} ions/cm^2 respectively. The increase in roughness from the pristine sample to the sample irradiated at the lower fluence value can be explained by the small number of pores in the

latter contributing an associatively small number of sampling counts at the lower height value. The progressive increase in surface roughness from the pristine sample through to the sample irradiated at the maximum fluence is characteristic of ablation induced by ion beam irradiation at high fluence. In *Figure 1 (C)* we observe significant degradation of the polymer film, coupled with an increase in surface roughness relative to the pristine sample. The degradation may be prospectively attributed to significant carbonisation of the specimen [27], resulting from excessive desorption or evolution of hydrogen and heavier molecules brought about by the greater irradiation fluence [28]. The observed variations in surface topography (predominantly manifested as increased surface roughness) brought about by the ion irradiation may prospectively enhance polyterpenol's adhesive properties in a similar fashion to that observed for other forms of ionising radiation [29, 30]. This may have important implications for bonding processes between the treated polymer and metallic electrodes or contacts, resulting, in turn, in improved performance of electronic devices incorporating the polymer [27].

4.2 Optical properties – ellipsometry

Refractive index and extinction coefficient values shown in *Figure 2* reveal that both the pristine and irradiated thin films are optically transparent across the spectral range investigated, indicating that these films may be suitable for applications relating to the protective encapsulation of various devices (including circuit boards and organic photovoltaics). The pristine specimen exhibited a refractive index and extinction coefficient comparable to those obtained previously [31], and irradiation at 1×10^{10} ions/cm^2 produced a refractive index comparable to that of the pristine specimen (i.e., both on the order of n = 1.55 at 500 nm). Subsequent irradiation at 1×10^{12} ions/cm^2 resulted in a decrease in refractive index to n = 1.52 at 500 nm.
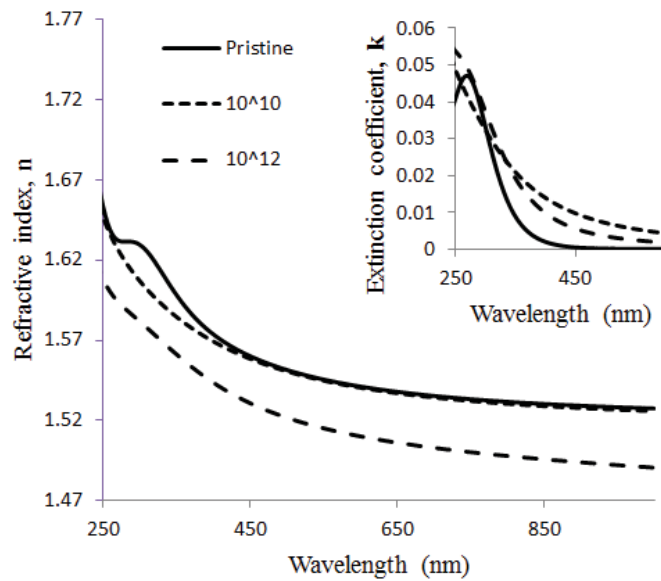
Figure 2. Refractive index and extinction coefficient (insert) for pristine and irradiated polyterpenol thin films

Whilst uncertainty continues to surround the matter of attributing variations in optical properties to either electronic or nuclear energy transfer mechanisms [32, 33], the optical findings presented above have been tentatively rationalised with respect to a number of key processes. Ion irradiation is known to lead to increased densification of the polymeric material resulting from dehydrogenation of the material and the subsequent increase of crosslinking within the penumbra. This, coupled with the formation of conjugated double and triple bonds [1], results in increased material density and an associated increase in refractive index. With this in mind, the minimal variation in refractive index exhibited by specimens irradiated at the lowest fluence can be attributed to the small extent of either increased void fraction and/or increased optical densification.

The substantial decrease in refractive index exhibited by specimens irradiated at the greatest fluence may be explained by the extensive density of entry and latent ion tracks, leading to an increased incorporation of void fraction within the material following the development of chain-scissions and ejection of polymeric material in the wake of the ions, which is further exacerbated by the thinness of the films. This void (or air) content has a substantially reduced refractive index relative to that of the polymer, which manifests as a reduced refractive index for the entire thin film.

These findings substantiate the capacity for ion irradiation to selectively modify the refractive index of plasma polymerised thin films. This indicates that it may be possible to employ ion irradiation processed plasma-polymers in the development of passive optical devices that incorporate waveguides accommodating a variety of different wavelengths (as determined by the waveguide's refractive index) [27].

4.3 *Surface and sub-surface topography - XRR*

Figure 3 represents the log(R) vs. Q/A^{-1} relationship for both a pristine polyterpenol thin film, and a film irradiated at a fluence of 1×10^{12} ions/cm^2. The figure clearly depicts the plateau at log(R) = 0 for incident X-ray angles below θ_c, for which total internal reflection occurs and reflectivity is held constant at R = 1. Exceeding θ_c results in a decrease in intensity of R (as $\sim Q_z^{-4}$), and this "Fresnel" reflectivity is furthermore overlaid with Kiessig fringes (or oscillations) resulting from interference between radiation reflected from the superstrate-polymer interface, and the polymer-substrate interface.

The period of these fringes (given as ΔQ_z) facilitated determination of the thickness (d) of the films by $d \approx 2\pi/\Delta Q_z$. XRR modelling revealed strong agreement between XRR and ellipsometry findings with respect to film thickness, with XRR thickness values approximating those obtained via ellipsometry to within a maximum variation of 3 nm. Additional modelling of the reflectivity data permitted the calculation of interfacial roughness (σ) between each of the stratified layers present within the specimen. Representative film roughness values provided by XRR modelling were found to deviate up to ± 1 nm from those provided by AFM, whereby the discrepancy between these two can be attributed to the disparity in the surface area probed by each instrument (i.e., 1×1 cm area for XRR, and 3×3µm for AFM).
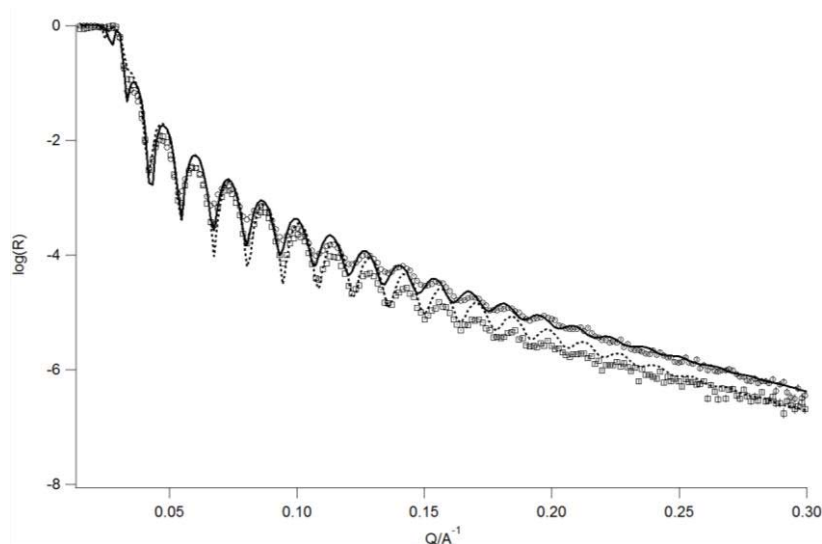
Figure 3. Representative XRR spectra for a pristine polyterpenol thin film, and a film irradiated to a fluence of 1×10^{12} ions/cm^2. Circles and squares represent the experimental data, and the solid and dashed lines are the calculated reflectivity obtained from the structural model (for the pristine and irradiated films respectively)

A summary of the key XRR findings are presented in *Table 1* below, detailing film thickness, scattering length density (SLD), and film surface roughness. The findings confirm the fabrication of thin films of less than 50 nm, and support the AFM findings which indicate an increase in surface roughness with increasing ion fluence. The decrease in SLD at the maximum ion fluence (representing a decrease in film density) further supports the assertion that the decrease in refractive index at this fluence may be attributed to an increase in the film's void content.

Table 1. Summary of XRR findings

Specimen	Film thickness (nm)	SLD	Roughness (superstrate-polymer interface) (nm)
Pristine Polyterpenol	43.99 ± 1.96	12.9 ± 0.9	0.49 ± 0.01
1×10^{10} ions/cm^2	46.31 ± 0.75	13 ± 1	0.52 ± 0.03
1×10^{12} ions/cm^2	42.62 ± 2.03	9.81 ± 0.07	1.12 ± 0.00

The ability of XRR to probe features at the interface between stacked layers was also capitalised upon to ascertain the substrate-polymer interfacial roughness, which was compared with that of the uncoated pristine substrate surface. In both instances, a roughness value on the order of 5Å was obtained, indicating that the plasma deposition process (and its competitive ablation process) brought about no detectable roughening of the substrate surface.

5. Conclusion

In this study we have demonstrated that 50 MeV I^{10+} irradiation of plasma-polymerised polyterpenol thin films can be employed to modify the material's optical properties (producing a substantial reduction in refractive index across all investigated wavelengths for specimens irradiated at 1×10^{12} ions/cm^2) and surface architecture (including the incorporation of nanopores, or substantial material etching). These findings indicate that SHI irradiation of plasma-polymers may be employed to fabricate materials suitable for use in membranes, nanotube-templates, and passive optical devices.

References

1.   E.H. Lee, *Ion-beam modification of polymeric materials - fundamental principles and applications.* Nuclear Instruments and Methods in Physics Research Section B: Beam Intereactions with Materials and Atoms, 1999. 151: p. 29.

2.   A.K. A. Tripathi, F. Singh, D. Kabiraj, D.K. Avasthi, J.C. Pivin, *Ion irradiation induced surface modification studies of polymers using SPM.* Nuclear Instruments and Methods in Physics Research Section B: Beam Intereactions with Materials and Atoms, 2005. 236: p. 186.

3. V.S.J. N.L. Mathakari, D. Kanjilal, V.N. Bhoraskar, S.D. Dhole, *Surface and structural changes in polyimide by 100 MeV Ag7+ ion irradiation.* Surface and Coatings Technology, 2009. 203: p. 2620.

4. G.R.R. E.H. Lee, L.K. Mansur, *Super-hard-surfaced polymers by high-energy ion-beam irradiation.* Trends in Polymer Science, 1996. 4(7): p. 229.

5. V.I.F. V. Ya. Kabanov, B. G. Ershov, A. I. Polikarpov, D. P. Kiryukhin, P. Yu. Apel, *Radiation Chemistry of Polymers.* High Energy Chemistry, 2009. 43(1): p. 5.

6. C. Dekker, *Solid-state nanopores.* Nature Nanotechnology, 2007. 2: p. 209.

7. P.Y. Apel, *Swift ion effects in polymers: industrial applications.* Nuclear Instruments and Methods in Physics Research Section B: Beam Intereactions with Materials and Atoms, 2003. 208: p. 11.

8. M. Ulbricht, *Advanced functional polymer membranes.* Polymer 2006. 47: p. 2217.

9. H. Yasuda, *Plasma Polymerization.* 1985, Orlanda, FL: Academic Press Inc.

10. H. Biederman, *Polymer films prepared by plasma polymerization and their potential applications.* Vacuum, 1987. 37(3-4): p. 367.

11. F.F. Shi, *Recent advances in polymer thin films prepared by plasma polymerization: Synthesis, structural characterization, properties and applications.* Surface and Coatings Technology, 1996. 82: p. 1.

12. S.W. Andy Brooks, Gareth Hennighan, Tin von Werne, *Plasma Polymerization: A Versatile and Attractive Process for Conformal Coating*, in *Proceedings of SMTA International.* 2012: Orlando, Florida.

13. S.-W.S. Kyu-Hyun Hwang, Eun Jung, Heeyeop Chae, Sung Min Cho, *Plasma-polymerized n-hexane and its utilization as multilayer moisture-barrier film with aluminium oxide.* Korean Journal of Chemical Engineering, 2013. 31(3): p. 528.

14.   J. Friedrich, *Mechanisms of Plasma Polymerization - Reviewed from a Chemical Point of View.* Plasma Processes and Polymers, 2011. 8: p. 783.

15.   K. Bazaka and M.V. Jacob, *Synthesis of radio frequency plasma polymerized non-synthetic Terpinen-4-ol thin films.* Materials Letters, 2009. 63: p. 1594.

16.   K. Bazaka and M.V. Jacob, *Post-deposition ageing reactions of plasma derived polyterpenol thin films.* Polymer Degradation and Stability, 2010. 95(6).

17.   M.V. Jacob, et al., *Electron-blocking hole-transport polyterpenol thin films.* Chemical Physics Letters, 2012. 528.

18.   K. Bazaka, et al., *Plasma-Enhanced Synthesis of Bioactive Polymeric Coatings from Monoterpene Alcohols: A Combined Experimental and Theoretical Study.* Biomacromolecules, 2010. 11: p. 2016.

19.   A. Nelson, *Co-refinement of multiple-contrast neutron/X-ray reflectivity data using MOTOFIT.* Journal of Applied Crystallography, 2006. 39(2): p. 273.

20.   K.P. Rainer Storn, *Differential Evolution - A Simple and Efficient Heuristic for Global Optimization over Continuous Spaces.* Journal of Global Optimization, 1997. 11(4): p. 341.

21.   A.S. P. Apel, R. Spohr, C. Trautmann, V. Vutsadakis, *Tracks of very heavy ions in polymers.* Nuclear Instruments and Methods in Physics Research Section B, 1997. 131(1-4): p. 55.

22.   I.V.B. P.Yu. Apel, V.R. Oganessian, O.L. Orelovitch, C. Trautmann, *Morphology of latent and etched heavy ion tracks in radiation resistant polymers polyimide and poly(ethylene naphthalate).* Nuclear Instruments and Methods in Physics Research Section B, 2001. 185(1-4): p. 216.

23.   R. Spohr, *Status of ion track technology - Prospects of single tracks.* Radiation Measurements, 2005. 40(2-6): p. 191.

24.   R.L. Clough, *High-energy radiation and polymers: a review of commercial processes and emerging applications.* Nuclear Instruments and Methods in Physics Research Section B, 2001. 185: p. 8.

25. S.D. L. Piraux, J.L. Duvail, A. Radulescu, S. Demoustier-Champagne, E. Ferain, R. Legras, *Fabrication and properties of organic and metal nanocylinders in nanoporous membranes.* Journal of Materials Research, 1999. 14(07): p. 3042.

26. S.K. Chakarvarti, *Track-etch membranes enabled nano-/microtechnology: A review.* Radiation Measurements, 2009. 44: p. 1085.

27. D.M. Ruck, *Ion induced modification of polymers at energies between 100 keV and 1 GeV applied for optical waveguides and improved metal adhesion.* Nuclear Instruments and Methods in Physics Research Section B, 2000. 166: p. 602.

28. J.S. Dorothee M. Ruck, Norbert Deusch, *Ion irradiation induced chemical changes of polymers used for optical applications.* Nuclear Instruments and Methods in Physics Research Section B, 1997. 131(1-4): p. 149.

29. A.A. Olgun Güven, Erdal Tan, *An atomic force microscopic study of the surfaces of polyethylene and polycarbonate films irradiated with gamma rays.* Radiation Physics and Chemistry, 1997. 50(2): p. 165.

30. G.K.W. H. Kupfer, *Plasma and ion beam assisted metallization of polymers and their application.* Nuclear Instruments and Methods in Physics Research Section B, 2000. 166: p. 722.

31. K. Bazaka and M.V. Jacob, *Synthesis of radio frequency plasma polymerized non-synthetic Terpinen-4-ol thin films.* Materials Letters, 2009. 63(18-19).

32. M.M. D. Fink, T. Lewis, P. Chadderton, H. Cannington, R.G. Elliman, D.C. McDonald, *Optically absorbing layers on ion beam modified polymers: A study of their evolution and properties.* Nuclear Instruments and Methods in Physics Research Section B, 1988. 32(1-4): p. 125.

33. G.B. J. Devenas, M. Fallavier, *Speculations on a mechanism for the ion beam induced degradation of polyimide.* Nuclear Instruments and Methods in Physics Research Section B, 1989. 39(1-4): p. 796.

4.2 HIGH FLUENCE SWIFT HEAVY ION SYNTHESIS OF NANOCRYSTALLINE AND AMORPHOUS CARBON FROM A PLASMA POLYMERISED POLYTERPENOL THIN FILM PRECURSOR MATERIAL

This paper examined the conversion of polyterpenol thin films into graphitic-polymer nanocomposites following exposure to 55 MeV I^{9+} SHIs at fluences > 10^{13} ions/cm^2. Surface restructuring and morphology was explored with atomic force microscopy and scanning electron microscopy. Retention of polyterpenol's chemical functionalities was verified with Fourier transform infrared spectroscopy, and the presence of nanocrystalline and amorphous carbon was substantiated with vibrational mode data collected via Raman spectroscopy. "High fluence swift heavy ion synthesis of nanocrystalline and amorphous carbon from a plasma polymerised polyterpenol thin film precursor material," has been submitted to the Journal of Applied Polymer Science. This paper involved collaboration with Dr. Rainer Siegele.

HIGH FLUENCE SWIFT HEAVY ION SYNTHESIS OF NANOCRYSTALLINE AND AMORPHOUS CARBON FROM A PLASMA POLYMERISED POLYTERPENOL THIN FILM PRECURSOR MATERIAL

Daniel S. Grant[a], Rainer Siegele[b], Kateryna Bazaka[a,c], Mohan V. Jacob[a,*]

[a] College of Science and Engineering, James Cook University, Townsville, Queensland 4811, Australia

[b] Institute for Environmental Research, Australian Nuclear Science and Technology Organisation, Lucas Heights, New South Wales 2234, Australia

[c] School of Chemistry, Physics, and Mechanical Engineering, Queensland University of Technology, Brisbane, Queensland 4000, Australia

* Corresponding author. Tel: +61-7-47814379 E-mail: mohan.jacob@jcu.edu.au

Abstract

Graphitic-polymer nanocomposites with nanocrystalline and amorphous carbon phases were prepared by swift heavy ion irradiation of polyterpenol thin films synthesised from an environmentally sustainable precursor by radio-frequency plasma enhanced chemical vapour deposition. Atomic force microscopy and scanning electron microscopy revealed fluence-dependent surface restructuring of the thin films leading to the formation of interconnected island structures, with no discernible delamination from the underlying electrically conductive aluminium substrate. Raman spectroscopy confirmed the development of D and G peaks associated with graphitic materials, whilst Fourier transform infrared spectroscopy indicated retention of the plasma polymer's chemical functionalities (including hydroxyl groups) within the material after irradiation. Graphitic-polymer nanocomposite films prepared by this dry and solvent free process have

numerous potential applications in biological assay, organic electronics, and membrane technology.

1. Introduction

Graphitic materials comprised of nanocrystalline and amorphous carbon structures have received considerable scientific interest owing to their unique characteristics that include high tensile strength [1], thermal conductivity [2], electrical conductivity [3], and high surface area [4]. Accordingly, efforts have been made to incorporate carbon based nanostructures and graphitic-polymer composites into a broad range of applications in renewable energy, supercapacitors/energy storage, mobile communications, gas sensing, and bioactive materials [5-8].

These materials have been fabricated using a variety of techniques, including exfoliation [9], pyrolysis chemical vapour deposition [10, 11], and magnetron sputtering [12]. These techniques are, however, often constrained by the need for metal catalysts, special substrate preparation, high processing temperatures or pressures, and complex procedures for transferring the film after synthesis [5, 13, 14].

One dry and low temperature alternative technology for the spatially localised *in situ* production of graphitic materials is that of swift heavy ion (SHI) irradiation of polymeric precursors. SHIs deposit a large amount of energy (upward of several hundred eV/Å) within a cylindrical region along the ion track, and subsequent ionisation processes produce chain scissions, crosslinking, and gas evolution within a modified defect-rich zone [15-18]. Modifications contingent upon the ion penetration depth, radius of the cylindrical ion track zone, and dominance of electronic or nuclear stopping, can be controlled by informed selection of the energy, mass, and fluence of the SHIs [17]. Modified parameters in the polymer's physical and chemical properties include composition, density, molecular weight, solubility, optical bandgap, and electrical conductivity [19-22].

Given its capacity to transform chemical composition and structure, SHI irradiation has been utilised to synthesise and modify a variety of polymeric and graphitic nanostructured materials. For instance, tetrahedral amorphous carbon insulators have been converted into graphitic nanowires and self-aligned structures [18, 23], and ions have been used to slice and weld single walled nanotubes [24]. Nucleation of conjugated carbon clusters has also been induced

in an assortment of traditional polymers, including polyethylene terephthalate (PET), polycarbonate (PC), and polymethylmethacrylate (PMMA), bringing about a consummate transformation and enhancement of their mechanical and electrical properties [25-29].

Contrary to the majority of papers that elucidate interactions between SHIs and comparatively thick (> 10's µm) traditional polymers (such as PET, PC, PMMA, etc.), this study focusses on the application of SHIs to a non-traditional polymeric material synthesised via radio frequency plasma enhanced chemical vapour deposition (RF-PECVD). In this process a variety of reactor configurations (internal/external electrode, inductively/capacitively coupled, etc.) and power sources (dc, ac, pulsed, etc.) have been employed to produce graphene and polymeric pinhole-free thin films with tailorable thickness, surface functionality, complex refractive index, and electrical conductivity [11, 30, 31]. The polymer under investigation in this study, polyterpenol, is a stable plasma polymer [32] that exhibits a diverse range of characteristics that make it suitable for use as an antibacterial coating [33], encapsulating or insulating layer for electronic devices [34, 35], and electron-blocking/hole-transport layer in organic transistors [36]. Low fluence SHI irradiation leading to porous microstructures with a variety of potential applications [37, 38] has already been documented for polyterpenol films irradiated at fluences ranging from 1×10^{10} to 1×10^{12} ions/cm^2 [39]. By increasing the fluence by two orders of magnitude (up to 2×10^{14} ions/cm^2), this study explores the conversion of polyterpenol into a functionalised graphitic-polymer composite incorporating nanocrystalline and amorphous carbon phases.

2. Experimental

Polished silicon wafers (100) were cut to size before being rinsed in acetone, sonicated (double distilled water, 50ºC, 30 min), rinsed in isopropanol, and blown dry. Aluminium layers were then applied to the Si substrates via vacuum coating. Polyterpenol thin films ~ 900 nm thick were deposited over the aluminium layers using capacitively coupled external electrode RF-PECVD (25 W, 60 min) in a custom-made glass reactor chamber. The polyterpenol films were synthesised from the terpinen-4-ol precursor monomer, a terpene alcohol distilled from *Melaleuca alternifolia* oil.

Irradiation was carried out with 55 MeV I^{9+} ions using the 10 MV ANTARES tandem accelerator (ANSTO) over an area of ~ 1 cm^2, with fluence varied from ~ 0.5 - 2×10^{14} ions/cm^2 by controlling the irradiation time. Beam current was kept below ~ 20 nA to minimise thermal heating effects.

The thickness of pristine films was determined via ellipsometry with an M-2000 J.A. Woollam Variable Angle Spectroscopic Ellipsometry instrument [40]. A lack of surface uniformity prohibited reliable determination of the thickness and optical properties of the irradiated films. Surface imaging was performed using a JEOL JSM-6700F scanning electron microscope (SEM) . Pristine polyterpenol films were coated with platinum to facilitate imaging, whilst no conductive coating was required for irradiated samples owing to their enhanced electrical conductivity. Vibrational mode peaks were obtained via Raman spectroscopy using a WITEC CRM200 Raman system with 488 nm (2.54 eV) excitation wavelength. Fourier transform infrared spectroscopy (FTIR) was performed in attenuated total reflectance (ATR) mode with a Perkin Elmer Spectrum 100 spectrometer (range: 4000-1000 cm^{-1}, scan number: 4, resolution: 4.00 cm^{-1}). Atomic force microscopy (AFM) was performed using an NT-MDT NTEGRA Prime instrument (255 kHz cantilever resonant frequency, 11.5 Nm^{-1} force constant, 3:1 tip aspect ratio and 10 nm curvature radius), and analysis was performed with the Nova 1.0.26.1487 software package.

3. Results and discussion

3.1 Scanning electron microscopy

Figure 1 shows SEM images of pristine and irradiated polyterpenol films. Image (a) in Figure 1 reveals the uniform, defect-free and smooth nature of the pristine polyterpenol film following RF-PECVD fabrication. Subsequent SHI irradiation at the lowest applied dose of 0.5×10^{14} ions/cm^2 shows widespread and uniform film restructuring (b). Higher magnification imaging indicates the formation of discrete island hubs interconnected by filaments as the applied fluence is increased from 0.5×10^{14} ions/cm^2 (c) to 2×10^{14} ions/cm^2 (d).
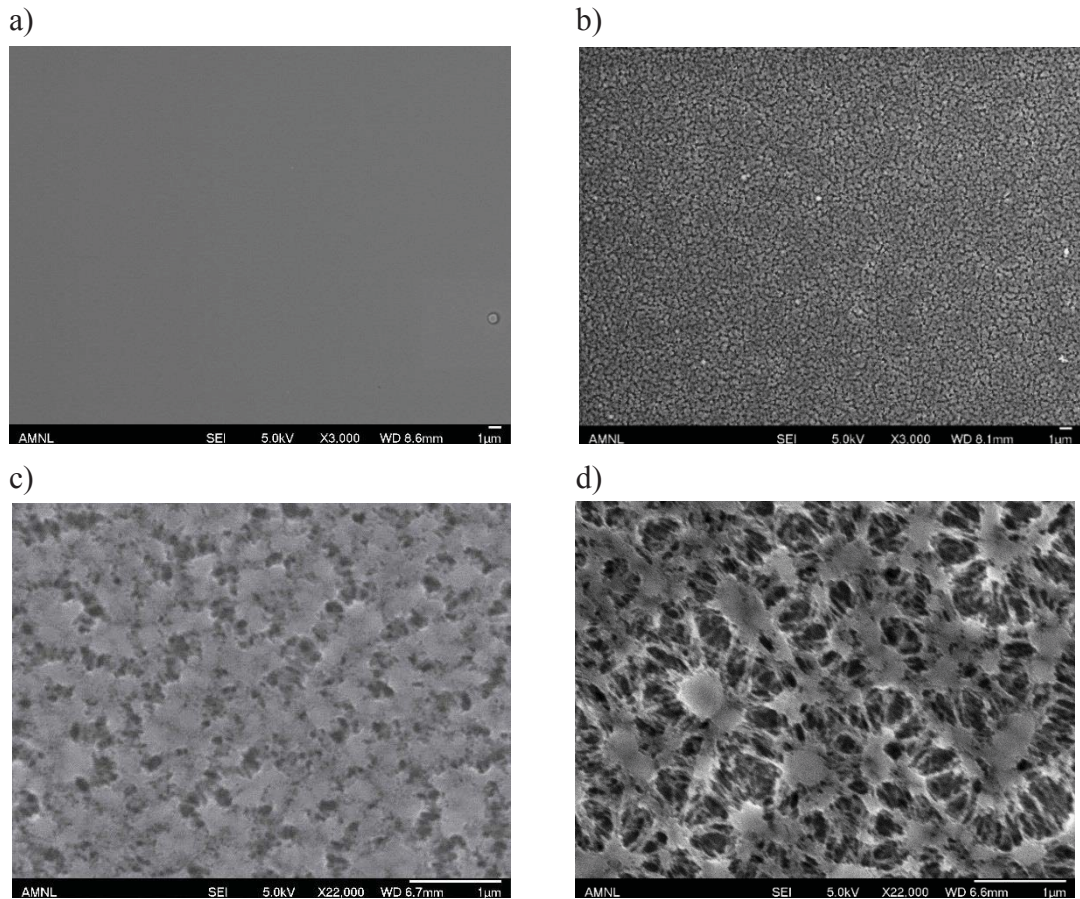
Figure 1. SEM images of pristine polyterpenol (a), and polyterpenol irradiated to 0.5×10^{14} ions/cm^2 (b)-(c), and 2×10^{14} ions/cm^2 (d)

Use of high energy (55 MeV) I^{9+} ions guarantees that virtually all bombarding ions come to rest within the supporting substrate medium [41]. This, coupled with the use of a fluence greater than $\sim10^{13}$ ions/cm^2, indicates that the observed morphological restructuring can be predominantly attributed to electronic energy loss mechanisms (excitation and ionisation) occurring within regions subjected to a multiple track overlap regime [42].

3.2 Raman spectroscopy

Raman spectra for pristine polyterpenol and polyterpenol irradiated to the maximum fluence of 2×10^{14} ions/cm^2 are given in Figure 2.
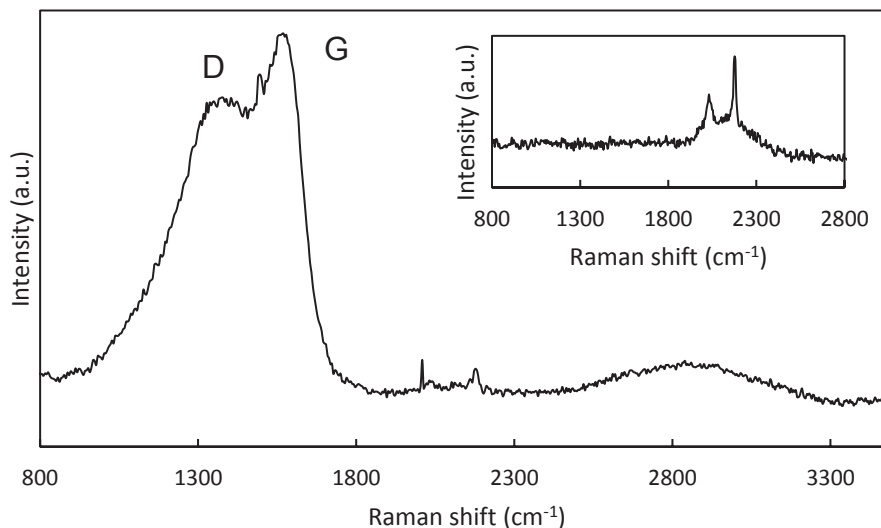
Figure 2. Raman spectra of pristine polyterpenol (insert), and polyterpenol irradiated to 2×10^{14} ions/cm^2

The pristine sample's spectrum is notably devoid of any features commonly associated with graphite or its derivatives. Following irradiation peaks associated with graphitic phases manifest, and peaks observed in the pristine film from ~1900 to 2400 cm^{-1} are also retained with low intensity. The intensity (taken as peak height) and wavenumbers of graphitic peaks were identified following spectra processing that consisted of baseline correction and Gaussian curve fitting (two prominent curves for the D and G peaks, and a small curve at the lower wavenumber shoulder of the D peak). The graphitic index, given as the I_D/I_G ratio, was also determined and used to calculate the nanocrystalline carbon cluster size (L_a) via the Tuinstra-Koenig relation given as [43]:

$$\frac{I_D}{I_G} = \frac{-126 + 0.033\lambda}{L_a} \; (\text{Å}) \qquad (1)$$

Where I_D and I_G are the intensities of the deconvoluted D and G peaks respectively, and λ is the wavelength of the excitation source in Å. Given that the irradiated material is not entirely comprised of nanocrystalline graphite, and that L_a is liable to underestimate the true cluster size due to the dominant effect of small crystallites [44], consideration must be given to the fact that Eq. 1 only provides an approximate indication of cluster size in this instance. An alternative

approach to calculating cluster size using D and G peak areas [45] yielded L_a values ~ 9 Å greater than those provided by Eq. 1 across all fluence values.

Processing results summarised in Table 1 show the presence of D and G peaks at ~ 1384 and 1580 cm^{-1} respectively, and an additional broad band over the region ~2500-3250 cm^{-1} that likely represents a confluence of G', D+G, G+D', and G'' second order modes [46].

Table 1. Peak locations, graphitic index, and approximate carbon cluster size as a function of fluence

Fluence (×10^{14} ions/cm^2)	D location (cm^{-1})	G location (cm^{-1})	I_D/I_G	L_a (Å)
0	-	-	-	-
0.5	1386	1580	1.08	32.4
1	1384	1580	1.19	29.4
2	1382	1580	1.25	28.0

The E_{2g} mode of graphite, given by the graphite G peak, is indicative of the presence of nanocrystalline graphite regions with C-C stretching of sp^2 carbon pairs arranged in rings or chains within the irradiated films. The disorder-induced D peak at ~1384 cm^{-1} corresponds to the breathing mode of A_{1g} and is forbidden in perfect graphite. Resultantly, its presence indicates the formation of sixfold aromatic rings in a disordered structure [47]. The broad width of the D peak, evident upon Gaussian curve fitting, also suggests a distribution of clusters with different orders and magnitudes [47]. The slight red shift of the D peak with increasing fluence represents a decrease in the number of ordered aromatic rings [48], though the magnitude of this shift may be partially offset by the decrease in cluster size which tends to shift D upwards [49, 50]. A low intensity peak at ~ 1100 cm^{-1} was also fitted during Gaussian deconvolution to account for the probable presence of sp^3 bonded diamond nanocrystals and their precursor structures [51, 52].

The graphitic index can be used to provide a measure of the degree of disorder in the film [53], and the observed increase in I_D/I_G with increasing fluence suggests that the higher fluence produces a greater degree of disorder in the films and an associated increase in elastic scattering. This trend also indicates

conversion of the polymer matrix into nanocrystalline graphite, as a predominance of sp^2 amorphous carbon resulting from high defect density would produce a decrease in I_D/I_G [54, 55]. Hence, from the position of the G peak and the graphitic index, we can assert that the irradiated polymer consists of both nanocrystalline and amorphous carbon phases. Furthermore, the increase in graphitic index with increasing fluence suggests an increase in the defect densities facilitated by the greater degree of overlap in defect regions. These subsequently produce more elastic scattering and a drive from the amorphous carbon phase towards nanocrystalline graphite organised in clusters of decreasing dimensions [54, 55].

3.3 Fourier transform infrared spectroscopy

The spectra for pristine polyterpenol, and polyterpenol irradiated to the intermediate fluence of $\sim 1 \times 10^{14}$ ions/cm^2 are provided in Figure 3. Measurements were performed in ATR mode and subjected to ATR correction post-processing. Skewing of peak intensities at the higher wavenumbers in the irradiated film may be attributed to the decreasing pathlength of the sample being probed, coupled with the reduction in film thickness following irradiation [56]. The assignment of excitation frequencies is provided in Table 2.
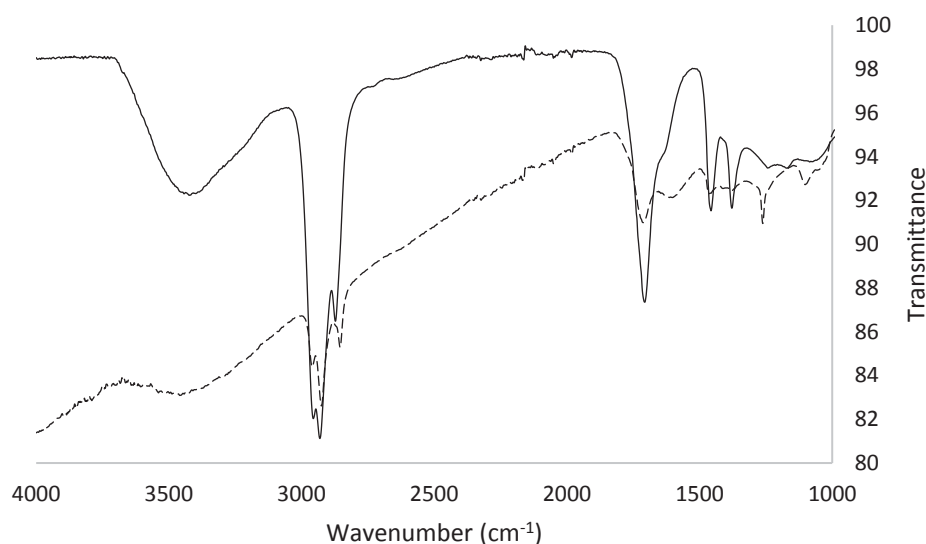

Figure 3. FTIR spectra for pristine polyterpenol (solid line) and polyterpenol irradiated to 1×10^{14} ions/cm^2 (dashed line)

Table 2. FTIR excitation frequency assignment [57, 58]

Assignment	Group frequency (cm^{-1})
Hydroxyl group, H-bonded OH stretch	~3450
Methyl asymmetric C-H stretch	2955, 2930
Methyl symmetric C-H stretch	2875
Alkenyl C=C stretch	~1660
Methyl asymmetric C-H bend	1459
Symmetric C-H bend	1380
C-O stretching of alkyl-substituted ether	1150, 1050

As observed for other conventional polymers [16], homogeneous reductions in peak intensities for post-irradiated polyterpenol films reveal significant elimination of OH and C-H groups, indicating hydrogen and oxygen evolution from the polymer matrix. In conventional polymers this degradation also represents scissioning of the main chain and elimination of monomeric units from the irradiated polymer [27], though this interpretation may not translate to polyterpenol, given the inherently disordered and branched structure of plasma polymers. Dangling bonds formed by the hydrogen and oxygen abstraction provide opportunities for subsequent recombination of carbon into a disordered network of π-conjugated bonds, and hence facilitate the formation of the nanocrystalline and amorphous carbon clusters identified in the Raman spectra. The retention of polyterpenol functional groups following irradiation is particularly desirable, given that these functionalities are influential in the previously stated electrical, encapsulation, and antibacterial properties of polyterpenol thin films. Functional group retention also suggests that the irradiated material is a confluence of polymeric and graphitic phases.

3.4 Atomic force microscopy

Surface morphological parameters obtained from AFM are presented in Table 3, and representative two-dimensional surface images of pristine and irradiated films are provided in Figure 4. As expected from the degree of film restructuring evident in SEM images, AFM confirms a considerable increase in the roughness of the films from R_{RMS} = 0.9 nm for pristine polyterpenol, to R_{RMS} = 20.1 nm for

films irradiated to a fluence of 2×10^{14} ions/cm^2. Skewness indicates almost symmetrical height distribution about the mean for the pristine film (R_{sk} = 0.09), whilst an increasing dominance of surface valleys is indicated by the negative skewness values of the irradiated films as the fluence increases. Initially these valleys manifest as frequent slight deviations (i.e., $R_{ku} < 3$), before the onset of a small number of extreme deviations (i.e., $R_{ku} < 3$) for irradiation at the maximum fluence.

Table 3. Surface morphological parameters as a function of fluence

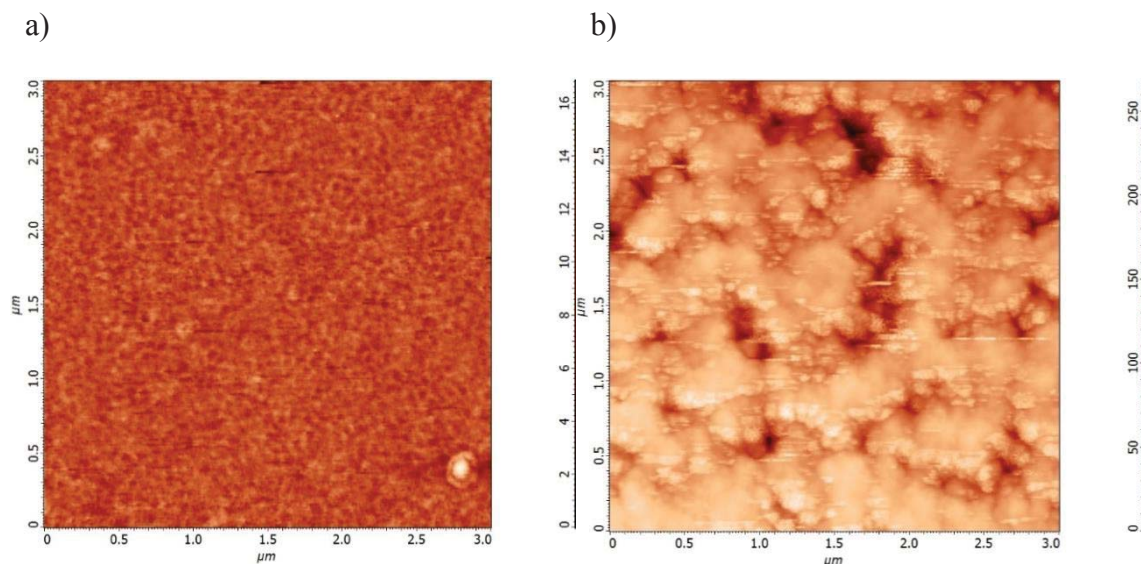| Fluence (×10^{14} ions/cm^2)	Surface parameter			
	Average roughness (R_{av}) nm	RMS roughness (R_{RMS}) nm	Skewness (R_{sk})	Kurtosis (R_{ku})
0	0.6	0.8	0.09	3.2
0.5	6.3	8.0	-0.43	0.4
1	14.7	19.0	-0.72	1.1
2	14.5	20.1	-1.01	3.4

a)   b)

Figure 4. 3×3 µm AFM images of (a) pristine and (b) irradiated (2×10^{14} ions/cm^2) films

Increases in polymer film roughness following irradiation have been observed in other polymer thin films [59], and plays an important role in a variety of physical

processes, including thermal and electrical conduction, and the adhesion strength of metals deposited over ion irradiated polymers [60]. Hence, the post-irradiation formation of nanostructures with an increase in roughness and a probable accompanying increase in exposure of polyterpenol's retained functional groups has potential implications for applications spanning thermal insulation, catalysts, absorbents, and biocompatibility [61-64].

4. Conclusion

In this study plasma polymerised polyterpenol thin films were converted into graphitic-polymer nanocomposite films using high energy SHI irradiation. The resulting thin films exhibited a trend towards the formation of discrete islands interconnected by filamentary structures as the fluence increased. The formation of these structures was accompanied by the nucleation of disordered clusters rich in π-conjugated carbon bonding, displaying a preferential increase in the presence of nanocrystalline graphitic clusters relative to amorphous carbon content with increasing fluence. Chemical functionalities specific to the plasma polymer were also retained within the irradiated material, albeit with reduced prevalence and a clear reduction in hydrogen and oxygen content.

References

1. J.N. Coleman, et al., *Small but strong: A review of the mechanical properties of carbon nanotube-polymer composites.* Carbon, 2006. 44: p. 1624.

2. A.A. Balandin, *Thermal properties of graphene and nanostructured carbon materials.* Nature Materials, 2011. 10: p. 569.

3. S.L. Candelaria, et al., *Nanostructured cardbon for energy storage and conversion.* Nano Energy, 2012. 1: p. 195.

4.   X. Zhao, et al., *Carbon nanosheets as the electrode material in supercapacitors.* Journal of Power Sources, 2009. 194(2): p. 1208.

5.   P. Greil, *Perspectives of Nano-Carbon Based Engineering Materials.* Advanced Engineering Materials, 2015. 17(2).

6.   G. Bongiorno, et al., *Electronic properties and applications of cluster-assembled carbon films.* Journal of Materials Science: Materials in Electronics, 2006. 17: p. 427.

7.   H. Feng, X. Wang, and D. Wu, *Fabrication of Spirocyclic Phosphazene Epoxy-Based Nanocomposites with Graphene via Exfoliation of Graphite Platelets and Thermal Curing for Enhancement of Mechanical and Conductive Properties.* Industrial and Engineering Chemistry Research, 2013. 52: p. 10160.

8.   Y. Sun and Gaoguan, *Graphene/polymer composites for energy applications.* Journal of Polymer Science Part B: Polymer Physics, 2013. 51(4): p. 231.

9.   K.S. Novoselov and A.K. Geim, *The rise of graphene.* Nature Materials, 2007. 6(3): p. 183.

10.   A. Michon, et al., *Graphene growth on AIN templates on silicon using propane-hydrogen chemical vapor deposition.* Applied Physics Letters, 2014. 104(071912).

11.   M. Othman, et al., *Low-temperature plasma-enhanced chemical vapour deposition of transfer-free graphene thin films.* Materials Letters, 2015. 158: p. 436.

12.   F. Guzman-Olivos, R. Espinoza-Gonzalez, and V. Fuenzalida, *Nanocrystalline carbon flakes deposited by RF magnetron sputtering.* Materials Letters, 2016. 167: p. 242.

13.   J. Penuelas, et al., *Surface morphology and characterization of thin graphene films on SiC vicinal substrate.* Physical Review B, 2009. 79(3): p. 033408.

14. D. Presto, V. Song, and D. Boucher, *P3HT/graphene composites synthesized using In situ GRIM methods.* Journal of Polymer Science Part B: Polymer Physics, 2017. 55(1): p. 60.

15. J. Davenas, et al., *Stability of polymers under ionising radiation: The many faces of radiation interactions with polymers.* Nuclear Instruments and Methods in Physics Research Section B, 2002. 191(1): p. 653.

16. T. Steckenreiter, et al., *Chemical modifications of PET induced by swift heavy ions.* Nuclear Instruments and Methods in Physics Research Section B, 1997. 131(1): p. 159.

17. S. Bouffard, B. Gervais, and C. Leroy, *Basic phenomena induced by swift heavy ions in polymers.* Nuclear Instruments and Methods in Physics Research Section B, 1995. 105(1): p. 1.

18. H.-G. Gehrke, et al., *Self-aligned nanostructures created by swift heavy ion irradiation.* Journal of Applied Physics, 2010. 107: p. 094305.

19. J. Davenas, et al., *Hydrogenated carbon layers produced by ion beam irradiation of PMMA and polystyrene films.* Nuclear Instruments and Methods in Physics Research Section B, 1990. 46(1-4): p. 317.

20. O. Puglisi and A. Licciardello, *Anomalous molecular weight distribution in ion irradiated polystyrene.* Nuclear Instruments and Methods in Physics Research Section B, 1994. 91(1-4): p. 436.

21. J.-P. Salvetat, et al., *Onset and growth of conduction in polyimide Kapton induced by swift heavy-ion irradiation.* Physical Review B, 1997. 55(10): p. 6238.

22. D.S.S. M. Mujahid, Shiuli Gupta, D.K. Avasthi, *Estimation of optical band gap and carbon cluster sizes formed in heavy ion irradiated polycarbonate.* Radiation Physics and Chemistry, 2005. 74(2): p. 118.

23. J. Krauser, et al., *Conductivity of nanometer-sized ion tracks in diamond-like carbon films.* Journal of Applied Physics, 2003. 94(3): p. 1959.

24. S. Dhara, *Formation, Dynamics, and Characterization of Nanostructures by Ion Beam Irradiation.* Critical Reviews in Solid State and Materials Sciences, 2007. 32(1-2): p. 1.

25. P. Murugaraj, et al., *The improved electromechanical sensitivity of polymer thin films containing carbon clusters produced in situ by irradiation with metal ions.* Carbon, 2010. 48: p. 4230.

26. D. Fink, et al., *Ion track-based electronic elements.* Vacuum, 2008. 82(9): p. 900.

27. E. Balanzat, N. Betz, and S. Bouffard, *Swift heavy ion modification of polymers.* Nuclear Instruments and Methods in Physics Research Section B, 1995. 105(1): p. 46.

28. R. Miksova, et al., *A study of the degradation of polymers irradiated by C^{n+} and O^{n+} 9.6 MeV heavy ions.* Polymer Degradation and Stability, 2015. 122: p. 110.

29. S. Arif, et al., *Impact of nucleation of carbocaceous clusters on structural, electrical and optical properties of Cr^+-implanted PMMA.* Applied Physics A, 2016. 122(9): p. 866.

30. J. Friedrich, *Mechanisms of Plasma Polymerization - Reviewed from a Chemical Point of View.* Plasma Processes and Polymers, 2011. 8: p. 783.

31. K. Bazaka, M.V. Jacob, and K. Ostrikov, *Sustainable Life Cycles of Natural-Precursor-Derived Nanocarbons.* Chemical Reviews, 2016. 116(1): p. 163.

32. K. Bazaka and M.V. Jacob, *Post-deposition ageing reactions of plasma derived polyterpenol thin films.* Polymer Degradation and Stability, 2010. 95(6).

33. K. Bazaka, et al., *Plasma-Enhanced Synthesis of Bioactive Polymeric Coatings from Monoterpene Alcohols: A Combined Experimental and Theoretical Study.* Biomacromolecules, 2010. 11: p. 2016.

34. K. Bazaka and M.V. Jacob, *Synthesis of radio frequency plasma polymerized non-synthetic Terpinen-4-ol thin films.* Materials Letters, 2009. 63(18-19).

35. M.V. Jacob, et al., *Fabrication and characterization of polyterpenol as an insulating layer and incorporated organic field effect transistor.* Thin Solid Films, 2010. 518(21).

36.   M.V. Jacob, et al., *Electron-blocking hole-transport polyterpenol thin films.* Chemical Physics Letters, 2012. 528.

37.   R. Spohr, *Status of ion track technology - Prospects of single tracks.* Radiation Measurements, 2005. 40(2): p. 191.

38.   S.K. Chakarvarti, *Track-etch membranes enabled nano-/microtechnology: A review.* Radiation Measurements, 2009. 44(9-10): p. 1085.

39.   D.S. Grant, et al., *Ion irradiation as a tool for modifying the surface and optical properties of plasma polymerised thin films.* Nuclear Instruments and Methods in Physics Research Section B, 2015. 360: p. 54.

40.   K. Bazaka, M.V. Jacob, and B.F. Bowden, *Optical and chemical properties of polyterpenol thin films deposited via plasma-enhanced chemical vapor deposition.* Journal of Materials Research, 2011. 26(8): p. 1018.

41.   M.E. Fragalà, et al., *Track Overlap Regime in Ion-Irradiated PMMA.* Journal of Polymer Science Part B: Polymer Physics, 1997. 36(4): p. 655.

42.   E.H. Lee, *Ion-beam modification of polymeric materials - fundamental principles and applications.* Nuclear Instruments and Methods in Physics Research Section B: Beam Intereactions with Materials and Atoms, 1999. 151: p. 29.

43.   F. Tuinstra and J.L. Koenig, *Raman Spectrum of Graphite.* Journal of Chemical Physics, 1970. 53: p. 1126.

44.   A. Cuesta, et al., *Comparative performance of X-ray diffraction and Raman microprobe techniques for the study of carbon materials.* Journal of Materials Chemistry, 1998. 8(12): p. 2875.

45.   L.G. Cançado, et al., *General equation for the determination of the crystallite size La of nanographite by Raman spectroscopy.* Applied Physics Letters, 2006. 88(16): p. 163106.

46.   E.H.M. Ferreira, et al., *Evolution of the Raman spectra from single-, few-, and many-layer graphene with increasing disorder.* Physical Review B, 2010. 82(12): p. 125429.

47. A.C. Ferrari and J. Robertson, *Interpretation of Raman spectra of disordered and amorphous carbon.* Physical Review B, 2000. 61(20): p. 14095.

48. D. Beeman, et al., *Modeling studies of amorphous carbon.* Physical Review B, 1984. 30(2): p. 870.

49. C. Mapelli, et al., *Common force field for graphite and polycyclic aromatic hydrocarbons.* Physical Review B, 1999. 60: p. 12710.

50. M.S. Rafique, et al., *Surface analysis correlated with the Raman measurements of a femtosecond laser irradiated CaF2.* Applied Surface Science, 2012. 258(7): p. 3178.

51. K. Okada, et al., *Effect of the excitation wavelength on Raman scattering of microcrystalline diamond prepared in a low pressure inductively coupled plasma.* Journal of Applied Physics, 2000. 88(3): p. 1674.

52. P.K. Bachmann and D.U. Weichert, *Optical characterization of diamond.* Diamond and Related Materials, 1992. 1(5-6): p. 422.

53. M.S. Dresselhaus, et al., *Defect characterization in graphene and carbon nanotubes using Raman spectroscopy.* Philosophical Transactions of the Royal Society A, 2010. 368(1932): p. 5355.

54. R. Saito, et al., *Raman spectroscopy of graphene and carbon nanotubes.* Advances in Physics, 2011. 60(3): p. 413.

55. M.M. Lucchese, et al., *Quantifying ion-induced defects and Raman relaxation length in graphene.* Carbon, 2010. 48(5): p. 1592.

56. J.M. Chalmers, *Infrared Spectroscopy in Analysis of Polymers and Rubbers*, in *Encyclopedia of Analytical Chemistry*, R.A. Meyers, Editor. 2011, John Wiley and Sons Ltd.

57. J. Ristein, et al., *A comparative analysis of a-C:H by infrared spectroscopy and mass selected thermal effusion.* Journal of Applied Physiology, 1998. 84(7): p. 3836.

58. J.W.A.M. Gielen, et al., *Optical and mechanical properties of plasma-beam-deposited amorphous hydrogenated carbon.* Journal of Applied Physics, 1996. 80: p. 5986.

59. C.R.B. Esteves, et al., *Effect of ion irradiation on the thermal stability of thin polymer films.* Nuclear Instruments and Methods in Physics Research Section B, 2013. 314: p. 71.

60. C.-H. Jung, et al., *The effects of energetic ion irradiation on metal-to-polymer adhesion.* Radiation Physics and Chemistry, 2012. 81: p. 919.

61. J. Cheng, et al., *Immediate fabrication of flower-like graphene oxide by ion beam bombardment.* Applied Surface Science, 2015. 357: p. 1975.

62. K. Bazaka, R.J. Crawford, and E.P. Ivanova, *Do bacteria differentiate between degrees of nanoscale surface roughness?* Biotechnol J, 2011. 6(9).

63. K. Bazaka, et al., *Anti-bacterial surfaces: natural agents, mechanisms of action, and plasma surface modification.* RSC Advances, 2015. 5: p. 48739.

64. E. Erdtman, et al., *A molecular-level computational study of the diffusion and solubility of water and oxygen in carbonaceous polyethylene nanocomposites.* Journal of Polymer Science Part B: Polymer Physics, 2016. 54(5): p. 589.

CHAPTER 5   DENSE PLASMA FOCUS IRRADIATION

This chapter details the discovery of inelastic deformation and surface structure formation in polyterpenol thin films following exposure to dense plasma focus (DPF) irradiation. As a form of non-cylindrical z-pinch plasma, the DPF environment exposes target films to a high-velocity kinetic shockwave, ionisation wavefront, hot plasma, ion beam, and energetic photons. These processes and species bring about a high heating slope and speed in the target film over the course of 10 – 100's of ns. Despite the thermosetting behaviour of plasma polymers, rapid transient thermal treatment delivered by DPF can facilitate thermoplastic behaviour before degradation processes can take effect.

5.1   INELASTIC DEFORMATION OF PLASMA POLYMERISED THIN FILMS FACILITATED BY TRANSIENT DENSE PLASMA FOCUS IRRADIATION

This paper highlights the ability of transient dense plasma focus treatment to induce inelastic deformation in highly crosslinked plasma polymer thin films. The presence and elemental composition of new 'bubble-like' structures formed on the surface of polyterpenol thin films were determined by scanning electron microscopy and energy dispersive X-ray analysis respectively. Pre- and post-irradiated polyterpenol thin film thickness was also determined via spectroscopic ellipsometry and modelling. "Inelastic deformation of plasma polymerised thin films facilitated by transient dense plasma focus irradiation," is published in Materials Research Express. This paper involved collaboration with A/Prof. Rajdeep Rawat.

INELASTIC DEFORMATION OF PLASMA POLYMERISED THIN FILMS FACILITATED BY TRANSIENT DENSE PLASMA FOCUS IRRADIATION

Daniel S. Grant[a], Rajdeep S. Rawat[b], Kateryna Bazaka[a,c], Mohan V. Jacob[a] *

[a] College of Science and Engineering, James Cook University, Townsville, Queensland 4811, Australia

[b] National Institute of Education, Nanyang Technological University, Singapore 637616

[c] School of Chemistry, Physics, and Mechanical Engineering, Queensland University of Technology, Brisbane, Queensland 4000, Australia

* Corresponding author. Tel: +61-7-47814379 E-mail: mohan.jacob@jcu.edu.au

Abstract

The high degree of crosslinking present in plasma polymerised thin films, coupled with their high molecular weight, imbues these films with properties similar to those of thermosetting polymers. For instance, such films tend to be relatively hard, insoluble, and to date have not exhibited plasticity when subjected to elevated temperatures. In this paper it is demonstrated that plasma polymers can, in fact, undergo plastic deformation in response to the application of extremely short-lived thermal treatment delivered by a dense plasma focus device, as evidenced by the evolution of bubble-like structures from the thin film. This finding suggests new avenues for texturing plasma thin films, and synthesising cavities that may find utility as thermal insulators or domains for material encapsulation.

Keywords: thin films; radiation processing; plasma polymer; dense plasma focus; inelastic deformation

1. Introduction

Owing to their high degree of crosslinking, plasma polymers typically exhibit thermal decomposition and degradation in response to the application of heat. This decomposition includes the scissioning of chemical bonds and vaporisation of molecular fragments, leading to significant mass loss and the formation of a brittle and charred carbonised material [1]. Thus, the vast majority of studies investigating the relationship between plasma polymers and temperature have focussed either on the influence of temperature on the growth response of these films [2, 3], or on the thermal stability of films post synthesis [1]. In contrast to prior work, this study focusses on the transient irradiation and thermal treatment of plasma polymer thin films with dense plasma focus (DPF) – a form of non-cylindrical z-pinch plasma device [4]. DPF devices expose target materials to a confluence of short-lived phenomena, including a high-velocity kinetic shockwave, ionisation wavefront, hot plasma, ion beam, extreme ultraviolet rays, and soft/hard X-rays [5]. Resultantly, for the first time it has been possible to demonstrate thermoplastic behaviour in plasma polymers in response to this unique treatment environment.

2. Materials and methods

Prior to deposition the polished silicon wafers were cut to size ($\sim$1×1 cm^2), rinsed in acetone, sonicated for 30 minutes in double distilled water, rinsed in isopropanol, and then blown dry. The precursor monomer, terpinen-4-ol, was introduced to the glow discharge without any additional processing. Film synthesis was undertaken using continuous wave radio frequency (13.56 MHz) plasma polymerisation in a custom-made glass reactor, as detailed elsewhere [6]. Deposition was performed for 60 minutes at 25 W and a pressure of 100 mTorr. The synthesised films were approximately 1170 nm thick, as determined via ellipsometry (J.A. Woollam variable angle spectroscopic ellipsometer).

Following film deposition, the samples were irradiated using a 3.3 kJ UNU/ ICTP DPF device [4] powered by a single 15 kV, 30-µF Maxwell capacitor. Prior to exposing the samples to a transient thermal load in the DPF device, a number of conditioning shots were fired (with the shutter closed and samples shielded from the radiation and hot dense decaying plasma) in order to ensure optimal

focussing/pinching efficiency of the DPF device. Samples were then treated with a single DPF shot in either an Ar or N_2 process gas, at a sample-to-anode distance ranging from 6 to 12 cm. Whilst these processing conditions influenced a number of polymer thin film chemical and physical properties (to be published separately), they exhibited no apparent influence over the prevalence, size, or shape of the bubble structures formed.

Following DPF treatment, scanning electron microscope (SEM) imaging was performed using a JEOL JSM-6700F instrument on platinum coated samples to confirm the presence and visual characteristics of bubble structures formed via inelastic deformation. SEM was coupled with an Oxford Instruments INCA x-sight 7421 for energy dispersive X-ray (EDX) analysis to confirm the carbon composition of the structures, and eliminate misidentification with possible copper impurities (from the DPF device anode) or silicon artefacts (from the substrate).

3. Results and discussion

As an example of the inelastic deformation wrought by DPF treatment, the SEM image coupled with EDX spectra presented in *Figure 1* indicates the presence of the thin film (C and O) over the silicon substrate (*B*), the C, N, and O composition of the bubble with some of the underlying substrate being detected (*C*), and the deficit of plasma polymer underneath the bubble at the locus of venting (*D*).

Figures 1 and *2* indicate that there is no distinct phase delineation or boundaries between the structures formed and the plasma polymer film that they evolve from. These structures exhibit a variety of morphologies including ripples, cracks, and perfectly smooth surfaces, and may be populated with venting pores. They are universally comprised of C and O, with the possible presence of nitrogen in N_2 irradiated films, and trace amounts of Pt arising from the application of a thin conductive coating to aid SEM imaging.

Bubble or blister formation following exposure to radiation has been reported in a number of other studies for traditional (i.e., non-plasma synthesised) polymers. Typically the formation of these structures has been attributed to the scissioning-induced evolution of gases from within the polymer matrix [7-9]. The timescale associated with the evolution of these volatile species ranges from hours up to several days, and the bubbles formed thereafter either show prolific surface coverage/distribution (in response to uniform surface irradiation) or precise spatial confinement (in response to localised radiation delivered by ion or electron beams).
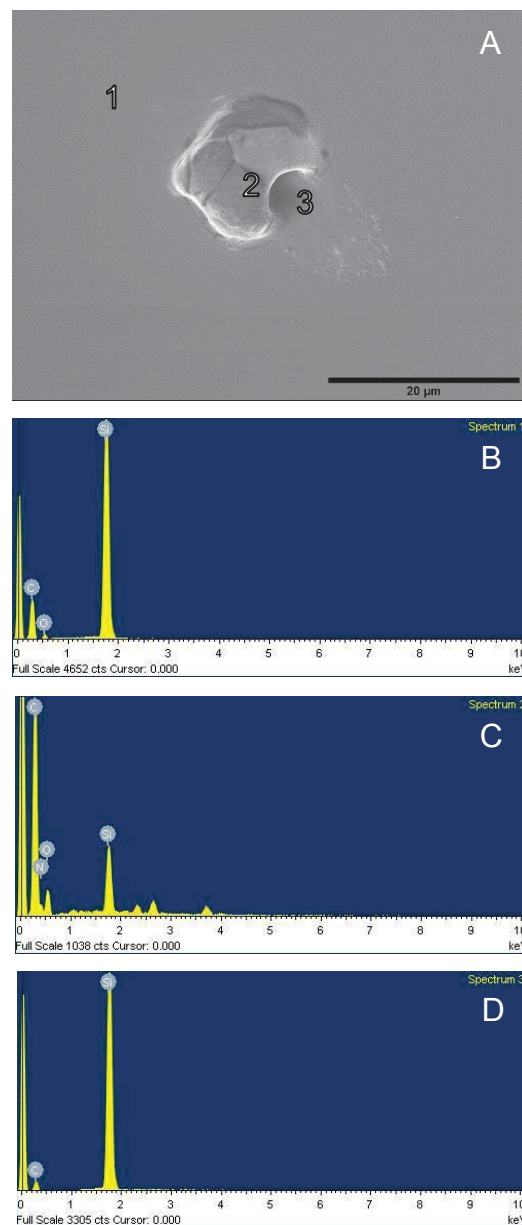

Figure 1. A) SEM image of a DPF induced structure, B) EDX spectrum at location 1, C) EDX spectrum at location 2, D) EDX spectrum at location 3
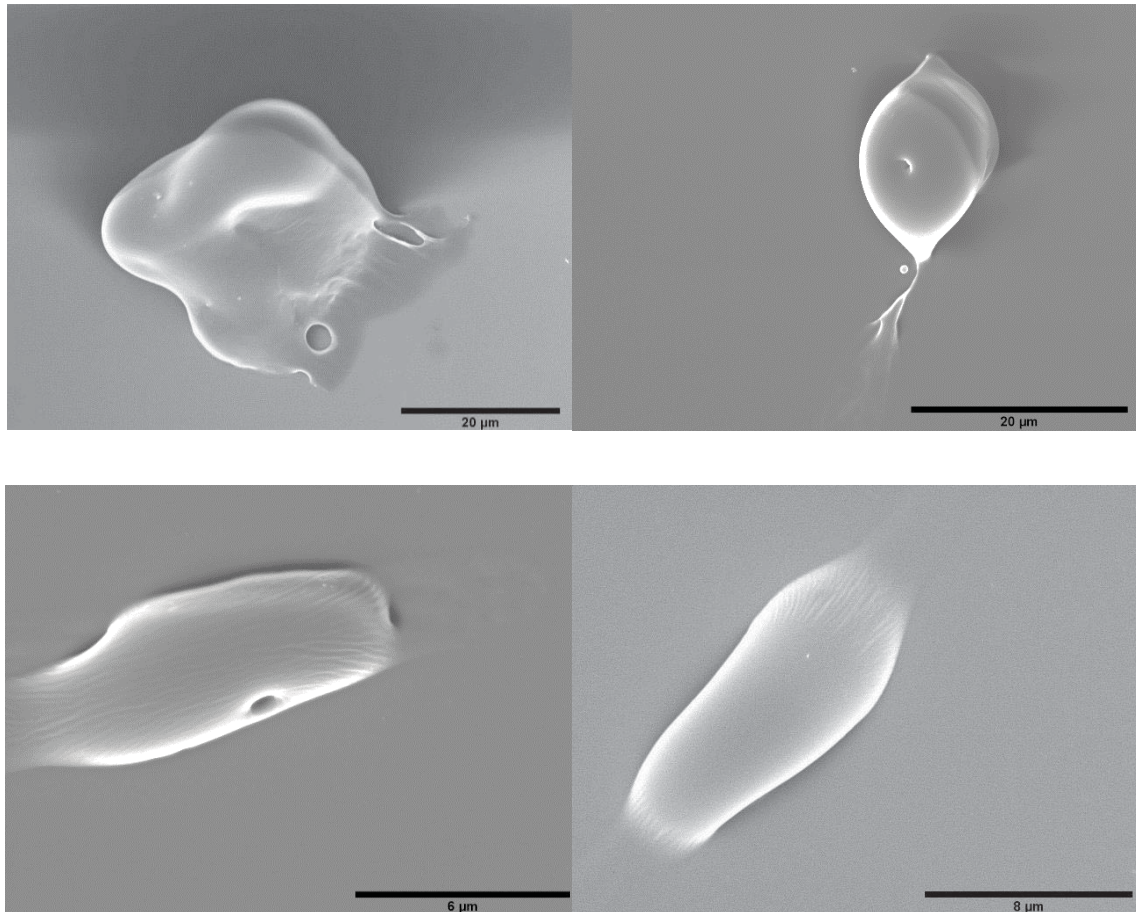
Figure 2. SEM images of DPF irradiation induced structures on separate samples

Given the extremely short DPF irradiation time and low surface density of the structures formed thereafter within the plasma polymer films, we have discounted the bubble growth mechanism proffered by previous studies in favour of an approach centred on the thermal expansion of pre-existing void content within the films as follows:

1. Pre-existing voids are present either within the thin film or at the interface between the film and substrate. [*Figure 3 A*]

2. The films are subjected to DPF irradiation with an approximate duration ranging from tens to hundreds of nanoseconds [10, 11]. In this phase the shock front, ionisation wavefront, plasma, ion beam, and high energy photons serve to bring about a transient heating slope that has been shown to reach as high as ~3600 K/µm and a heating speed that can reach up to ~40 K/ns at a sample-to-anode distance of 4 cm [12]. [*Figure 3 B*]

123

3. This rapid increase in material temperature induces a rise in the pressure of gaseous species present within void spaces. Assuming that the elevated temperature is also liable to exceed the plasma polymers' melting point, the pressure exerted by these species is free to take advantage of the films' transient plasticity to grow the void volume into the observed bubble structures. [*Figure 3 C*]

4. Termination of structure growth occurs in response to the development of defects in the structure's 'skin' (which facilitate gas venting), or as a result of rapid cooling of the polymeric material beneath its melting point, subsequently allowing the structure's cohesive forces to counterbalance the pressure of the energetic gas species. [*Figure 3 D]*
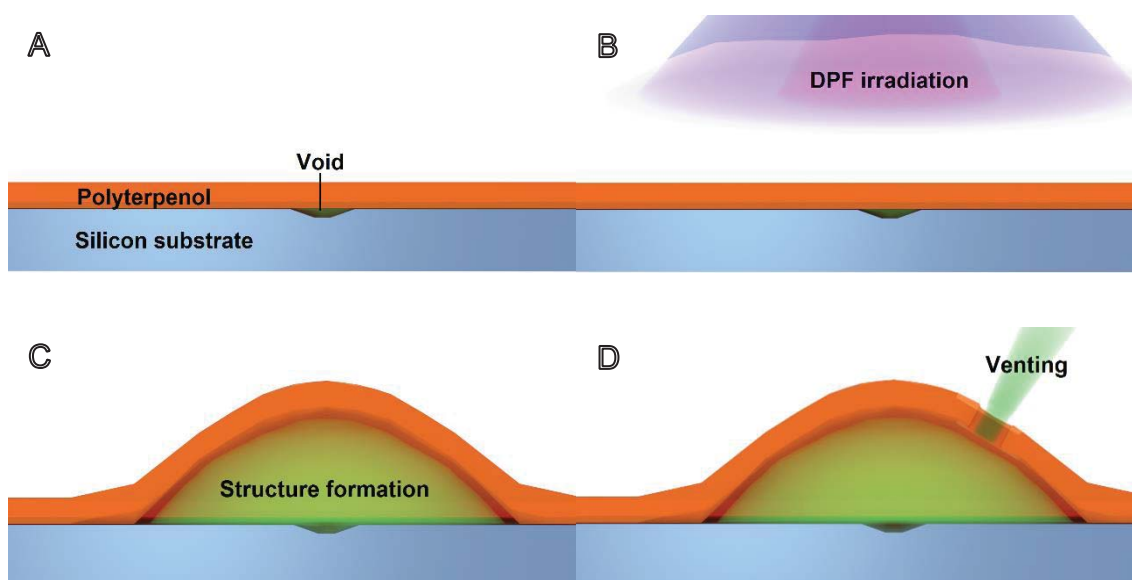
Figure 3. Mechanism of postulated structure formation following transient DPF processing: A) Original void content, B) DPF irradiation, C) Expansion of void content and structure formation, D) Void content venting

In previous studies the application of thermal treatment (starting in the tens of degrees and terminating in the hundreds of degrees Celsius) to plasma polymer thin films has resulted in significant decomposition of the films, with the evolution of volatile degradation products and eventual transformation into a carbonaceous residue [13, 14]. In these studies temperature elevation occurred in controlled increments (e.g., 10 K increments held constant for 5 min to ensure thermal equilibrium) over the course of several hours. This approach to thermal treatment

may have exacerbated film decomposition, given that the rate of thermal decomposition is not only a function of the temperature, but also of the amount and nature of the decomposition processes that proceeded it [15]. Thus, in these studies the possibility of heating-induced plasticity was precluded by the onset of complete decomposition occurring before the thin films could undergo a phase change.

Transient DPF treatment may circumvent a number of factors that contributed to the total thermal decomposition of plasma polymers in prior studies. For example, the extremely high heating slope and rate of heating ensured that the entire film could be elevated above its melting temperature without first being subjected to a protracted temperature rise regime that permits complete decomposition before the melting temperature can be reached. The short duration of the cooling process that followed after intense transient heating also allowed for retention of the plasma polymer before complete decomposition and vaporisation could take place.

4. Conclusion

The action of inelastic deformation, as evidenced by the formation of bubble-like structures, presented itself as an unintended (though in retrospection not unexpected) phenomenon following the exposure of plasma polymerised thin films to DPF irradiation. This development suggests the utility of DPF treatment in destructive identification of plasma polymer void content, relieving internal film mechanical stress, and surface microstructure texturing.

Acknowledgements

References

1.   A. Hollander and J. Thome, *Degradation and Stability of Plasma Polymers*, in *Plasma Polymer Films*, H. Biederman, Editor. 2004, Imperial College Press. p. 386.

2.   F.J. Aparicio, et al., *Wide Range Control of the Chemical Composition and Optical Properties of Propanethiol Plasma Polymer Films by Regulating*

the Deposition Temperature. Plasma Processes and Polymers, 2016. 13: p. 814.

3.   H. Kersten, et al., *The energy balance at substrate surfaces during plasma processing.* Vacuum, 2001. 63: p. 385.

4.   S. Lee, et al., *A simple facility for the teaching of plasma dynamics and plasma nuclear fusion.* American Journal of Physics, 1988. 56(1): p. 62.

5.   R.S. Rawat, *High-Energy-Density Pinch Plasma: A Unique Nonconventional Tool for Plasma Nanotechnology.* IEEE Transactions on Plasma Science, 2013. 41: p. 701.

6.   M.V. Jacob, et al., *Fabrication of a novel organic polymer thin film.* Thin Solid Films, 2008. 516: p. 3884.

7.   Siddhartha, et al., *Formation of Blisters in Kapton Polymer by the Effect of 1.25 MeV Gamma Irradiation.* Journal of Applied Polymer Science, 2011. 120: p. 2928.

8.   A. Sharma, et al., *Effects of 50 MeV Li3+ Ion Irradiation on Kapton Films.* Journal of Macromolecular Science: Part A - Chemistry, 2005. 42(2): p. 149.

9.   S. Unai, et al., *Influence of MeV H+ ion beam flux on cross-linking and blister formation in PMMA resist.* Maejo International Journal of Science and Technology, 2012. 6(01): p. 70.

10. A. Patran, et al., *Spectral study of the electron beam emitted from a 3 kJ plasma focus.* Plasma Sources Science and Technology, 2005. 14(3): p. 549.

11. R. Verma, et al., *Compact sub-kilojoule range fast miniature plasma focus as portable neutron source.* Plasma Sources Science and Technology, 2008. 17(4): p. 045020.

12. G. Sanchez and J. Feugeas, *The thermal evolution of targets under plasma focus pulsed ion implantation.* Journal of Physics D: Applied Physics, 1997. 30(6): p. 927.

13. I. Kuritka, et al., *Thermal stability of plasma deposited polysilanes.* Polymer Degradation and Stability, 2006. 91: p. 2901.

14. K. Bazaka and M.V. Jacob, *Post-deposition ageing reactions of plasma derived polyterpenol thin films.* Polymer Degradation and Stability, 2010. 95(6).

15. C.L. Beyler and M.M. Hirschler, *Thermal Decomposition of Polymers*, in *SFPE Handbook of Fire Protection Engineering* P.J. DiNenno, Editor. 2001, Springer: Quincy, MA.

CHAPTER 6   GAMMA IRRADIATION

Whilst the process employed to synthesise PECVD thin films is inherently sterile, plasma sterilisation has yet to receive international status as an officially regulated and standardised sterilisation technique. Therefore, polyterpenol thin films must demonstrate functional stability following exposure to an approved sterilisation technique before their commercial uptake within the biomedical industry can be considered. As such, this chapter examines the post-irradiation response of polyterpenol thin films to gamma radiation delivered at a variety of doses below, equal to, and above that required to accomplish biological sterilisation.

6.1   ORGANIC BIOELECTRONIC PLASMA POLYMERISED POLYTERPENOL THIN FILMS – PRESERVATION OF PROPERTIES RELEVANT TO BIOMEDICAL AND ORGANIC ELECTRONIC APPLICATIONS FOLLOWING EXPOSURE TO STERILISING DOSES OF GAMMA RADIATION

This paper outlines the capacity for polyterpenol thin films to retain select physical and chemical properties following exposure to sterilising doses of gamma radiation. Film thickness, refractive index, and extinction coefficient were determined with spectroscopic ellipsometry and modelling. Surface morphology was examined with atomic force microscopy, and the preservation of chemical functionalities was verified with Fourier transform infrared spectroscopy. Electrical properties including capacitance, dielectric constant, and resistivity were characterised with LCR meters and high precision source meters. "Organic bioelectronics plasma polymerised polyterpenol thin films – preservation of properties relevant to biomedical and organic electronic applications following exposure to sterilising doses of gamma radiation," is in press with the Journal of Materials Science: Materials in Electronics. This paper involved collaboration with Dr. Justin Davies and Mrs Connie Banos.

ORGANIC BIOELECTRONIC PLASMA POLYMERISED POLYTERPENOL THIN FILMS – PRESERVATION OF PROPERTIES RELEVANT TO BIOMEDICAL AND ORGANIC ELECTRONIC APPLICATIONS FOLLOWING EXPOSURE TO STERILISING DOSES OF GAMMA RADIATION

Daniel S. Grant[a], Kateryna Bazaka[a,b], Justin B. Davies[c], Connie Banos[c], Mohan V. Jacob[a,*]

[a] College of Science and Engineering, James Cook University, Townsville, QLD 4811, Australia

[b] School of Chemistry, Physics, and Mechanical Engineering, Queensland University of Technology, Brisbane, QLD 4000, Australia

[c] Australian Nuclear Science and Technology Organisation, Lucas Heights, NSW 2234, Australia

* Corresponding author: Tel: +61-7-47814379. E-mail: mohan.jacob@jcu.edu.au

Abstract

Plasma polymers such as polyterpenol have been investigated for use as biofunctional coatings, insulating/dielectric layers in electronics, and adhesion promoting interlayers in organic electronics. The commercialisation of plasma polymers in these and other biomaterial-related applications is contingent upon their ability to resist degradation in response to sterilising and potentially damaging ionising radiation, such as gamma rays. Hence, this study focusses on the stability of plasma polymerised polyterpenol thin films following exposure to gamma radiation doses ranging from 0 to 100 kGy. Irradiated films were subjected to ellipsometry, current-voltage, dielectric, Fourier transform infrared,

and atomic force microscopy characterisation. Stability of polyterpenol was evidenced by the observed lack of radiation-induced variation in its complex refractive index, optical band gap, relative permittivity, dc conductivity, surface chemical functionalities, and surface morphology.

1. Introduction

Bioelectronics presents a multitude of opportunities for enhancing patient quality of life and longevity through improved monitoring and treatment driven by a confluence of sensor-driven data collection and intelligent electrical actuators, as evidenced by well-established devices such as implantable pacemakers [1], cochlear implants [2], and glucose monitors [3]. Development of the next-generation of bioelectronic devices is already underway, with research into electronic controlled drug release systems [4], electrode arrays for neuroprosthesis [5], resorbable electronic sensors (for monitoring intracranial pressure, temperature, pH, fluid flow, acoustics, etc.) [6-8], and flexible piezoelectric thin film energy harvesters to power these devices [9]. Successful commercialisation of these advanced applications is contingent upon the advent of new materials, including organic bioelectronic materials, that can satisfy a gamut of constraints imposed by both the physical demands of the devices and the biological environments in which they operate, defining the need to simultaneously preserve electronic performance and biological function [7].

For organic bioelectronic materials and devices these constraints manifest in a variety of forms, including the need for biocompatibility [10, 11], surfaces that resist bacteria biofilm formation and ensuing infection [12], clean interfacial boundaries with strong adhesion between layers [5], and biodegradation to obviate secondary surgery [13]. To satisfy these requirements materials are often designed to specifically serve as either device encapsulating layers, or as active components within the bioelectronic device. Encapsulating layers facilitate control over the device's interaction with the biological medium by protecting against biofluid-induced corrosion [5], inhibiting pathogen adhesion and proliferation [14, 15], and mediating immunogenic responses [10]. Active component materials facilitate operation of the device by performing a variety of roles, such as charge carrier transportation or blocking [8], promoting interlayer bonding [16], or acting as dielectrics for capacitors, transistors, and component isolation [17, 18].

The performance and economics of bioelectrionic devices can benefit from the development of a single class of renewable organic bioelectronic materials that can simultaneously satisfy biological and electronic constraints; here, plasma

polymerisation may present as a viable contender for the synthesis of this class of materials. This process employs a cold plasma environment rich in neutral species, metastables, ions with temperatures close to ambient at 300 K, electrons with temperatures in excess of 1×10^4 K, and energetic photons with wavelengths down to the extreme UV region [19]. Precursor monomers introduced into this environment are subjected to ionisation, fragmentation, and recombination begetting polymeric thin film deposition [20]. Contrary to conventional polymers, plasma polymers are not comprised of regularly repeating monomeric units. Instead, they represent a polymeric matrix constructed from fragments of the original precursor/s, with these fragments spanning a spectrum of power-dependent products ranging from almost intact monomeric units, to individual constituent atoms from the original precursor/s. The final result is the formation of a highly disordered and crosslinked hydrogenated carbon structure, with significant presence of trapped free radicals that cannot readily undergo recombination due to reduced chain mobility stemming from extensive crosslinking [21].

Plasma polymerisation technology incorporates several attractive features into a single-step process for thin film organic bioelectronic material synthesis. For example, the presence of high energy ionising species facilitates the destruction of microorganisms, leading to inherent and economical bio-decontamination of material surfaces (including heat-sensitive surfaces) exposed to the non-thermal plasma [22-25]. The films demonstrate conformational coverage, allowing homogeneous or micro/nano-patterned coatings to be applied to devices with irregular geometries, including nails, plates, stents, and meshes [26-29]. Strong adhesion to a wide variety of substrate materials relevant to the biomedical field (including ceramics, metals, and polymers) is also evidenced and made possible by surface cleaning, activation, and formation of covalent bonds induced by the plasma environment. Finally, the type and density of biomedically-relevant chemical functional groups on these pin-hole free films can be selectively tailored by informed selection of deposition conditions, choice of precursor/s, and masking or diffusion gradient techniques [30-33].

The plasma polymer under investigation in this study, polyterpenol, possess properties pertinent to the biological and electronic requirements of organic

bioelectronic materials. Previous studies have provisioned the utility of polyterpenol as: an electrically insulating coating for electrical components [34], electron blocking – hole transport layer in organic electronic devices [35], coating to control magnesium biodegradation [36], and as an antibacterial coating [37]. Polyterpenol also addresses the demand for green chemistry and sustainable production, being synthesised from the natural terpinen-4-ol precursor, a monocyclic terpenoid alcohol extract from *Melaleuca alternifolia* (aka. tea tree oil). Before plasma polymers such as polyterpenol can find commercial success in the field of organic bioelectronics, it must first be shown that these polymers can retain the properties that underpin their organic bioelectronic utility following exposure to a commercial sterilisation technique, such as gamma irradiation.

Gamma irradiation at a standardised dose of ~25 kGy is one of the foremost methods employed in the sterilisation of polymers for pharmaceutical and biomedical applications [38-40]. This approach is used in preference to steam/heat or chemical techniques that can damage the target materials and leave behind harmful residues, or electron beams techniques that may provide unacceptable variation in sterilisation performance depending upon the material's composition [41-43]. As a form of uncharged radiation, gamma rays impart energy to polymeric materials via three dominant mechanisms: photoelectron absorption, pair production, and Compton scattering [44]. These photon-material interactions result (either directly or indirectly) in the subsequent generation of ionised absorber atoms, energetic photo-, recoil- , or Auger electrons, and further photon production from either atomic de-excitation processes or positron annihilation. Species thus formed often possess sufficient energy (i.e., energy > 10 eV) to sever chemical bonds, and resultantly induce crosslinking and chain-scissioning [45-47].

In instances where the rate of crosslinking exceeds that of chain-scissioning, gamma radiation has been shown to enhance the mechanical properties of a wide range of polymer-related materials, including polymer fiber reinforced concrete [48], carbon nanotube reinforced polymers [49], and synthetic biodegradable polymers [50]. Such crosslinking also serves to increase the conductivity of polymer composites, with possible applications in dosimetry [51]. Gamma radiation's capacity to polymerise monomeric units has also been employed to

synthesise polymers with antimicrobial properties [52] and smart biocompatible hydrogels [53]. With respect to crosslinking's complementary process of chain-scissioning, the associated reduction in molecular weight can enhance the workability and incorporation of polymer components into coatings and inks, and polymer recycling outcomes [54]. More often, however, chain-scissioning brings about undesirable degradation in the mechanical, electrical, optical, and chemical properties of the polymer [55-57]. This degradation serves to limit the utility and life expectancy of biomedical polymers subjected to radiation sterilisation processes [58], as evidenced by doses as low as 30 kGy significantly decreasing the duration and uniformity of antibiotic elution from biodegradable polymer composites [59], and irradiation at the standard 25 kGy sterilising dose inducing degradation in the mechanical properties of biodegradable medical polymers [40].

Countering this degradation has necessitated a sustained effort to synthesise and study radiation resistant polymeric materials [60], though this effort has, however, almost completely overlooked the novel class of plasma polymers [61]. In recognition of this oversight, this study seeks to advance the standing of plasma polymerised polyterpenol as a stable organic bioelectronic material by establishing a relationship between sterilising gamma radiation, and those material properties of polyterpenol that are of biological and electronic relevance.

2. Experimental

2.1 Sample fabrication

Metal-insulator-metal (MIM) structures were fabricated on glass substrates, as detailed in Figure 1 (left). The glass substrates (Knittle Glass, standard slides) were cleaned in Extran and distilled water, sonicated for 30 min in distilled water at 50ºC, rinsed in isopropanol, and then blown dry. Following cleaning, conductive aluminium layers (Advent Research Materials AL5020) were deposited onto the glass substrates with a HHV Vacuum coating unit (12A4D). Polyterpenol layers (~ 300 nm thick) were deposited over the aluminium layers using a 13.56 MHz continuous wave capacitively-coupled plasma polymerisation setup detailed in Figure 1 (right). Prior to polymerisation, the custom-made cylindrical glass reactor vessel (length: 0.75 m, internal diameter: 0.07 m) was

flushed with argon gas for 60 s to dislodge loose contaminants and displace atmospheric gas. Terpinen-4-ol sourced from Australian Botanical Products Ltd. was used as the precursor monomer without any supplemental processing, and the plasma polymerisation process was performed for 30 min at an applied power of 25 W and starting pressure of ~ 200 mTorr. Following irradiation, additional aluminium layers were applied over masked polyterpenol layers to complete the MIM structures.

The aforementioned plasma polymerisation process was applied to polished silicon substrates (100) for 60 min at 25 W to prepare ~ 700 nm thick samples for ellipsometry and atomic force microscopy (AFM) analysis. The silicon substrates were rinsed in isopropanol then blown dry before polymer deposition. The same plasma polymerisation regime (i.e., 60 min, 25 W) was applied to 25×5 mm potassium bromide (KBr) discs (International Crystal Laboratories, part: 0002C-133) to prepare samples for transmission Fourier transform infrared (FTIR) spectroscopy analysis.
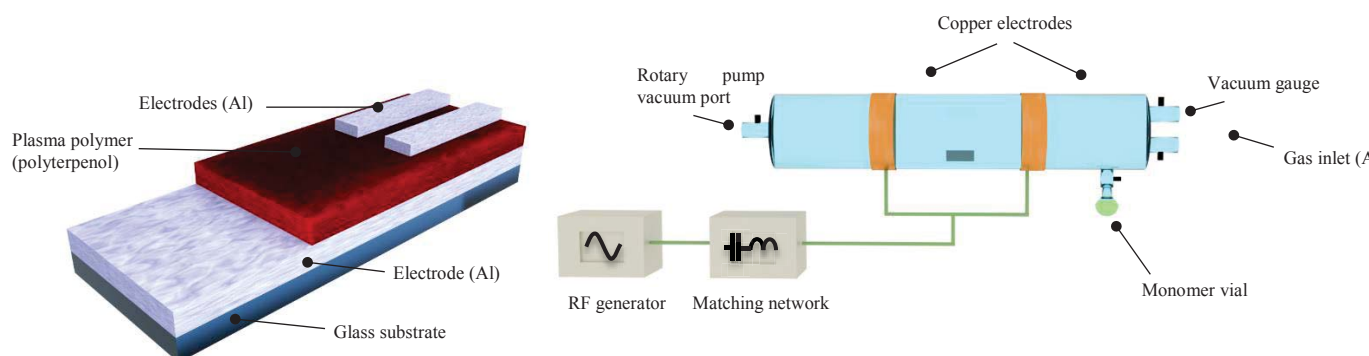
Figure 1. Metal-insulator-metal structure (left), and radio frequency plasma polymerisation setup (right)

2.2 Sample irradiation

Samples were irradiated at doses of 0, 0.1, 1, 10, 25, 50, and 100 kGy using the Gamma Technology Research Irradiator (GATRI) at the Australian Nuclear Science and Technology Organisation (ANSTO). Gamma radiation was provided by Co-60 sources at a dose rate of 1.97 kGy/h under ambient conditions (~ 23 ºC) in air. Dose rates were determined via Fricke dosimeters [62], with the associated uncertainty of 2.0% providing a confidence level of ~ 95%. Whilst

polymers display degradation in response to thermal treatment, oxidation, and hydrolysis [21, 63], prior studies on plasma polymerised polyterpenol thin films have shown minimal aging under ambient laboratory conditions [64]. This, coupled with the use of pristine unirradiated reference samples, allowed any observed variation in film properties to be confidently ascribed to the influence of gamma radiation.

2.3 Sample characterisation

The optical parameters for magnitude ratio (Ψ) and phase difference (Δ) of reflected p- and s-polarised light were obtained on silicon substrate samples with an M-2000 J.A. Woollam Variable Angle Spectroscopic Ellipsometry (VASE) instrument over the wavelength region of 200 – 1000 nm (6.2 – 1.2 eV) at incident angles of 55º, 60º, and 65º. These parameters were then used to construct a model (Cauchy dispersion layer over Si) using WVASE32 software to determine film thickness and complex refractive index (i.e., $\boldsymbol{N} = n + ik$).

Capacitance measurements were performed on the MIM structures using a Hioki 3522-50 LCR HiTESTER with 100 test points over a frequency range of 1 Hz – 10 kHz. Current-voltage characteristics were determined using a Keithley 2636A System SourceMeter over a voltage range of 0.2 – 20 V. Step sizes of ~ 0.2 V were applied over a hold time of 50 ms/point, and current was measured at a range of 1 µA. All electrical characterisation was performed at a temperature of ~ 25ºC.

FTIR transmission scans of the KBr substrate samples were taken with a Perkin Elmer Spectrum 100 spectrometer (range: 4000 – 450 cm^{-1}, scan number: 4, resolution: 4.00 cm^{-1}).

3 × 3 µm tapping mode surface scans of the silicon substrate samples were performed with an NT-MDT NTEGRA Prime atomic force microscope fitted with an NSG10 probe (255 kHz cantilever resonant frequency, 11.5 Nm^{-1} force constant, 3:1 tip aspect ratio, and 10 nm curvature radius). Subsequent data analysis was performed with the Nova 1.0.26.1487 software package.

3. Results and discussion

3.1 Optical properties

Real refractive index (*n*) and extinction coefficient (*k*) components of the complex refractive index at representative doses of 0, 50, and 100 kGy are given as a function of wavelength in Figure 2. Maximum variance in the real refractive index ranged from ~ 1.7 at 200 nm to 1.50 at 1000 nm, and the extinction coefficient varied from ~ 0.1 at 200 nm to 8×10^{-6} at 1000 nm, with neither parameter demonstrating appreciable variability in response to the applied radiation.
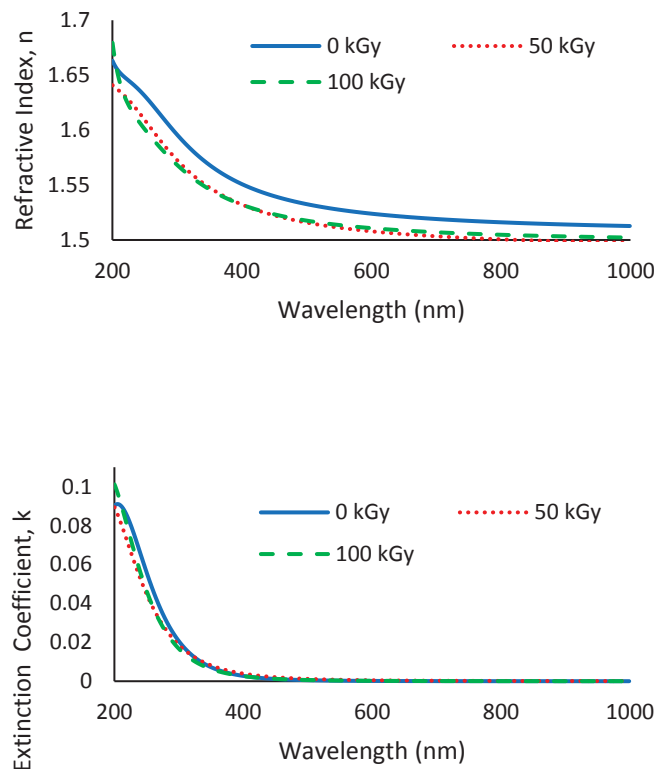
Figure 2. Refractive index (top) and extinction coefficient (bottom) as a function of wavelength for samples irradiated at 0, 50, and 100 kGy

The real refractive index of polymers is dependent upon a number of physical and chemical parameters, including the molecular refraction (*R*), molecular weight *(M)*, and molecular volume *(V)* of the polymer's constituent atomic and molecular units, as represented by the Lorentz-Lorenz equation [65-67]:

$$\frac{n^2-1}{n^2+2} = \frac{R}{M}\frac{M}{V} \quad (1)$$

137

Within amorphous hydrogenated carbon (a-C:H) films, including those synthesised via plasma techniques, it has also been shown that the refractive index depends upon the film's density, and the ratio of sp^3/sp^2 bonds [68, 69]. Given the dependence of *n* on all of these parameters, the negligible variance in *n* indicates that polyterpenol expressed no preferential crosslinking or chain-scissioning in response to the applied gamma radiation, and that the concentration of atomic and molecular groups contributing to the molar refraction (i.e., *R/M*) remained unaltered.

The real refractive index provides critical information about the propagation of light through the polymer and the refraction of light at interfaces between the polymer and materials adjacent to it [70]. As such, it is a defining parameter in the design of polymers for optical waveguides [68, 71], optical lenses [72], encapsulating layers for organic light emitting diodes [73], and photodetectors for biochemical sensing and *in vivo* imaging [74, 75]. The operation of these devices and their protective encapsulating layer frequently calls for the use of low *k* polymers so as to minimise light or signal attenuation. Resultantly, the observed stability of polyterpenol's real refractive index and low extinction coefficient following irradiation suggests that it may be a viable candidate for incorporation into the synthesis of optical biomedical devices.

Extinction coefficient data was further interrogated to yield information about the optical absorption coefficient α by way of the relation [76]:

$$\alpha(\lambda) = \frac{4\pi k}{\lambda}, \ or \ \alpha(v) = \frac{4\pi k}{c/v} \quad (2)$$

The absorption data within the higher energy region was then related to the optical energy gap via the Tauc equation [77]:

$$\alpha(v)hv = B\left(hv - E_{opt}\right)^{m} \quad (3)$$

Where E_{opt} is the optical energy band gap, *hv* is the incident photon energy, *m* represents the form of electronic transition (given as indirect allowed transition with *m* = 2 for polyterpenol [34]) and *B* is a constant related to electrical conductivity, refractive index, and the width of the tail of the localised states.

Equation (3) was rearranged to provide a Tauc plot of $(\alpha h v)^{1/2}$ vs. hv, and a MATLAB program was written to approximate E_{opt} by fitting and extrapolating the linear section of each curve to the energy axis intercept. Representative Tauc plots are provided for polyterpenol irradiated at 0, 50, and 100 kGy in Figure 3.
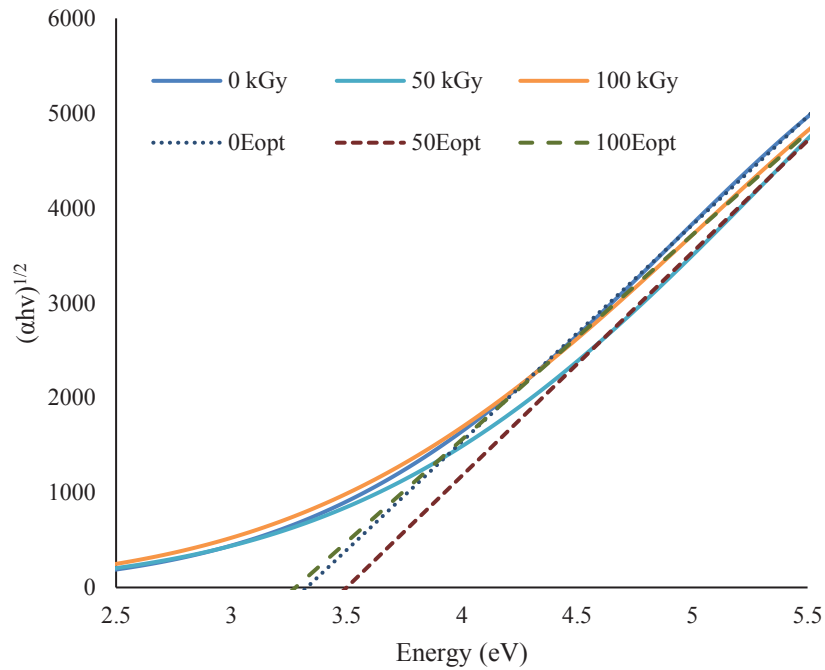

Figure 3. Tauc plot for samples irradiated at 0, 50, and 100 kGy

The optical energy gap provides a measure of the energy at which a rapid increase occurs in the absorption coefficient (i.e., the fundamental absorption edge), owing to the absorption of photons and subsequent promotion of electrons across the fundamental gap from the highest occupied continuous energy level to the lowest unoccupied continuous energy level [78]. Using the Tauc plot method, E_{opt} values ranging from 3.29 to 3.50 eV were observed (see Table 1), suggesting that polyterpenol occupies a middle ground between semiconductor ($E_{gap} < 3$ eV) and insulator ($E_{gap} > 4$ eV) materials [79]. This classification may be subject to change if there exists appreciable disparity between the optical and electronic band gap of polyterpenol.

Table 1. Optical energy gap as a function of dose

Dose (kGy)	0	0.1	1	10	25	50	100
E_{opt} (eV)	3.33	3.29	3.33	3.33	3.35	3.35	3.50

The optical energy gap of organic semiconductors is dependent upon a number of parameters, including their chemical composition, extent of π-conjugation, temperature, and pressure [80]. With environmental factors held constant, the lack of variation in E_{opt} values supports earlier inferences drawn from the stability of the real refractive index – viz. minimal changes occur in polyterpenol's underlying chemical composition and structure following gamma irradiation.

3.2 Dielectric properties

The real part of the relative permittivity, ε_r, is given by [81]:

$$\varepsilon_r = \frac{C}{C_0} \qquad (4)$$

Where C is the experimentally determined capacitance in F, and C_0 is the equivalent capacitance *in vacauo*. C_0 can in turn be calculated from the sample's geometry as $C_0 = \varepsilon_0 A/d$, allowing ε_r at sonic frequencies to be calculated by [81]:

$$\varepsilon_r = \frac{C}{C_0} = \frac{DC}{\varepsilon_0 A} \qquad (5)$$

Where D is the film thickness in m, ε_0 is the permittivity *in vacuo* given as 8.854×10^{-12} F m^{-1}, and A is the cross-sectional area in m^2.

Drawing on optical results presented earlier, the real refractive index of polyterpenol can be related to its relative permittivity and relative permeability (μ_r) by [82]:

$$n = \sqrt{\varepsilon_r \mu_r} \qquad (6)$$

By allowing the relative magnetic permeability of the polymeric material to approximate to 1, the relationship can be rearranged to give ε_r at optical frequencies as:

$$\varepsilon_r = n^2 \qquad (7)$$

Using Equations (5) and (6) the relative permittivity has been calculated at sonic frequencies ranging from 0.1 to 10 kHz, and at optical frequencies representing ultraviolet (400 nm) and infrared (800 nm) wavelengths bounding the visible spectrum, and one wavelength within the visible region (600 nm).

140

Table 2. Relative permittivity from capacitive and optical measurements

Dose (kGy)	Relative permittivity, ε_r					
	Sonic frequencies			Optical frequencies		
	0.1 kHz	1 kHz	10 kHz	375 THz	500 THz	749 THz
0	3.50	3.45	3.39	2.30	2.32	2.41
0.1	3.70	3.64	3.59	2.27	2.29	2.35
1	3.74	3.69	3.64	2.27	2.29	2.36
10	4.19	4.13	4.06	2.27	2.29	2.36
25	4.37	4.25	4.15	2.27	2.29	2.36
50	4.03	3.95	3.87	2.25	2.27	2.35
100	4.06	3.91	3.80	2.26	2.28	2.35

A polymer's relative permittivity depends on factors such as temperature [83], frequency [84], chemical composition [85], and water content [86], and can be decomposed into three contributing components as [87]:

$$\varepsilon_r = \varepsilon_{electronic} + \varepsilon_{ionic} + \varepsilon_{orientational} \quad (8)$$

Stability of polyterpenol's relative permittivity across the sonic range of frequencies may be attributed to low ionic polarization of the film's molecular structure, suggesting that polyterpenol is predominantly apolar [26]. The encroachment of ε_r values into the 3.5 to 5 range does, however, imply some degree of polar nature, which is to be expected given the presence of hydroxyl side groups and trapped free radicals [88]. The contribution of these ionic and orientational components to the relative permittivity decreases with increasing frequency in the sonic range, reflecting their reduced capacity to follow variations in the applied field. Stability of the relative permittivity across the range of applied doses implies minimal variation in the contributing electronic, ionic, and orientational components. This stability may be attributed to the film's high degree of crosslinking, which serves to limit molecular mobility and hence the contribution of orientational components to the permittivity [89, 90].

The relative permittivity provides a measure of a material's capacity to store energy in an electric field and is a key parameter in material selection for capacitors, insulators, and dielectric gates in organic thin film transistors at sonic frequencies [91], as well as dielectric resonator antennas at optical frequencies [92]. In this respect, pristine and irradiated polyterpenol compares favourably with dielectric polymers derived from natural and synthetic precursors, including plasma polymerised methyl methacrylate ($\varepsilon_r = 3.86$), Aloe vera ($\varepsilon_r = 3.39$), poly(vinyl alcohol) ($\varepsilon_r = 1.99$), poly(methyl methacrylate) ($\varepsilon_r = 3.45$), and poly(4-vinylphenol) ($\varepsilon_r = 2.18$) [18, 93]. The attractiveness of polyterpenol as a dielectric material in bioelectronic devices may be further enhanced by plasma polymerisation's capacity to overcome performance-limiting boundary interface inhomogeneities common to solution-based processing, and difficulty in applying organic dielectrics to organic semiconductors due to their low surface energy [94, 95].

3.3 Electrical properties

Current density (J) was calculated using experimentally determined current and voltage values under dc conditions, with representative J-V curves for 0, 50, and 100 kGy doses given in Figure 4 for samples with thickness values of 346, 301, and 328 nm respectively. Variations in absolute current density values may be attributed to differences in the thickness of the samples used, given that increasing thickness leads to reduced current density in plasma polymerised thin films [96]. Despite this thickness dependence, information about the modes of conduction can still be extracted from the shape of the curves.
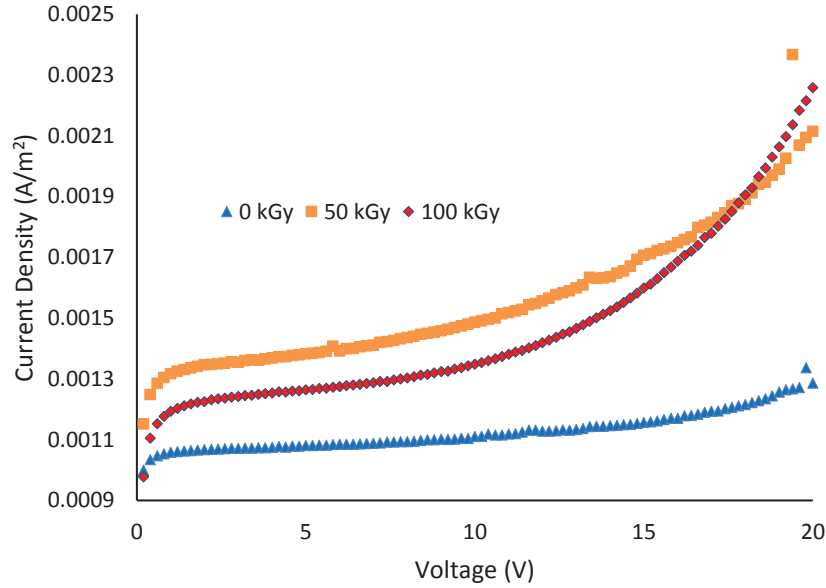
Figure 4. J-V relationship as a function of gamma radiation dose

The very low field region (~0 – 1.5 V) may be described by a power law relation as [97]:

$$J \propto V^n \qquad (9)$$

This advances to a linear Ohmic relationship above 1.5 V which can modelled as:

$$J = \mu n_0 e \frac{V}{D} \quad (10)$$

Where μ is charge carrier mobility, n_0 is the free charge carrier density, and e is the electronic charge. This linearity breaks down around the ~10 - 15 V region and a non-Ohmic relationship is established between J and V. The dependence of the J-V relationship on applied voltage and film thickness indicates that current conduction may be modelled by a number of mechanisms, including Poole-Frenkel (PF) conduction, Richardson-Schotty (RS) conduction, and Space Charge Limited Conduction (SCLC) [98-100]. If present, PF/RS conduction can be determined by linearity in the plot of $\ln J$ vs $V^{0.5}$, whilst SCLR conduction can be confirmed by linearity in the plot of $\ln J$ vs. $\ln V$ (for SCLC) [101].
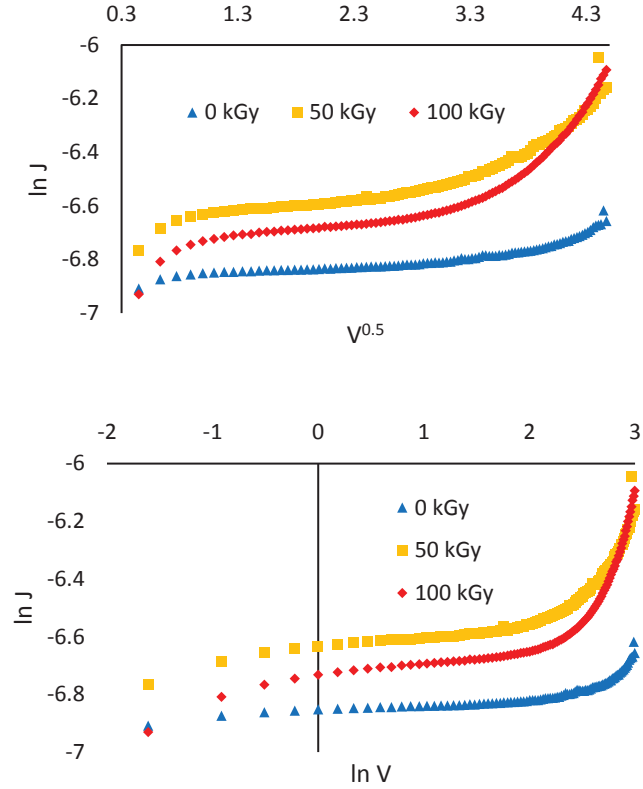
143

Figure 5. ln J vs. V$^{0.5}$ (top), and ln J vs. ln V (bottom) for samples irradiated to 0, 50, and 100 kGy

From Figure 5 it is apparent that neither PF/RS or SCLC exhibit prominent linearity relative to each other, enforcing the likelihood that the mode of conduction within the voltage range under investigation can be attributed to a confluence of electrode- and bulk-limited mechanisms, including the material's trap barrier potential being lowered by the application of a high electric field, electric-field assisted transfer of energetic electrons from the metal to the polymer at the electrode-polymer interface, and the filling of traps [102].

DC electrical conductivity (σ) was calculated over the range of 0.2 – 20 V using the experimentally measured current and voltage values as:

$$\sigma = \frac{D}{RA} = \frac{ID}{VA} \qquad (11)$$

Where I is the current in A, D is the sample thickness in m, V is the applied voltage in V, and A is the cross-sectional area in m^2. The dielectric's resistivity (ρ) is by

definition given as the reciprocal of σ and is also provided in Table 3 at 1 and 20 V.

Table 3. Conductivity and resistivity as a function of dose

Dose (kGy)	σ (pS·cm^{-1})		ρ (MΩ·m)	
	1 V	20 V	1 V	20 V
0	3.66	0.22	2731	44943
0.1	3.90	0.21	2561	48498
1	3.03	0.16	3296	62289
10	3.36	0.20	2975	50535
25	5.31	0.77	1884	13033
50	4.33	0.35	2311	28781
100	3.92	0.37	2550	26942

Gamma radiation can produce transient increases in a polymer's electrical conductivity due to the radiation-induced formation of charge-carrying electrons and holes [103]. Post-irradiation, polymers are also known to show altered long-term electrical conductivity in response to variations in irradiation factors such as total dose, dose rate, and air/vacuum environment [104, 105]. These factors influence the occurrence of competing crosslinking and chain-scission mechanisms, with chain-scissioning supporting free radical formation and the subsequent development of defects in conduction pathways through the material, giving rise to reduced conductivity. Conversely, crosslinking and the recombination of free radicals can facilitate the formation of new electrical pathways and thus increase the polymer's conductivity [106, 107]. In this instance a lack of preferential crosslinking or chain-scissioning has resulted in polyterpenol displaying no marked variation in electrical conductivity following irradiation, with the conductivity order of magnitude of all samples remaining in the 10^{-12} S/cm range. This falls within the conductivity range of electrical insulators [108], and is a favourable outcome in support of polyterpenol's use as an insulating interlayer or encapsulating organic bioelectronic material.

3.4 Chemical properties

Variations in chemical structure and composition as a function of applied dose were explored using FTIR spectroscopy, with accompanying transmission spectra and absorption frequency assignments provided in Figure 6 and Table 4 respectively.
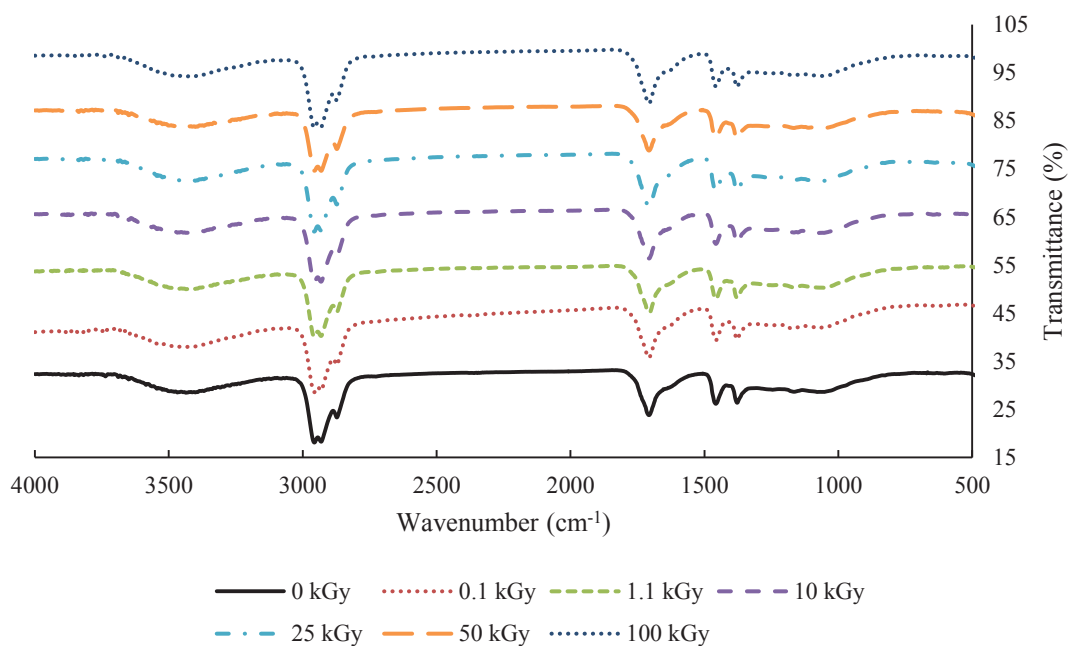
Figure 6. FTIR transmission spectra for pristine and irradiated films (spectra offset for clarity)

Table 4. FTIR group frequency assignment [109, 110]

Group Assignment	Group Frequency (cm^{-1})
Hydroxyl group, H-bonded OH stretch	~3450
Methyl asymmetric C-H stretch	2955, 2930
Methyl symmetric C-H stretch	2875
Alkenyl C=C stretch	~1660
Methyl asymmetric C-H bend	1459
Symmetric C-H bend	1380
C-O stretching of alkyl-substituted ether	1150, 1050

Gamma irradiation at doses as low as 18 kGy have been shown to induce dehydrogenation and variation in the presence of double/triple bonds in plasma polymerised polypyrroles [61], whilst doses below 0.1 kGy produce oxidation and p-type doping in organic semiconducting oligomers such as pentacene [111]. In contrast to the onset of these chemical modifications at low doses, polyterpenol FTIR spectra revealed no appreciable variation in peak intensity, frequency shift, or the formation/elimination of peaks in response to the applied radiation. This indicates that the films expressed no preference for either crosslinking (no additional C=C) or chain-scissioning, and furthermore the lack of an increase in oxygen functionalities (i.e., OH, C-O) suggests that even though the irradiation treatment was carried out in an air environment known to increase radical formation and degradation [112], it resulted in no additional oxidation of the films. The destructive effects of ionising radiation (i.e., chain-scissioning and free radical formation) may have been moderated by the inherently disordered and crosslinked nature of the plasma polymer. Furthermore, undesirable radical-mediated reactions within plasma polymers can be terminated by the recombination of two radicals [21], and as such the deleterious effects of radicals produced by the gamma irradiation may have been moderated by the abundance of pre-existing trapped plasma-generated radicals available for recombination and termination.

The antibacterial and bioactive properties of polyterpenol have previously been attributed to the incorporation of intact terpinen-4-ol monomer structures, and the presence of polar carbon-oxygen and oxygen-hydrogen groups that enhance the polymer's hydrophilicity [37]. Demonstrating the preservation of these groups at a gamma irradiation dose of 100 kGy (four time in excess of the standard ~ 25 kGy dose used in sterilising procedures) is an important step towards validating the biomedical utility of polyterpenol thin films following gamma sterilisation.

3.5 Morphological properties

Polymer thin film morphology is dependent upon a variety of parameters such as molecular weight and polydispersity index [80], and has shown considerable rearrangement following exposure to gamma radiation [113]. In the case of polyterpenol, however, retention of the pristine film's smooth and defect-free surface features is observed in films irradiated at all dose values. Metrics given

in Table 5 for average roughness (R_a), RMS roughness (R_q), surface skewness (R_{skw}) and coefficient of kurtosis (R_{kur}) revealed no prominent variations in surface architecture as a result of irradiation.

Table 5. 3×3 µm AFM metrics for pristine and irradiated films

Dose (kGy)	R_a (nm)	R_q (nm)	R_{skw}	R_{kur}
0.0	0.47	0.59	0.22	0.26
0.1	0.42	0.53	0.12	0.31
1.0	0.24	0.31	0.25	0.29
10.0	0.48	0.61	0.16	0.32
25.0	0.43	0.55	0.19	0.17
50.0	0.29	0.36	0.14	0.09
100.0	0.42	0.53	0.12	0.05

AFM images for 3×3 µm sites (Figure 7) revealed a lack of powder formation, indicating that polymerisation occurred predominantly at the substrate surface and not in the gas phase [20]. This indicates that low pressure was maintained throughout the deposition process, resulting in long mean free paths and low collision rates for molecular fragments within the plasma volume. Surface morphology was marginally dominated by peaks relative to troughs, as evidenced by $R_{skw} > 0$, and the variation in height values is predominantly comprised of frequent small-amplitude deviations, demonstrated by $R_{kur} < 3$.
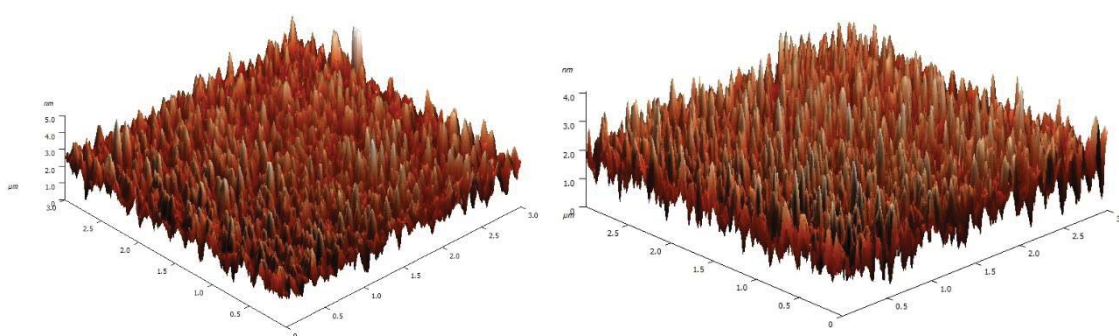

Figure 7. AFM 3D images of pristine (left), and irradiated film (100 kGy) (right)

Surface morphology is critical to both the electronic and biological performance of organic bioelectronic devices. For instance, surface porosity is a major factor influencing the leakage current density of organic dielectric layers [114], and the performance of devices with organic dielectric – organic semiconductor interfaces (such as phototransistors and organic thin film transistors) is dependent, in part, on the surface roughness of the materials at the junction interface [115, 116]. On the biological front a number of processes (including the adhesion, alignment, and proliferation of cells) are mediated by surface patterning and roughness [26]. Similarly, polyterpenol's bioactive properties are also strongly dependent upon surface roughness and architecture [117, 118], and the preservation of these morphological traits following irradiation is an important step in validating its organic bioelectronics utility.

4. Conclusion

The realisation of next-generation bioelectronics devices is dependent upon the development of renewable, non-toxic, and biocompatible organic bioelectronic materials that can pass biomedical sterilisation procedures with their properties intact. With this demand in mind, this study focussed on characterising the response of plasma polymerised polyterpenol thin films to gamma irradiation at maximum doses of up to 100 kGy. Polyterpenol thin films possess a host of chemical and physical properties with concomitant applications ranging from gate dielectrics in transistors to antibacterial coatings. Post-irradiation preservation of the suite of properties that underlie its performance in these applications allows us to present polyterpenol as a viable organic bioelectronic candidate material capable of satisfying both biological and electronic performance constraints.

Acknowledgements

References

1. G.D. Nelson, *A brief history of cardiac pacing.* Texas Heart Institute Journal, 1993. 20(1): p. 12.

2.   W.M. Rabinowitz, et al., *Better speech recognition with cochlear implants.* Nature, 1991. 352(6332): p. 236.

3.   D.A. Gough, et al., *Function of an implanted tissue glucose sensor for more than 1 year in animals.* Science translational medicine, 2010. 2(42): p. 42ra53.

4.   R. Farra, et al., *First-in-human testing of a wirelessly controlled drug delivery microchip.* Science translational medicine, 2012. 4(122): p. 122ra21.

5.   F.G. Yamagishi, *Investigation of plasma-polymerized films as primers for parylene-c coatings on neural prosthesis materials.* Thin Solid Films, 1991. 202(1): p. 39.

6.   S.-K. Kang, et al., *Bioresorbable silicon electronic sensors for the brain.* Nature, 2016. 730(7588): p. 71.

7.   M.D. Angione, et al., *Carbon based materials for electronic bio-sensing.* Materials Today, 2011. 14(9): p. 424.

8.   C. Liao, et al., *Flexible Organic Electronics in Biology: Materials and Devices.* Advanced Materials, 2015. 27: p. 7493.

9.   G.-T. Hwang, et al., *Flexible Piezoelectric Thin-Film Energy Harvesters and Nanosensors for Biomedical Applications.* Advanced Healthcare Materials, 2015. 4(5): p. 646.

10.   D.F. Williams, *On the mechanisms of biocompatibility.* Biomaterials, 2008. 29: p. 2941.

11.   B.D. Ratner and S.J. Bryant, *Biomaterials: Where We Have Been and Where We Are Going.* Annual Review of Biomedical Engineering, 2004. 6: p. 41.

12.   N. Gour, K.X. Ngo, and C. Vebert-Nardin, *Anti-Infectious Surfaces Achieved by Polymer Modification.* Macromolecular Materials and Engineering, 2014. 299: p. 648.

13. T.H. Barrows, *Degradable implant materials: a review of synthetic absorbable polymers and their applications.* Clinical Materials, 1986. 1(4): p. 233.

14. S. Lischer, et al., *Antibacterial burst-release from minimal Ag-containing plasma polymer coatings.* Journal of the Royal Society Interface, 2011. 8(60): p. 1019.

15. T.D. Michl, et al., *Nitric oxide releasing plasma polymer coating with bacteriostatic properties and no cytotoxic side effects.* Chemical Communications, 2015. 51(32): p. 7058.

16. J.-M. Hsu, et al., *Encapsulation of an Integrated Neural Interface Device With Parylene C.* IEEE Transactions on Biomedical Engineering, 2009. 56(1): p. 23.

17. J.P. Seymour, et al., *The insulation performance of reactive parylene films in implantable electronic devices.* Biomaterials, 2009. 30: p. 6158.

18. J.-S. Lim, et al., *Plasma polymerized methyl methacrylate gate dielectric for organic thin-film transistors.* Organic Electronics, 2010. 11(5): p. 951.

19. R. d'Agostino, et al., *Low-Temperature Plasma Processing of Materials: Past, Present, and Future.* Plasma Processes and Polymers, 2005. 2(1): p. 7.

20. J. Friedrich, *Mechanisms of Plasma Polymerization - Reviewed from a Chemical Point of View.* Plasma Processes and Polymers, 2011. 8: p. 783.

21. A. Hollander and J. Thome, *Degradation and Stability of Plasma Polymers*, in *Plasma Polymer Films*, H. Biederman, Editor. 2004, Imperial College Press. p. 386.

22. M. Laroussi, *Low Temperature Plasma-Based Sterilization: Overview and State-of-the-Art.* Plasma Processes and Polymers, 2005. 2: p. 391.

23. M. Moreau, N. Orange, and M.G.J. Feuilloley, *Non-thermal plasma technologies: New tools for bio-decontamination.* Biotechnology Advances, 2008. 26: p. 610.

24. M. Moisan, et al., *Low-temperature sterilization using gas plasmas: a review of the experiments and an analysis of the inactiviation mechanisms.* International journal of pharmaceutics, 2001. 226(1): p. 1.

25. S. Adler, M. Scherrer, and F.D. Daschner, *Costs of low-temperature plasma sterilization compared with other sterilization methods.* Journal of Hospital Infection, 1998. 40(2): p. 125.

26. E. Sardella, et al., *Homogeneous and Micro-Patterned Plasma-Deposited PEO-Like Coatings for Biomedical Surfaces.* Plasma Processes and Polymers, 2004. 1: p. 63.

27. E. Kulaga, et al., *Mechanically Responsive Antibacterial Plasma Polymer Coatings for Textile Biomaterials.* Plasma Processes and Polymers. 11: p. 63.

28. P. Khalilpour, et al., *Ag/SiOxCy plasma polymer coating for antimicrobial protection of fracture fixation devices.* Journal of Biomedical Materials Research B: Applied Biomaterials, 2010. 94B(1): p. 196.

29. M. Santos, M.M.M. Bilek, and S.G. Wise, *Plasma-synthesised carbon-based coatings for cardiovascular applications.* Biosurface and Biotribology, 2015. 1: p. 146.

30. M. Zelzer, et al., *Investigation of cell-surface interactions using chemical gradients formed from plasma polymers.* Biomaterials, 2008. 29(2): p. 172.

31. M.S. Kim, F. Khang, and H.B. Lee, *Gradient polymer surfaces for biomedical applications.* Progress in Polymer Science, 2008. 33(1): p. 138.

32. D. Mangindaan, et al., *Creation of biofunctionalized plasma polymerized allylamine gradients.* Journal of Polymer Science Part B: Polymer Physics, 2013. 51(18): p. 1361.

33. S. Lerouge, et al., *Nitrogen-Rich Plasma Polymer Coatings for Biomedical Applications: Stability, Mechanical Properties and Adhesion Under Dry and Wet Conditions.* Plasma Processes and Polymers, 2015. 12: p. 882.

34. K. Bazaka and M.V. Jacob, *Synthesis of radio frequency plasma polymerized non-synthetic Terpinen-4-ol thin films.* Materials Letters, 2009. 63(18-19).

35.   M.V. Jacob, et al., *Electron-blocking hole-transport polyterpenol thin films.* Chemical Physics Letters, 2012. 528.

36.   K. Bazaka, N. Ketheesan, and M.V. Jacob, *Polymer Encapsulation of Magnesium to Control Biodegradability and Biocompatibility.* Journal of Nanoscience and Nanotechnology, 2014. 14(10): p. 8087.

37.   K. Bazaka, et al., *Plasma-Enhanced Synthesis of Bioactive Polymeric Coatings from Monoterpene Alcohols: A Combined Experimental and Theoretical Study.* Biomacromolecules, 2010. 11: p. 2016.

38.   F. Sakar, et al., *Nano drug delivery systems and gamma radiation sterilization.* Pharmaceutical Development and Technology, 2016: p. 1.

39.   G.P. Jacobs, *A Review of the Effects of Gamma Radiation on Pharmaceutical Materials.* Journal of Biomaterials Applications, 1995. 10: p. 59.

40.   K. Gorna and S. Gogolewski, *The effect of gamma radiation on molecular stability and mechanical properties of biodegradable polyurethanes for medical applcations.* Polymer Degradation and Stability, 2003. 79(3): p. 465.

41.   E.P. Jr., et al., *Ethylene oxide's role as a reactive agent during sterilization: Effects of polymer composition and device architecture.* Journal of Biomedical Materials Research Part B, 2013. 101B(4): p. 532.

42.   J.A. Beck, *Process variation in electron beam sterilization.* Radiation Physics and Chemistry, 2011. 81(8): p. 1236.

43.   W.A. Rutala and D.J. Weber, *Disinfection, sterilization, and antisepsis: An overview.* American Journal of Infection Control, 2016. 44: p. e1.

44.   G.F. Knoll, *Radiation Detection and Measurement.* 2nd ed. 1989, New York: Wiley.

45.   K. Makuuchi and S. Cheng, *Radiation Processing of Polymer Materials and its Industrial Applications.* 2012, New Jersey: Wiley.

46. J. Davenas, et al., *Stability of polymers under ionising radiation: The many faces of radiation interactions with polymers.* Nuclear Instruments and Methods in Physics Research Section B, 2002. 191(1): p. 653.

47. J.K. Thomas, *Fundamental aspects of the radiolysis of solid polymers, crosslinking and degradation.* Nuclear Instruments and Methods in Physics Research Section B, 2007. 265: p. 1.

48. G. Martinez-Barrera, et al., *Mechanical properties of polypropylene-fiber reinforced concrete after gamma irradiation.* Composites: Part A, 2011. 42: p. 567.

49. P.S.R. Sreekanth and S. Kanagaraj, *Influence of multi walled carbon nanotubes reinforcement and gamma irradiation on the wear behaviour of UHMWPE.* Wear, 2015. 334-335: p. 82.

50. N. Akter, et al., *Fabrication and mechanical characterization of biodegradable and synthetic polymeric films: Effect of gamma radiation.* Radiation Physics and Chemistry, 2012. 81: p. 995.

51. U.A. Sevil, et al., *Gamma and electron dose response of the electrical conductivity of polyanilise based polymer composites.* Radiation Physics and Chemistry, 2003. 67: p. 575.

52. T.B. Mostafa, A. Awadallah-F, and M.M.K. Shehata, *Gamma radiation synthesis optimization of a novel polymer and its possible applications in antimicrobial and antitumor fields.* Medicinal Chemstry Research, 2012. 22: p. 479.

53. E. Suljovrujic and M. Micic, *Smart poly(oligo(propylene glycol) methacrylate) hydrogel prepared by gamma radiation.* Nuclear Instruments and Methods in Physics Research Section B, 2015. 342: p. 206.

54. R.L. Clough, *High-energy radiation and polymers: a review of commercial processes and emerging applications.* Nuclear Instruments and Methods in Physics Research Section B, 2001. 185: p. 8.

55. E.S. Kempner, *Direct effects of ionizing radiation on macromolecules.* Journal of Polymer Science Part B: Polymer Physics, 2011. 49(12): p. 827.

56. C.V. Stephenson, B.C. Moses, and W.S. Wilcox, *Ultraviolet irradiation of plastics. I. Degradation of physical properties.* Journal of Polymer Science Part A: Polymer Chemistry, 1961. 55(162): p. 451.

57. D.M. Pinkerton and K.R.L. Thompson, *Polytetrafluoroethylene: Effects of γ-radiation on fine structure.* Journal of Polymer Science Part B: Polymer Physics, 1972. 10(3): p. 473.

58. J. Chen, et al., *Organic polymer materials in the space environment.* Progress in Aerospace Sciences, 2016. 83: p. 37.

59. C.-Y. Hsiao, et al., *The influence of γ irradiation and ethylene oxide treatment on the release characteristics of biodegradable poly(lactide-co-glycolide) composites.* Polymer Degradation and Stability, 2012. 97: p. 715.

60. M. Tavlet and S. Ilie, *Behaviour of Organic Materials in Radiation Environment*, in *1999 Fifth European Conference on Radiation and Its Effects on Components and Systems*. 1999, IEEE. p. 6.

61. O.G. Lopez, et al., *Gamma-Irradiation to Modify Properties in Polypyrroles Synthesized by Plasmas.* Macromolecular Symposia, 2013. 325-326: p. 96.

62. H. Fricke and E.J. Hart, *12: Chemical Dosimetry*, in *Radiation Dosimetry*, F.H. Attix, W.C. Roesch, and E. Tochilin, Editors. 1966, Academic Press: New York and London.

63. I. Kuritka, et al., *Thermal stability of plasma deposited polysilanes.* Polymer Degradation and Stability, 2006. 91: p. 2901.

64. K. Bazaka and M.V. Jacob, *Post-deposition ageing reactions of plasma derived polyterpenol thin films.* Polymer Degradation and Stability, 2010. 95(6).

65. H. Dislich, *Plastics as Optical Materials.* Angewandte Chemie International Edition, 1979. 18(1): p. 49.

66. J.C. Seferis, *Polymer Handbook.* 3rd ed. 1989, New York: Wiley.

67. *Lange's Handbook of Chemistry*. 16th ed. 2005, New York; London: McGraw-Hill Professional.

68. T. Sato, K. Moriki, and M. Yumoto, *Refractive Index Control of Polymer Film by Plasma CVD for designing an Optical Waveguide.* IEEJ Transactions on Electrical and Electronic Engineering, 2010. 5: p. 416.

69. S. Choi, et al., *Wide wavelength-range optical studies of hydrogenated amorphous carbon films: from 700 nm to 10 μm.* Applied Surface Science, 2001. 169-170: p. 217.

70. M. Born and E. Wolf, *Principles of Optics: Electromagnetic Theory of Propagation, Interference and Diffraction of Light*. 7th ed. 2003, Cambridge, UK: Cambridge University Press.

71. K. Moriki, et al., *Fabrication of an optical polymer waveguide by plasma-enhanced polymerization.* Electronics and Communications in Japan, 2009. 92(4): p. 21.

72. T. Matsuda, et al., *Optical material of high refractive index resin composed of sulfur-containing aliphatic and alicyclic methacrylates.* Journal of Applied Polymer Science, 2000. 76(1): p. 45.

73. H.-J. Yen and G.-S. Liou, *Enhanced near-infrared electrochromism in triphenylamine-baed aramids bearing phenothiazine redox centers.* Journal of Materials Chemistry, 2010. 20: p. 9886.

74. Z. Guo, et al., *Recent progress in the development of near-infrared fluorescent probes for bioimaging applications.* Chemical Society Reviews, 2013. 43(1): p. 16.

75. H. Zhang, et al., *Transparent Organic Photodectector using a Near-Infrared Absorbing Cyanine Dye.* Scientific Reports, 2015. 5: p. 9439.

76. M. Saito, et al., *Optical constants of polymer coatings in the infrared.* Infrared Physics & Technology, 1994. 36: p. 1125.

77. J. Tauc, *The Optical Properties of Solids: Preceedings of course 34*. 1966, New York: Academic Press.

78.   K. Arshak and O. Korostynska, *Advanced Materials and Techniques for Radiation Dosimetry.* 2006, Norwood, MA: Artech House Books. 219.

79.   J.C.S. Costa, et al., *Optical band gaps of organic semiconductor materials.* Optical Materials, 2016. 58: p. 51.

80.   A. Facchetti, *π-Conjugated Polymers for Organic Electronics and Photovoltaic Cell Applications.* Chemistry of Materials 2011. 23: p. 733.

81.   R.C. Dorf, ed. *The Electrical Engineering Handbook.* Second ed. 2000, CRC Press LLC: Boca Raton.

82.   A.A. Dakhel, *Mechanisms of dc-current transfer in tris(acetylacetonato)iron(III) films.* Journal of Non-Crystalline Solids, 2007. 353(16): p. 1529.

83.   T.Z. Rizvi and M.A. Khan, *Temperature-dependent dielectric properties of slightly hydrated horn keratin.* International Journal of Biological Macromolecules, 2008. 42(3): p. 292.

84.   M. Shahbazi, A. Bahari, and S. Ghasemi, *Structural and frequency-dependent dielectric properties of PVP-SiO2-TMSPM hybrid thin films.* Organic Electronics, 2016. 32: p. 100.

85.   F. Bibi, et al., *A Review: Origins of the Dielectric Properties of Proteins and Potential Development as Bio-Sensors.* Sensors, 2016. 16(8): p. 1232.

86.   M.S. Venkatesh and G.S.V. Raghavan, *An Overview of Microwave Processing and Dielectric Properties of Agri-food Materials.* Biosystems Engineering, 2004. 88(1): p. 1.

87.   H. Jiang, et al., *The relationship between chemical structure and dielectric properties of plasma-enhanced chemical vapor deposited polymer think films.* Thin Solid Films, 2007. 515: p. 3513.

88.   A.v. Hippel, et al., *Photocurrent, Space-Charge Buildup, and Field Emission in Alkali Halide Crystals.* Physical Review, 1953. 91(3): p. 568.

89.   K. Endo, K. Shinoda, and T. Tatsumi, *Plasma deposition of low-dielectric-constant fluorinated amorphous carbon.* Journal of Applied Physics, 1999. 86(5): p. 2739.

90.   C.G.A. Lima, et al., *DC conductivity and dielectric permittivity of collagen-chitosan films.* Materials Chemistry and Physics, 2006. 99(2): p. 284.

91.   H.E. Katz and J. Huang, *Thin-Film Organic Electronic Devices.* Annual Review of Materials Research, 2009. 39: p. 71.

92.   L. Zou, et al., *Efficiency and Scalability of Dielectric Resonator Antennas at Optical Frequencies.* IEEE Photonics Journal, 2014. 6(4): p. 4600110.

93.   L.Q. Khor and K.Y. Cheong, *Aloe vera gel as natural organic dielectric in electronic application.* Journal of Materials Science: Materials in Electronics, 2013. 24(7): p. 2646.

94.   P.J. Diemer, et al., *Vibration-Assisted Crystallization Improves Organic/Dielectric Interface in Organic Thin-Film Transistors.* Advanced Materials, 2013. 25(48): p. 6956.

95.   R. Hamilton, et al., *High-performance polymer-small molecule blend organic transistors.* Advanced Materials, 2009. 21(10-11): p. 1166.

96.   R.B. Sarker and A.H. Bhuiyan, *Electrical conduction mechanism in plasma polymerized 1-Benzyl-2-methylimidazole thin films under static electric field.* Thin Solid Films, 2011. 519: p. 5912.

97.   L.J. Anderson and M.V. Jacob, *Electrical characterisations of plasma polymerised linalyl acetate.* Materials Science and Engineering B, 2012. 177: p. 311.

98.   S. Sivaraman and M.R. Anantharaman, *Determination of charge carrier transport in radio frequency plasma polymerized aniline thin films.* Journal of Physics D: Applied Physics, 2010. 43(5): p. 055403.

99.   C.J. Mathai, et al., *Mechanism of electrical conduction in plasma polymerized furfural thin films.* Thin Solid Films, 2002. 416(1): p. 10.

100.   R. Matin and A.H. Bhuiyan, *Electrical transport mechanism in plasma polymerized 2, 6, diethylaniline thin films.* Thin Solid Films, 2011. 519(11): p. 3462.

101. T.Y. Kim, et al., *Electrical conduction of polyimide films prepared from polyamic acid (PAA) and pre-imidized polyimide (PI) solution.* eXPRESS Polymer Letters, 2007. 1(7): p. 427.

102. F.-C. Chiu, *A Review on Conduction Mechanisms in Dielectric Films.* Advances in Materials Science and Engineering, 2014. 2014: p. 1.

103. P. Hedvig, *Radiation-induced electrical conductivities in polyamide copolymers.* Journal of Polymer Science Part A: Polymer Chemistry, 1964. 2(9): p. 4097.

104. Q. Yao, L. Liu, and C. Li, *Studies on electrical conductivity of gamma irradiated polyaniline.* Polymer Bulletin, 1993. 31(5): p. 601.

105. M. Wolszczak, J. Kroh, and M.M. Abdel-Hamid, *Some aspects of the radiation processing of conducting polymers.* Radiation Physics and Chemistry, 1995. 45(1): p. 71.

106. M.C. Kane, R.J. Lascola, and E.A. Clark, *Investigation on the effects of beta and gamma irradiation on conducting polymers for sensor applications.* Radiation Physics and Chemistry, 2010. 79: p. 1189.

107. G.M. Nasr, M.M. Badawy, and E. Ateia, *Effects of radiation and storage time on conductive NBR/LDPE blends.* Polymer Degradation and Stability, 1998. 60(2-3): p. 333.

108. A. Kiesow and A. Heilmann, *Deposition and properties of plasma polymer thin films made from thiophenes.* Thin Solid Films, 1999. 343: p. 338.

109. J. Ristein, et al., *A comparative analysis of a-C:H by infrared spectroscopy and mass selected thermal effusion.* Journal of Applied Physiology, 1998. 84(7): p. 3836.

110. J.W.A.M. Gielen, et al., *Optical and mechanical properties of plasma-beam-deposited amorphous hydrogenated carbon.* Journal of Applied Physics, 1996. 80: p. 5986.

111. H.N. Raval, et al., *Investigation of effects of ionizing radiation exposure on material properties of organic semiconducting oligomer - Pentacene.* Organic Electronics, 2013. 14: p. 1467.

112. K. Arakawa, et al., *Radiation-induced oxidation of polyethylene, ethylene-butene copolymer, and theylene-propylene copolymer.* Journal of Polymer Science Part A: Polymer Chemistry, 1982. 20(9): p. 2681.

113. Z. Xu, et al., *Nano-structure and property transformations of carbon systems under γ-ray irradiation: a review.* RSC Advances, 2013. 3(27): p. 10579.

114. D.P. Singh, Y.N. Mohapatra, and D.C. Agrawal, *Dielectric and leakage current properties of sol-gel derived calcium copper titanate (CCTO) thin films and CCTO/ZrO2 multilayers.* Materials Science and Engineering B, 2009. 157(1-3): p. 58.

115. J.W. Bae, et al., *Triacetate cellulose gate dielectric organic thin-film transistors.* Organic Electronics, 2017. 41.

116. H.-L. Park, et al., *Effect of morphological and physicochemical properties of dielectric-organic semiconductor interfaces on photoresponse of organic phototransistors.* Thin Solid Films, 2016. 619: p. 297.

117. R.J. Crawford, et al., *Surface topographical factors influencing bacterial attachment.* Advances in Colloid and Interface Science, 2012. 179: p. 142.

118. K. Bazaka, et al., *Plasma-assisted surface modification of organic biopolymers to prevent bacterial attachment.* Acta Biomater, 2011. 7(5).

CHAPTER 7   CONCLUSIONS AND FUTURE WORK

7.1 FINDINGS

Technology can play a pivotal role in meeting many of the challenges faced by humanity in the 21st century, and its advance is underpinned in no small measure by the development of new materials. Here, the novel characteristics of plasma polymers mark them as attractive materials for supporting technological innovation spanning several domains, including the transition from inorganic electronics to organic electronics, and the development of antibacterial surfaces for biomedical devices. Despite their potential utility, the commercial uptake of plasma polymers within certain technologies has been hampered by property limitations (e.g., low electrical conductivity), poor understanding of the plasma chemistry within the synthesis environment, and limited information about their stability following exposure to biomedically sterilising doses of radiation.

The aim of this thesis was to enhance the utility of plasma polymerised polyterpenol thin films derived from the environmentally sustainable terpinen-4-ol/tee tree oil precursor. In doing so, this thesis has characterised the plasma chemistry used to synthesise polyterpenol, and explored the material's response to various radiation regimes. The radiation-induced tailoring of polyterpenol thin film properties, and their biomedical sterilisation, opens up new avenues for achieving technological innovation driven by the use of a plasma polymer synthesised from a natural resource using a green-chemistry approach.

7.1.1 Terpenoid Plasma Environment

The relationship between synthesis parameters and plasma environment was explored using mass spectrometry and ion energy analysis. A comparative positive ion mode analysis of terpinen-4-ol and *M. alternifolia* oil plasmas revealed marked differences in the type and abundance of *m/z* species at 5 W. Terpinen-4-ol exhibited peaks at *m/z* 43 ($C_3H_7^+$), 71 ($C_5H_{11}^+$ or $C_4H_7O^+$), 81, 93, 111 ($C_8H_{15}^+$), 137 ($[M + H]^+ - H_2O$), 155 ($[M + H]^+$), 171, 273, 292 ($[2M + H]^+ - OH$), and 309 ($[2M + H]^+$). Despite being comprised of a diverse cocktail of terpenes (including terpinen-4-ol), *M. alternifolia* only displayed peaks at *m/z* 81, 93, 122, 137, and 155 at low power. Subsequent increases in power served to

diminish the disparity between terpinen-4-ol and *M. alternifolia* plasma environments, with comparable abundance of *m/z* 95, 137, and 155 and other low molecular weight species present at 50 W. This unifying trend towards smaller molecular fragments was also accompanied by significant elimination of species above *m/z* 155, including 171, 273, 292, and 309 peaks.

Quartz crystal microbalance data revealed mass deposition rates of 5.6, 55.2, and 42.3 $\mu g/m^2 s$ for glow discharges supplied with terpinen-4-ol monomeric precursors at nominal generator powers of 5, 25, and 50 W respectively. Assuming comparable flow rates and pressures, the reduction in mass deposition rate from 25 W to 50 W may indicate that an adsorption-desorption equilibrium is beginning to become a rate-limiting process. This may be in response to increased substrate temperature (induced by higher applied power), or increased abstraction and sputtering facilitated by a shift in the ion energy distributions towards higher energy values. This latter explanation is supported by data obtained via an energy probe coupled to the quadrupole mass spectrometer, which revealed a positive correlation between maximum ion energy values and applied power. Specifically, maximum ion energies of ~ 13.7, 18.4, and 24.1 eV were observed for applied powers of 5, 25, and 50 W respectively.

Residual gas analysis of terpinen-4-ol plasmas at 5, 25, and 50 W revealed a trend towards the proliferation of low *m/z* species with increasing power, with considerable abundance of *m/z* 2 (H_2), 18 (H_2O), 28 ($CO^{\cdot+}$ or $C_2H_4^{\cdot+}$), 43 ($C^3H_7^+$), 55 ($C_4H_7^+$ or $C_3H_3O^+$), and 71 ($C_5H_{11}^+$ or $C_4H_7O^+$) species. Similarities between the *no plasma* and 5 W plasma spectra suggest that minimal plasma-induced terpinen-4-ol monomer fragmentation occurs at this low power, though non-trivial concentrations of the monomer are still present in 25 and 50 W plasmas.

The antibacterial properties of films prepared from the two precursors have also been demonstrated, with terpinen-4-ol and *M. alternifolia* plasma polymer coatings showing reduced *Staphylococcus aureus* biofilm thickness and biovolume relative to the uncoated glass control. Phase contrast images of human fibroblasts incubated in the presence of the coatings revealed healthy cell size and morphology similar to that of cells incubated in the presence of the inert glass control, suggesting cytocompatibility of the coatings and limited leaching of

biologically active agents into the liquid media. Contact cytocompatibility has also been shown with Balb/c mice macrophage cells incubated in the presence of the coated and control samples.

7.1.2 Swift Heavy Ion Irradiation

Polyterpenol thin films were exposed to high energy ions under low and high fluence regimes. In the first case, 50 MeV I^{10+} swift heavy ion irradiation at low fluence ($\leq 1 \times 10^{12}$ ions/cm^2) produced polyterpenol thin films with well-defined nano-scale ion entry tracks, as revealed by atomic force microscopy. X-ray reflectometry findings indicated that this irradiation was accompanied by an increase in superstrate-polymer interface roughness from 0.49 ± 0.01 nm for pristine films to 1.12 ± 0.01 nm for films irradiated to the maximum fluence of 1×10^{12} ions/cm^2. X-ray reflectometry also revealed minor reduction in the scattering length density from an initial value of 12.9 ± 0.9 for pristine films to 9.81 ± 0.07 for films exposed to the maximum fluence. This reduction in scattering length density was accompanied by optical densification leading to a reduction in refractive index and an increase in extinction coefficient across the 250-1000 nm wavelength region investigated via spectroscopic ellipsometry.

Swift heavy ion irradiation with 55 MeV I^{9+} ions at high fluence up to 2×10^{14} ions/cm^2 transformed polyterpenol into a morphologically restructured polymer-graphitic composite. Scanning electron microscopy analysis revealed that the smooth, defect free, pristine thin films progressed to a uniform restructured state consisting of discrete island-like hubs interconnected by filamentary structures as the applied fluence increased. This morphological restructuring is accompanied by the formation of discrete G and D peaks, corresponding to E_{2g} graphite at ~ 1580 cm^{-1} and A_{1g} breathing modes at ~1384 cm^{-1} respectively. These peaks indicate the presence of nanocrystalline graphite regions comprised of sp^2 carbon pairs arranged in both ordered and disordered sixfold aromatic rings and chains, with greater fluence leading to increased nanocrystalline graphite content. This transformation was accompanied by retention of polyterpenol's chemical functionalities, including OH, C-H, and C-O groups, albeit at reduced peak intensities resulting from hydrogen and oxygen evolution.

7.1.3 Dense Plasma Focus Irradiation

Despite similarities between plasma polymers and thermosetting polymers, inelastic deformation was successfully induced in highly crosslinked polyterpenol by transient dense plasma focus irradiation. Scanning electron microscopy revealed the development of bubble-like structures rising from the surface of the thin films, likely in response to the thermally-induced expansion of pre-existing void content trapped within the film. It is postulated that this manifestation of inelastic deformation occurs in four stages: 1. Void content is inherently present in the thin films following plasma deposition; 2. DPF exposure produces a high heating slope (up to ~ 3600 K/μm) and heating speed (up to ~ 40K/ns) in the sample over a treatment period of 10's to 100's of ns; 3. This rapid temperature rise increases the pressure of species trapped within void content regions, allowing for the growth of bubble structures within the polymer melt; 4. Structure growth terminates in response to rapid cooling of the polymer, or the development of defects/holes in the structure's 'skin'. Previous studies on the thermal treatment of polyterpenol and other plasma polymers have universally resulted in decomposition of the thin films and formation of a carbonaceous residue. In contrast to these studies, it is advanced that short-lived transient DPF irradiation allows the polymer to enter a melt state, deform, and resolidify, all before thermal degradation mechanisms can exert a dominant effect.

7.1.4 Gamma Irradiation

Polyterpenol thin films demonstrated stability following exposure to gamma irradiation at doses four times in excess of that employed in standard biomedical sterilisation. Minimal variation in both the real and imaginary components of the complex refractive index suggest negligible change in underlying film density, sp^3/sp^2 bonding ratio, and the concentration of atomic and molecular groups. Relative permittivity determined from capacitive measurements remained within $3.39 - 4.37$ across sonic frequencies spanning $0.1 - 10$ kHz, with the associated low ionic polarization suggesting that polyterpenol is predominantly apolar. The stability of the relative permittivity within this frequency range may also be attributed to the highly crosslinked nature of the film, which serves to limit molecular mobility and thus the contribution of orientational components. Current-voltage curves within the studied voltage region ($0.2 - 20$ V) revealed that charge

carrier movement is likely to be due to a confluence of Poole-Frenkel, Richardson-Schotty, and Space Charge Limited conduction. DC conductivity, σ, varied from 0.22 – 0.37 pS/cm following the application of 20 V to pristine and 100 kGy irradiated films respectively. This electrically semiconductor/insulating behaviour is supported by 3.33 – 3.50 eV optical energy gap values derived from Tauc plot analysis of extinction coefficients for pristine and 100 kGy irradiated films. Fourier transform infrared spectroscopy also revealed no discernible change in chemical functionalities between the pristine films, and those irradiated up to the maximum 100 kGy dose.

7.2 POTENTIAL APPLICATIONS AND RECOMMENDATIONS FOR FUTURE WORK

The findings presented within this thesis suggest several natural avenues for future investigation into the radiation processing of polyterpenol, and the conversion of research findings into applications.

7.2.1 Terpenoid Plasma Environment

Macroscopic understanding of the relationship between deposition conditions (i.e., R.F. power, pressure, flow rate, etc.) and deposition rate permits economic refinement of the polyterpenol deposition process. Specifically, the polyterpenol film thickness can be reliably set by selecting an appropriate deposition time for a given set of deposition conditions, eliminating use of the present 'trial-and-error' approach. Determining that ion kinetic energy within terpinen-4-ol reactive plasma can be controlled by careful selection of the generator power (without the need for substrate biasing) also permits tailoring of processes that are sensitive to energetic ion bombardment (including material etching, degradation, and physisorption of molecular ions).

Information provided by quadrupole mass spectrometer residual gas analysis permits tuning of plasma parameters (specifically power) to arrive at the desired terpinen-4-ol fragmentation scheme and subsequent provisioning of fragment and monomer species available for incorporation into the plasma polymer deposit. In particular, it is now confirmed that significant abundance of the terpinen-4-ol monomer within the plasma environment can be accomplished by

operating at low applied power (e.g., 5 W). This, in turn, suggests that polyterpenol thin films intended for biomedical applications, where surface chemical functionality is particularly important, should be synthesised at the lowest available power so as to preserve the bioactive properties of terpinen-4-ol within the polymer deposit.

Positive ion mode data suggests a convergence in the type and abundance of cationic species present within both terpinen-4-ol and *M. alternifolia* plasma environments as the power is increased. This finding serves to enhance the economics of terpenoid-based plasma polymer film synthesis by allowing selection of the less processed (and hence less costly) *M. alternifolia* precursor mixture in films that are to be produced at high power and used in physically protective coating applications. Conversely, if the preservation of terpinen-4-ol chemical functionality is of relevance to the final application of the film (e.g., in biomedical coatings), then use of the distilled monomer in a low power plasma environment is essential.

Cytocompatibility of both the terpen-4-ol and *M. alternifolia* plasma polymer films, coupled with their antibacterial action against *S. aureus*, suggests potential applications for these films as bioactive coatings for indwelling implants, drug eluting surfaces, and organic bioelectronic devices. Exposure of polyterpenol thin films to a wider variety of eukaryotic and prokaryotic microorganisms under *in vivo* and *in vitro* conditions may strengthen the case for its use biomedical devices.

7.2.2 Swift Heavy Ion Irradiation

Porous polyterpenol films synthesised with low fluence swift heavy ion irradiation may find utility as controlled-release drug loading platforms, filtration membranes, and templates for the production of micro- or nano-scale metallic rods. The utility of thin films with ion track pores showing fluence-dependent surface density can be materially advanced by first determining if the dimensions of these pores can be controlled via the application of chemical or physical etching techniques. Further work may then be undertaken to produce free-standing SHI irradiated polyterpenol films (i.e., without a substrate), before experimentally establishing the feasibility of using these porous films in the aforementioned applications.

166

Polyterpenol conversion into a micro- and nano-structured polymer-graphitic phase composite material following exposure to high fluence SHIs can be capitalised upon in a number of ways. First, masking technique may be applied to spatially confine the ion beam-induced graphitic conversion process, allowing for the creation of electrically conductive polyterpenol layers that can serve as electrodes or conduction regions within organic electronic devices. Retention of polyterpenol's chemical functionality, along with the significantly increased surface area, also suggest likely applications for the processed material in temperature and gas sensing applications. Additional studies into the conductivity of the processed film under different atmospheres and temperatures can serve to validate this premise.

7.2.3 Dense Plasma Focus Irradiation

The discovery of inelastic deformation behaviour in polyterpenol following exposure to transient dense plasma focus treatment can be built upon with additional studies focussing on the use of controlled void content to produce thin film cavities/structures of defined size, shape, and surface density. These structures may then serve as platforms suitable for drug loading, or to imbue the film with thermally insulating qualities.

Internal stresses created within plasma polymers during the deposition process also serve as a key limiting factor in the maximum thickness that can be achieved before curling/peeling behaviour manifests. The DPF induced melt state may alleviate such stresses, and additional studies should be undertaken to determine if DPF treatment can be used to produce plasma polymer coatings with substantially increased thickness, along with a consummate increase in barrier properties and longevity in wear-related applications.

7.2.4 Gamma Irradiation

Retention of biomedically relevant physical and chemical properties following exposure to high doses of gamma radiation suggest that polyterpenol is a suitable candidate for the encapsulation of bioelectronic and biomedical devices. Previous studies demonstrating the antimicrobial and cytocompatibility behaviour of polyterpenol thin films should be replicated on gamma sterilised films to verify that post-irradiation retained properties do indeed translate across to retained

bioactivity. Post-irradiation characterisation of adhesion strength, hardness, and breakdown voltage may strengthen the case for polyterpenol's use as an adhesion-promoting interlayer within bioelectronics devices, or physical/electrical protective coating.

Additional studies into the exposure of polyterpenol thin films to gamma radiation under a broader range of conditions may deliver useful insight into the film's stability mechanisms and supplementary avenues for processing. For example, sample irradiation within an inert atmosphere will eliminate the possibility of radiation-induced oxidation during the irradiation process, and may serve to enhance polyterpenol's stability response. Successively higher doses may also be applied in order to determine a maximum dose threshold for polyterpenol irradiation, and possibly serve as a means for stimulating degradation of what is otherwise a highly crosslinked and durable polymeric material.

7.2.5 Supplementary Future Work

All aspects of our understanding of polyterpenol radiation processing would benefit from expansion in the scope of irradiation conditions and characterisation techniques applied. In the interests of providing reasonable parameters to the scope increases of future studies, priority may be given to first broadening the suite of radiation species to include X-rays, UV rays, and electrons. In conjunction with those species already investigated, this would permit the formation of a comprehensive framework that can describe polyterpenol-radiation interactions and property changes. Molecular mass data provided by fundamental gel permeation chromatography studies on irradiated polyterpenol films also presents itself as a high priority target for future studies. The resulting data may yield vital information about the polymer's net preference for exhibiting either crosslinking or chain-scissioning following exposure to different irradiation conditions (species, energies, doses, etc.). Such information will permit the development of guidelines demarcating the boundaries between useful irradiation of polyterpenol, and the onset of molecular degradation.

7.3 CONCLUDING STATEMENT

This thesis has contributed new information to the understanding of terpenoid plasma environments, and the response of plasma polymerised polyterpenol thin films to various forms of ionising radiation.

Specifically, identification of the type and abundance of species generated within terpinen-4-ol and *Melaleuca alternifolia* oil reactive plasmas allows for informed and economical selection of precursor and deposition conditions. Processing with low fluence swift heavy ions has produced polyterpenol thin films with modified optical properties, and latent ion tracks suitable for a variety of applications. The multiple overlapping track regime generated by swift heavy ion irradiation at high fluence transformed polyterpenol into a chemically functionalised graphitic-polymer nanocomposite with significant morphological restructuring. Dense plasma focus irradiation has been used to facilitate the first instance of inelastic deformation in a plasma polymer, as evidenced by the development of bubble-like surface structures following the thermally induced expansion of trapped void content. Demonstrating the preservation of polyterpenol's physical and chemical properties following exposure to gamma radiation at doses up to 100 kGy was an essential step towards the commercial uptake of polyterpenol in biomedical applications.

These accomplishments, coupled with their associated publications and the review paper completed in the course of this thesis, have served to expose and elevate the importance of radiation processing as a tool in the development of plasma polymerised polyterpenol thin films in sustainable organic electronic and biomedical applications.